

**DEVELOPMENT AND PERFORMANCE EVALUATION OF
FRESNEL LENS AND PHASE CHANGE MATERIAL ASSISTED
PORTABLE SOLAR DESALINATION SYSTEM FOR FRESH WATER
PRODUCTION**

HO ZHI YONG

MASTER OF ENGINEERING SCIENCE

LEE KONG CHAIN FACULTY OF ENGINEERING AND
SCIENCE
UNIVERSITI TUNKU ABDUL RAHMAN
June 2021

**DEVELOPMENT AND PERFORMANCE EVALUATION OF
FRESNEL LENS AND PHASE CHANGE MATERIAL ASSISTED
PORTABLE SOLAR DESALINATION SYSTEM FOR FRESH WATER
PRODUCTION**

By

HO ZHI YONG

MASTER OF ENGINEERING SCIENCE

A dissertation submitted to the Department of Mechanical and Material
Engineering, Lee Kong Chian Faculty of Engineering and Science,
Universiti Tunku Abdul Rahman,
in partial fulfilment of the requirements for the degree of
Master of Engineering Science
June 2021

ABSTRACT

DEVELOPMENT AND PERFORMANCE EVALUATION OF FRESNEL LENS AND PHASE CHANGE MATERIAL ASSISTED PORTABLE SOLAR DESALINATION SYSTEM FOR FRESH WATER PRODUCTION

Passive solar still is one of the solutions on water scarcity in coastal and rural regions due to its uncomplicated design as well as its least demand for electrical energy. However, passive solar still often has low efficiency and productivity due to its limitation on enhancement approach. Concentrated solar power (CSP) is one of the well-known features being used on solar desalination. Reflective CSPs are mostly used on active solar still as it require solar tracker for its high sensitivity to solar flux. In this study, a less sensitive refraction based CSP feature is introduced to improve the performance of passive solar stills. The performance evaluation in terms of efficiency and productivity was conducted on 2 differently designed passive double slope single basin solar still coupled with Fresnel lens (FRL). Both prototypes show similar trends in augmentation of efficiency and productivity. The theoretical values of daily water yield show a good match with the experimental values. The highest water yield recorded from a prototype coupled with Fresnel lens is 3.19 L/m²day. With FRL, the efficiency of the prototype has reached to 37% from 28% for the conventional design. An increase in productivity (g/kJ) by 60% as compared to the conventional still is also observed. Further studies are conducted to identify the effect of Phase Change Material (PCM) being used as energy storage of the designed passive solar still. PCM alone stabilize the process with an enhanced productivity. However, when coupled with Fresnel lens, the existing design of PCM filled tubes placed in the solar still's basin did not show significant improvement due to heat loss to the surrounding. The collected freshwater from the 35,000 ppm saline solution produced by the prototypes is of very high quality and complies well with the World Health Organization (WHO) standard.

ACKNOWLEDGEMENTS

I would like to thank everyone who had contributed to the successful completion of this research. I would like to express my gratitude to my research supervisors, Dr. Rubina Bahar and Dr. Koo Chai Hoon for their invaluable advice, guidance and enormous patience throughout the development of the research. It is also important to mention the support from Institution of Mechanical Engineers (IMechE) through The Global Engineering Design Solution Challenge 2019.

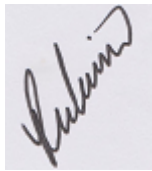
In addition, I would like to thank UTARRF for providing the UTAR Research Scholarship Scheme. The opportunity to work as a researcher in the project (Vote No. 6200/R20 and No. 6251//K02) is much appreciated.

I would also like to express my gratitude to my loving parents and friends who had helped and given me encouragement throughout this research. Lastly, I would like to thank Universiti Tunku Abdul Rahman for giving me the opportunity to contribute in this research with the facilities provided by them.

APPROVAL SHEET

This dissertation report entitled “**DEVELOPMENT AND PERFORMANCE EVALUATION OF FRESNEL LENS AND PHASE CHANGE MATERIAL ASSISTED PORTABLE SOLAR DESALINATION SYSTEM FOR FRESH WATER PRODUCTION**” was prepared by **HO ZHI YONG** and submitted as partial fulfilment of the requirements for the degree of Master of Engineering Science at Universiti Tunku Abdul Rahman.

Approved by:



(Dr. Rubina Bahar)
Supervisor
Department of Mechanical and Material
Engineering
Lee Kong Chian Faculty of Engineering
and Science
Universiti Tunku Abdul Rahman

Date: 22nd June 2021



(Dr. Koo Chai Hoon)
Co-supervisor
Department of Civil Engineering
Lee Kong Chian Faculty of Engineering
and Science
Universiti Tunku Abdul Rahman

Date: 22nd June 2021

**LEE KONG CHIAN FACULTY OF ENGINEERING AND SCIENCE
UNIVERSITI TUNKU ABDUL RAHMAN**

Date: 22nd June 2021

SUBMISSION OF DISSERTATION

It is hereby certified that Ho Zhi Yong (ID No: 19UEM00437) has completed this dissertation entitled “*Development and performance evaluation of Fresnel Lens and phase change material assisted portable solar desalination system for fresh water production*” under the supervision of Dr. Rubina Bahar (Supervisor) from the Department of Mechanical and Material Engineering, Lee Kong Chian Faculty of Engineering and Science, and Dr. Koo Chai Hoon (Co-Supervisor) from the Department of Civil Engineering, Lee Kong Chian Faculty of Engineering.

I understand that University will upload softcopy of my dissertation in pdf format into UTAR Institutional Repository, which may be made accessible to UTAR community and the public.

Your truly,



(HO ZHI YONG)

DECLARATION

I hereby declare that the dissertation is based on my original work except for quotations and citations which have been duly acknowledged. I also declare that it has not been previously or concurrently submitted for any other degree at UTAR or other institutions.



(HO ZHI YONG)

Date: 22nd June 2021

TABLE OF CONTENTS

	Page
ABSTRACT	ii
ACKNOWLEDGEMENTS	iii
APPROVAL SHEET	iv
SUBMISSION OF DISSERTATION	v
DECLARATION	vi
TABLE OF CONTENTS	vii
LIST OF TABLES	ix
LIST OF FIGURES	x
LIST OF SYMBOLS/ ABBREVIATIONS	xii
CHAPTER	
1 INTRODUCTION	1
1.1 General Introduction	1
1.2 Importance of Study	4
1.3 Problem Statement	4
1.4 Aim and Objectives	5
1.5 Scope and Limitation of the Study	6
1.6 Contribution of Study	7
1.7 Outline of the Report	7
2 LITERATURE REVIEW	8
2.1 Introduction	8
2.2 Solar Desalination	8
2.3 Solar Still	11
2.4 Variable Affecting the Performance of Solar Still	15
2.5 Existing Approaches to Improve Performance of Passive Solar Still	17
2.6 Concentrated Solar Power (CSP)	21
2.7 Thermal Energy Storage (TES)	28
2.8 Summary	34
3 RESEARCH METHODOLOGY	36
3.1 Introduction	36

3.2 Design of the Solar Still	38
3.3 Preliminary Test	42
3.4 Experimental Procedures	48
3.5 Theoretical Calculation	53
4 RESULTS	59
4.1 Introduction	59
4.2 Conventional Solar Still	60
4.3 Fresnel Lens Solar Still	63
4.4 Phase Change Material Solar Still	66
4.5 Combination of Fresnel Lens and Phase Change Material	69
4.6 Effect of Water Volume	72
4.7 Summary	77
5 DISCUSSIONS	80
5.1 Introduction	80
5.2 Theoretical Model	80
5.3 Effect of Fresnel Lens	83
5.4 Effect of Phase Change Material	86
5.5 Combination of Fresnel Lens and Phase Change Material	89
5.6 Quality of the Distillate	92
5.7 Cost of the Distillate	92
5.8 Summary	95
6 CONCLUSION AND RECOMMENDATION	96
6.1 Conclusion	96
6.2 Recommendation for Future Work	97
REFERENCES	99
APPENDICES	105
Appendix A: Experimental Error and Uncertainty Analysis	105
Appendix B: Experimental Data	112
Appendix C: Publication	143

LIST OF TABLES

Table		Page
3.1	Solar Still Configurations	37
3.2	Parameter of Solar Stills	50
3.3	Properties of PCM and FRL	51
3.4	Instruments for different measurement	52
4.1	Experimental Protocol	59
4.2	Productivity and Efficiency of Conventional Solar Stills	63
4.3	Productivity and Efficiency under FRL Effect	66
4.4	Productivity and Efficiency of Conventional and PCM Solar Still	69
4.5	Productivity and Efficiency of Conventional and MSS A and B	72
4.6	Productivity and Efficiency of FRL and MSS A and B	76
5.1	Comparison of Actual and Theoretical Yield	81
5.2	Water Conductivity Test	92
5.3	Cost of solar still model A	93
5.4	Cost of solar still model B	93
5.5	Comparison between present work and existing stills	94

LIST OF FIGURES

Figure		Page
2.1	Schematic diagram of a single effect single basin solar still	12
2.2	Schematic diagram of active solar still with flat plate collector and circulation system	14
2.3	Parabolic dish solar still	22
2.4	Single slope single basin solar still coupled with compound parabolic concentrator concentric tubular solar still	25
2.5	Difference between FRL and conventional lens	28
2.6	Schematic diagram of the conventional solar still and PCM solar still	33
3.1	Overall flow chart of the research	36
3.2	CAD drawing of double slope single basin solar still	39
3.3	Desalination process	40
3.4	Solar Path Diagram and Sun Chart	41
3.5	Schematic Drawing of the slope angle	41
3.6	Prototype solar still for preliminary test	42
3.7	Temperature Range of Model A (Without FRL)	43
3.8	Temperature Range of Model A (With FRL)	44
3.9	PCM tubes CAD drawing	44
3.10	Temperature trend of Solar Still without PCM	45
3.11	Temperature trend of Solar Still with Paraffin Wax	46
3.12	Temperature trend of Solar Still with Petroleum Jelly	46
3.13	Temperature trend of Solar Still with Petroleum Jelly with Scraps	47
3.14	Water Yield per average solar irradiation	48
3.15	(a) Petroleum Jelly (b) PCM tubes	48
3.16	Deformation of the acrylic board	49
3.17	Photograph of the solar stills	50
3.18	Flow chart of the experiment routine	52
3.19	Schematic of the modelling element	54
3.20	Direction of the incident solar radiation towards Model B	57

4.1	Temperature and Solar Irradiance of Conventional Model A	61
4.2	Temperature and Solar Irradiance of Conventional Model B	61
4.3	Hourly Water Yield of Conventional Still	62
4.4	Temperature and Solar Irradiance of FRL Model A	64
4.5	Temperature and Solar Irradiance of FRL Model B	64
4.6	Hourly Water Yield of FRL Still	65
4.7	Temperature and Solar Irradiance of PCM Model A	67
4.8	Temperature and Solar Irradiance of PCM Model B	67
4.9	Hourly Water Yield of conventional and PCM Stills	68
4.10	Temperature and Solar Irradiance of MSS A (with FRL and PCM)	70
4.11	Temperature and Solar Irradiance of MSS B (with FRL and PCM)	70
4.12	Accumulated Water Yield of Conventional and Modified Solar Stills	71
4.13	Temperature and Solar Irradiance of FRL Model B (4500mL)	73
4.14	Accumulated Water Yield of FRL Model B	74
4.15	Temperature and Solar Irradiance of MSS B (4500mL)	75
4.16	Hourly Water Yield of MSS Model B	76
4.17	Productivity and Efficiency of Model A	77
4.18	Productivity and Efficiency of Model B	78
5.1	photograph of the shaded regions.	83
5.2	Arrangement of FRL in the experiment	84
5.3	Solar flux concentrated on the side of the basin	85
5.4	Bubbles forming in CSP Solar Still where FRL is used	86
5.5	Schematic diagram of Unsubmerged PCM	87

LIST OF SYMBOLS/ ABBREVIATIONS

FRL	Fresnel lens
CSP	Concentrated Solar Power
TES	Thermal Energy Storage
PCM	Phase Change Material
MSS	Mixed Solar Still
$Q_{c,w-g}$	Convective heat transfer from saline water to glass lid (W/m ²)
$Q_{e,w-g}$	Evaporative heat transfer from saline water to glass lid (W/m ²)
$Q_{r,w-g}$	Radiation heat transfer from saline water to glass lid (W/m ²)
T_w	Water Temperature (°C)
T_g	Glass Lid Temperature (°C)
p_w	Water Saturation Pressure above water surface (N/m ²)
I(t)	Solar Irradiance (W/m ²)
p_g	Water Saturation Pressure below Glass lid (N/m ²)
m_{yield}	Mass of Yield (kg)
A_w	Area of water surface (m ²)
A_b	Area of basin (m ²)
A_{Total}	Total area of absorption (m ²)
Δt	Difference in time (sec)
$h_{fg,sw}$	Saline Water Latent heat of Vaporization (kJ/kg)
$h_{fg,w}$	Water Latent heat of Vaporization (kJ/kg)
P	Solar Power (W)
E	Energy (kJ)

CHAPTER 1

INTRODUCTION

1.1 General Introduction

Water is indeed the most crucial key to life. Even though it is well-known that 70% of our planet is covered by water, only 3% are consumable freshwater. Only 0.5% of the total amount of fresh water is accessible in nature (Srithar et al., 2016; Fathy et al., 2018; Chen et al., 2019). Up until today, billions around the world are suffering water scarcity throughout the year (Mekonnen and Hoekstra, 2016). As the population continues to grow, water scarcity will be the major challenge to face in the coming years (Liu et al., 2017; Mancosu et al., 2015). A different strategy to obtain fresh water must be developed before the water scarcity turns into a bigger issue.

Desalination is one of the general ways to resolve water scarcity (March et al., 2014). Reverse Osmosis and fuel-based desalination plants are the current trends to produce freshwater. (Alnaimat et al., 2018). However, both of these methods are energy and cost intensive (Ahmadvand et al., 2019; Delgado-Torres et al., 2020). In other words, these approaches may not be feasible for rural regions where there is an inadequacy of energy supply. Moreover, relying on desalination from the methods could result in global warming, thus they are not the ultimate solution to water scarcity (Elimelech and Phillip, 2011).

As a viable solution, researchers have focused their interest toward renewable energies (Manju and Sagar, 2017). Renewable energy (RE) based desalination has been in practice for years. Among various RE desalination systems, 80% is based on solar energy (Delgado-Torres et al., 2020). Most importantly, solar desalination is proven viable in a remote area (Pugsley et al., 2016). Solar still is a small to medium scale solar desalination unit that operates with a simple working mechanism suitable in rural regions. However, low water yield and efficiency are the existing challenges that still need to be taken care of.

Researches are being carried out to enhance the productivity of solar stills by various method (Srithar et al., 2016; Kabeel et al., 2016; Fathy et al., 2018). In most of the cases, active solar still has higher productivity compared to that of passive solar stills. Despite the higher yield, the complicated design and high cost of active solar still might not be the ideal solution for the arid region where electricity is absent or unstable. Therefore, passive solar still is the major economically feasible way to provide fresh water. It must be further enhanced to meet the required productivity (Dawoud and Al Mulla, 2012; Shatat et al., 2016).

Many studies have been conducted to enhance the productivity of solar stills. Different methods were performed to alter certain parameters to improve the productivity. Modification on evaporation rate, condensation rate, and solar power input are the basic approaches implemented. For instance, the development on wick solar stills and stepped stills to enhance the evaporation

rate; use of fins to increase the thermal energy received; multi-effect desalination (MED) to enhance the condensation rate; thermal storage to prolong the desalination process; concentrated solar power (CSP) to increase solar flux per unit area; and hybridization of mentioned modifications (Arunkumar et al., 2019). Out of those, CSP has the highest potential and has been constantly used to hybridize with other technologies.

Generally, CSP is not applied to passive solar still. The high tracking precision and design complexity are the major obstacles of CSP features. Compared to reflective CSP, such as Parabolic trough, Fresnel Lens (FRL) has the advantage of lower cost, higher efficiency, smaller size, and requires less tracking precisions (Pham et al., 2018; Al-Dohani et al., 2018; Ma et al., 2019). Such properties opened up the potential of FRL being coupled with passive solar still. It is, therefore, worth the effort to investigate the feasibility and performance of FRL as CSP to enable another branch of enhancement on passive solar still.

Phase Change Material (PCM) on the other hand, is a common productivity enhancement option for both active and passive solar still. Unlike common enhancement strategies, instead of increasing the input (Solar Power), PCM retains thermal energy. Conventionally, PCM is immersed in the feed water to absorb the heat directly from the water. Part of the heat absorbed by the desalination system stored inside PCM in the form of sensible and latent heat. At a point when the thermal supply is reduced, PCM act as a temporary heat supply. Thermal energy will be discharged from PCM to the feed water due to

temperature difference, thus prolong the desalination process. PCM has been used as a combination of other enhancement methods for its high compatibility (Kabeel et al., 2018a; Yousef et al., 2019).

1.2 Importance of Study

Water desalination through renewable energy is one of the most viable way of solving water scarcity in rural regions. Among all technologies, passive solar desalination plays a crucial role. The enhancing approaches used in the study could contribute to a novel passive solar desalination system that is technically viable in the remoted, energy deprived with an adequate amount of freshwater.

1.3 Problem Statement

Reflection-based solar power concentration has been the trend of CSP solar stills during the past decade. Refraction-based CSP could be the alternative for such solar stills. The major drawback for refraction based CSP was due to the large size of the conventional convex lens. FRL shares the similar optical property of the conventional lens but can be made thinner without affecting the optical performance. FRL has been used in water heating applications throughout the years (Mahmoud et al., 2013; Zhao et al., 2018; Wang et al., 2019). In the field of solar desalination, it is also proven FRL coupled solar stills have significant improvement in term of productivity (Palomino-Resendiz et al., 2018; Sriram et al., 2019; Muraleedharan et al., 2019; Mu et al., 2019). However,

the studies mentioned were based on FRL active solar still. Study involving FRL in passive solar still has yet to be explored.

PCM has been mostly used as thermal transfer fluid in active solar still (Fathy et al., 2018; Hassan et al., 2019). In the passive solar still, PCM is used as stationary thermal storage attached to the basin. However, work about the combination of PCM and FRL based CSP on passive solar still is rarely reported in the available Journal database. Both FRL and PCM possess a unique and independent working mechanism that is capable to enhance the performance of thermal desalination. FRL can be used to boost up the water temperature and evaporation rate, while PCM can be used to stabilize and prolong the desalination process. The effect of combining FRL and PCM on passive solar still is unknown.

In this study, FRL and PCM were coupled with a passive solar still. The productivity of the solar still with different configurations was investigated to identify the effect of FRL, PCM, and both combined on passive solar stills.

1.4 Aim and Objectives

This research aims to investigate on the feasibility of utilising concentrated solar power (CSP), together with the aid of thermal storage through the phase change material (PCM) in developing solar stills with enhanced production.

- i. To study the performance of Fresnel Lens and Phase Change Material in solar desalination under tropical climate.
- ii. To develop a portable passive solar desalination system associated with Fresnel Lens and Phase Change Material.
- iii. To evaluate the performance and economic feasibility of the solar desalination system.

1.5 Scope and Limitation of the Study

The scope of the research is to experimentally study the effect of FRL and PCM and the combination of both on passive solar still and identify the improvement they could make. Experiments with each configuration must be carried out to achieve the goal.

The solar still used in the study is targeted to serve in the rural area. Least maintenance and simple design are the considerations while designing the prototypes. At the same time, the solar still should be made with low cost to cater to the major community living under water scarcity. This limits the option for enhancement for solar still. Features that would further improve the performance of FRL and PCM such as solar tracking and thermal transfer circulation system are therefore out of bounds.

The experiments were conducted outdoor on different days. It is not possible to conduct the experiments in identical meteorological condition.

Parameters such as ambient temperature, wind velocity, cloud movement may still cause minor influences on the accuracy of the result.

1.6 Contribution of Study

In this study, the effect of FRL and its combination with PCM on the performance of solar desalination could be identified. The outcome of this research open up a new in sight on the novel enhancement method of conventional solar still. The potential of associating FRL and PCM on conventional solar still will be unveiled. The outcome of the research could contribute to the improvement and development of future household solar still design.

1.7 Outline of the Report

The thesis consists of six chapters. The first chapter briefly explains the concept of solar desalination, its field of study, and the objectives of the research. Chapter two provides a literature review summarise the outcomes from similar researches. The research methodology is described in Chapter three. Chapter four presents the observation of the experimental result, while Chapter five discusses the outcome from the results. Chapter six summarises the finding of the research and provides suggestions for future research.

CHAPTER 2

LITERATURE REVIEW

2.1 Introduction

In this chapter, the process of solar desalination was studied to identify the research gap in the field of solar desalination. The literature review focused on various types of solar desalination, variables affecting solar desalination, concentrated solar power (CSP), and phase change material (PCM). In the first section, types of solar desalination, together with solar stills were discussed. The second section emphasized on the variables affecting solar desalination. CSP, FRL, thermal storage, and PCM were introduced in the last section of the chapter.

2.2 Solar Desalination

Desalination is an approach to separate salt and water from saline water. Most commercial-grade desalination plants use fossil fuel to supply the energy required for water desalination. This is undoubtedly a high financial and energy consuming method to obtain fresh water in countries suffering from water scarcity. Nevertheless, fossil fuel-based water desalination is not a long term solution to water shortage. Apart from its significantly high energy-intensive, fossil fuel-based desalination also contributes to environmental pollution (Shatat

et al., 2013). Renewable energy-based desalination is slowly replacing fossil fuel in regions lacking infrastructures (Shatat et al., 2013). Among the renewable sources such as wind energy, solar energy, and geothermal energy, solar desalination possesses the highest potential in the renewable energy sector and is widely used in for freshwater production (Shatat et al., 2013). Solar desalination is capable to solve three issues faced by the conventional thermal desalination, which are water scarcity, fossil energy depletion and environmental degradation (Gorjian and Ghobadian, 2015). Moreover, the most areas suffering from water shortage are endowed with high solar irradiation (Pouyfaucou and García-Rodríguez, 2018a). Thus, solar desalination is believed to be the most practical solution for freshwater production in arid regions.

2.2.1 Indirect Solar Desalination

Majority of the matured commercial solar desalination plants are indirect solar desalination (Pugsley et al., 2018). In indirect solar desalination system, solar energy is either harnessed in the form of thermal energy through the solar thermal collector or converted into electrical power through photo-voltaic (PV) solar panels. Solar thermal-based indirect solar desalination includes Multi-stage Flash (MSF), Multi-Effect Distillation (MED), Membrane desalination (MD), and Reverse Osmosis (RO) (Ali et al., 2011). On the other hand, Electrodialysis (ED) and PV based RO are based on the electrical energy harvested (Ali et al., 2011). Out of the indirect solar desalination technologies mentioned, MSF, MED, and RO are the most dominant and matured technologies (Pugsley et al., 2018).

Compared to the thermal-based MSF and MED, RO is less energy-intensive and therefore is more cost-competitive (Ali et al., 2011). RO uses high pressure to feed saline water through a semi-permeable membrane which only water molecules can pass through. Due to its advantage in cost-competitiveness, RO is becoming a trend with more utilization than MSF and MED in the recent decade (Pugsley et al., 2018). However, RO, MSF, and MED are much more appropriate for large scale desalination plants. It is not economically viable to implement such technologies on small scale individual solar desalination.

2.2.2 Direct Solar Desalination

Direct solar desalination, on the other hand, distills the saline water solely and directly with the energy obtained from the sun. The conversion, from solar energy to thermal energy, together with the desalination process is carried out in the same device (Pouyfaucou and García-Rodríguez, 2018b). Solar still and humidification-dehumidification desalination is under the category of direct solar desalination as both of them use solar energy as input to provide the heat required for the desalination process (Ali et al., 2011). In terms of operational simplicity, direct solar desalination is relatively less complicated compared to indirect solar desalination. Moreover, solar still is said to be economically viable for small-scale, household production (Shatat et al., 2013).

However, direct solar desalination is yet to become a true solution to water scarcity due to its low freshwater production compared to other desalination processes. Thus, researches and modifications to improve the performance of solar still are required to solve the water scarcity in remote areas (Shatat et al., 2013).

2.3 Solar Still

Solar still is a basic desalination device falls under the category of direct solar desalination. The working concept of solar still is based on hydrological cycle (Ali et al., 2011). Conventional solar still is a small scale desalination device consists of a blackened basin, transparent slope, thermal insulated wall, and a collecting chamber located at the lower end of the slope (Ali et al., 2011; Altarawneh et al., 2017). Sunlight passed through the transparent slope are harnessed by the blackened basin. The harvested solar energy is later transferred to saline water inside the basin. The heat is used to increase the temperature of saline water and eventually, evaporate the saline water. The water vapour is then condensate on the inner surface of the transparent slope. The condensate is than collected in the collector chamber. The mentioned progress is the working concept for basic, conventional single effect solar still (Altarawneh et al., 2017). The yield of such solar still falls between 1.5 to 3 L/m², which is considered low and thus not widely used (Altarawneh et al., 2017; Awasthi et al., 2018).

Several types of solar still have been modified and developed to improve the performance of solar still. Solar stills can be classified into two categories, which is passive solar still and active solar still. Passive solar still solely utilise the solar energy harvested from the sun throughout the desalination process to obtain the yield (Awasthi et al., 2018). On the other hand, active solar still often coupled with external devices such as pumps, cooler, and solar tracker, to aids in the desalination process. In active solar still, solar energy is harnessed indirectly for water heating (Ali et al., 2011).

2.3.1 Passive Solar Still

As mentioned, passive solar still relies only on natural sunlight. This indicates that passive solar still is relatively less complicated compared to active solar still. Therefore, passive solar still often require the least maintenance and can be constructed with low cost (Awasthi et al., 2018). Despite its relatively low water yield, passive solar still is an ideal option for arid regions (Awasthi et al., 2018).

The conventional single effect single basin solar still is a typical example of passive solar still. Researches based on such basic solar still were conducted to develop on novel passive solar still with improved performance (Awasthi et al., 2018). Figure 2.1 shows the schematic diagram of the conventional single effect single basin solar still.

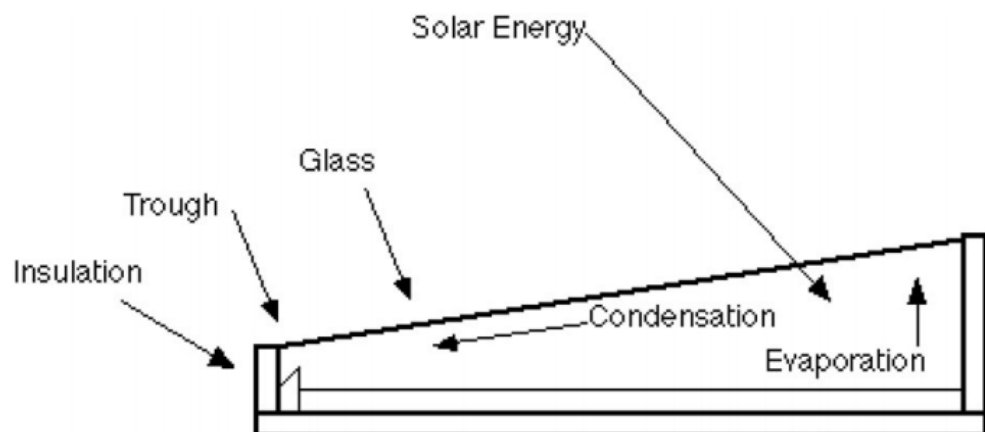


Figure 2.1: Schematic diagram of a single effect single basin solar still (Awasthi et al., 2018)

Derived from basin solar still, several types of passive solar stills were designed. Reflector solar still, wick type solar still and stepped type solar still are the common passive solar stills inspired by an inclined solar still (Awasthi et al., 2018). The reflectors enlarge the solar power input of the desalination system, and therefore increase the yield output of the solar still (Tanaka, 2009). In the wick type solar still, wick material absorbs the saline water from the basin through capillary action. After that, wick exposed to sunlight heated the small portion of water pulled up by the wick material. This greatly increases the evaporation rate of the still (Manikandan et al., 2013). The stepped type solar still increases the heat transfer between water and basin by spreading the feed water in small volumes across the basin. Such phenomenon greatly increases the evaporation rate (Awasthi et al., 2018).

2.3.2 Active Solar Still

Active solar still improves the water yield performance by increasing its thermal input, rate of evaporation, and rate of condensation as well (Sampathkumar et al., 2010). Unlike passive solar still, active solar still enhance its performance with the aid of alternative thermal source and mechanical devices. Additional solar energy input can be provided to active solar still through solar collectors and pre-heated thermal transfer fluid, while the condensation rate is often increased with a regenerative device, such as cold water condenser.

Solar collector, also known as concentrated solar power (CSP), is one of the common devices being used to improve the performance of active solar still.

Figure 2.2 shows an active solar still integrated with a flat plate solar collector. Other than the solar energy received by the solar still itself, the solar flux collected by the solar collector was also contributed to the desalination system as well (Sampathkumar et al., 2010). Circulation system is often used to effectively transfer the heat from the solar collector back to the solar still. Such CSP associated solar still greatly increases the overall temperature of the desalination system and thus higher water yield output (Sampathkumar et al., 2010).

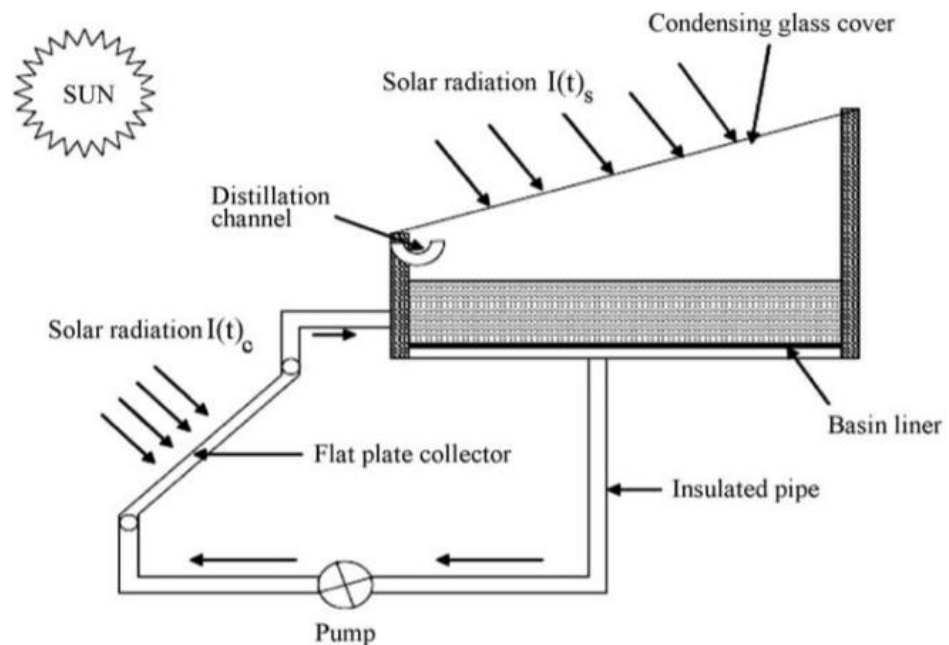


Figure 2.2: Schematic diagram of active solar still with flat plate collector and circulation system (Tiwari et al., 2009)

Preheat water active solar still increases the thermal input by obtaining thermal energy from a preheated fluid such as waste hot water from power plants and industries (Sampathkumar et al., 2010). The heat is transferred from wastewater to the solar still through a heat exchanger and circulation system (Sampathkumar et al., 2010). Such configuration increases the thermal gain of the active solar still, thus the evaporation rate of the feed water.

Regenerative active solar still increases the water yield output by increasing the condensation rate of the solar still (Sampathkumar et al., 2010). Coldwater flows were applied on the condensation surface of the solar stills. The condensation thus transfers its heat gained from vaporization of distillate to the cold water. This will cause a huge gap in temperature difference between condensation slope and the feed water, therefore increase the condensation rate of the solar still (Sampathkumar et al., 2010).

2.3.3 Multi-Effect Desalination (MED)

Multi-effect solar still refers to multi basin solar stills in an enclosed desalination system, with one basin on top of another. As the feed water in one of the basin evaporated, the water vapour begins to condensate beneath the basin of the upper chamber. The latent heat released during condensation will be absorbed by the feed water in the upper basin (Xiong et al., 2013). Therefore, the latent heat released from a basin is used as the alternative heat source of another basin. This method minimizes the heat loss of the desalination system.

2.4 Variable Affecting the Performance of Solar Still

Numerous studies have been conducted to identify the impact of variables affecting the performance of solar stills. Knowing the parameters helps in designing prototypes for the research.

2.4.1 Water Depth

Water mass or water depth of feed water in the basin affects the rate of temperature increment and overall water temperature in the desalination system. The larger the water mass, the more thermal energy is required to heat up the system. Studies have proven that the productivity of the solar still is inversely proportional to the water depth of the solar still (Kumar et al., 2017; Rajamanickam and Ragupathy, 2012; Kabeel et al., 2019a; Omara et al., 2017). Thus, in the ideal scenario, a low water depth must be kept throughout the experiment to obtain maximum productivity.

2.4.2 Free Surface Area

The surface area of the water exposed to the air, also known as the free surface area, decides the evaporation rate of the solar still (Samuel et al., 2016). Large free surface area indicates large evaporation for feed water. Wick solar still was developed to obtain a significantly high free surface area of feed water through capillary action (Samuel et al., 2016).

2.4.3 Slope Related Parameters

The thickness of the slope cover is one of the parameters affecting the transmission of solar intensity into the basin (Morad et al., 2015). The thicker the slope cover, the lesser the solar intensity is capable to transmit into the feed water. That will thus reduce the efficiency of the solar still (Morad et al., 2015). The temperature of the cover also plays an important role in the condensation

rates. The temperature difference between feed water and the slope cover is directly proportional to the condensation rate of the solar still (Morad et al., 2017).

The inclination angle of the transparent is optimum when closed to the latitude angle of the experiment region (Khalifa, 2011; El-Samadony et al., 2016). The slope angle affects the amount of solar flux transmitted. Numerous studies have been done to identify the ideal slope angle for different types of solar still. However, the results vary and inconsistent in different locations (Rufuss et al., 2016). Thus, the optimal slope angle of the solar should follow the location latitude of the research.

2.4.4 Climate Condition

Climatic parameter such as wind velocity, ambient temperature, and cloud movements are difficult to control while. However, these parameters have proven effects on the productivity of solar stills (Muftah et al., 2014). High wind velocity and low ambient temperature increase the condensation rate of the distillate, while cloud movement affects the solar intensity received by solar still (Muftah et al., 2014).

2.5 Existing Approaches to Improve Performance of Passive Solar Still

The approaches and techniques used to improve the performance of solar still are in fact based on the variables mentioned in the previous section. Ultimately, the productivity of the solar still is improved by:

- Increase thermal input of the solar still
- Increase rate of evaporation
- Increase rate of condensation

Several enhancement techniques that manipulate the above parameters have been used on solar to improve the efficiency and productivity of the solar still.

2.5.1 Wick Type Solar Still

Wick material like cotton and sponge is capable to increase the evaporation rate of the feed water. Feed water is absorbed by the wick material through capillary action, thus increases the free surface area.

Sharon et al. (2017) conducted an experimental work to compare the performance of tilted solar still with basin and with blackened wick. A basin with the dimensions of 1250 x 920 x 50-mm constructed with 2 mm thick of aluminium has been placed in single slope solar still. The basin has been divided into 12 identical compartments. Another similar solar still is associated with a blackened wick attached to a feed water tank. The result of the study shows that the water yield of the basin type is ranged from 4.48 to 4.99 L/day while the wick type is ranged from 4.54 to 4.62 L/day.

2.5.2 Stepped Type Solar Still

High water depth is not preferred as that indicates low heat transfer and high thermal inertia. Stepped solar still is designed to maintain a minimum water depth, while at the same time improve the heat transfer between basin (solar absorber) and saline water.

Saadi et al. (2018) has conducted an experiment to compare the performance of conventional single slope solar still with a modified vertical multi-tray evaporator (MTE) stepped solar still in Algeria. Both solar stills have a similar basin setup. The basins have an area of 0.35 m^2 and was made out of 0.7 mm thick of galvanized iron coupled with insulation. The slope angle was 36° from the horizontal. The MTE still has an internal vertical evaporator on the wall which consist of 18 triangular trays purposed to increase the evaporation area. The entire setup was sealed with silicone rubber to prevent leaking. The experimental result indicates that the stepped solar still performs better in term of productivity. Conventional solar still provides water yield of 2.85 kg/m^2 , while the modified stepped still provide water yield of 5.82 kg/m^2 .

2.5.3 Finned Type Solar Still

Fins are practically used in thermal dynamic applications. It increases the contacting surface between 2 mediums, thus increasing the heat transfer. The fins also increase the solar irradiance absorptivity of the solar still.

Rabhi et al. (2017) experimentally studied the water yield performance of modified single slope solar still with pin absorber and external condenser. The basin is covered with a layer of wick pinned with fins to increase solar absorptivity of the still. With the help of external condenser, the modified solar still has its solar efficiency of 43.7% and water yield of 3.492 l/m² day, which was 32.18% greater than conventional solar still.

2.5.4 Solar Reflector

Omara et al. (2016) investigated single slope solar still coupled with internal reflectors and corrugated absorber. Two single slope single basin solar still with identical dimension has been designed, while one remains as conventional solar still and another was integrated with internal reflectors and corrugated absorber. The area of the basin used is 0.5 m². Mirrors have been placed on the internal walls (back and sides) of the modified solar still. Black painted corrugated absorber has been placed on the basin to increase the solar absorbance. The saline water depth of both solar stills is left constantly at 1 cm with a feeding inlet. Part of the absorber was left out of the saline water surface due to low water depth. The corrugated absorber was covered with a layer of the wick. Eventually, capillary action will drag the saline water up after the saline water in the soaked wick evaporated. Thus, enhance the rate of evaporation. The working concept is similar to wicked solar still. The water yield result for conventional solar still and modified solar still are 2 L/m² and 4.1 L/m² respectively. The improvement in productivity of such modification is 145.5%.

2.6 Concentrated Solar Power (CSP)

Concentrated solar power (CSP) device or solar collector is an effective technique that is widely used on solar power generator, solar power plant, and large scale solar desalination system. The main purpose of utilizing a CSP device is to concentrate solar radiation from an area of aperture area (larger area) to receiver area (smaller spot) in order to generate high temperature on the receiver. Generally, CSP technology can be classified into 4 major categories, which is parabolic dish, parabolic trough, solar power tower, and linear Fresnel (Abdullah, et al., 2018).

Despite that CSP is commonly used on large scale desalination plant, some of the CSP devices are still feasible on small to medium scale basin type solar still (Sathyamurthy, et al., 2017). CSP solar stills often integrated with other techniques mentioned in Section 2.5 to further improve the performance of the solar still.

2.6.1 Solar Dish Concentrator

Parabolic dish or solar dish concentrator is a curvy dish device that reflects sunlight on the solar receiver, which is located on its focal point (Abdullah, et al., 2018). The focal distance of the solar dish concentrator changes overtime following the movement of the sun. To maximize the solar intensity received, solar dish concentrators are often integrated with a dual-axis solar tracker (Abdullah, et al., 2018). Despite its complicated mechanism, solar dish concentrator is still relatively mobile compared to other CSP devices (Abdullah,

et al., 2018). When coupled with solar still, the solar receiver of the solar dish concentrator is replaced with the basin (Arunkumar et al., 2015a; Bahrami et al., 2019). Figure 2.3 is the schematic diagram of parabolic dish solar still in the study of Bahrami (Bahrami et al., 2019).

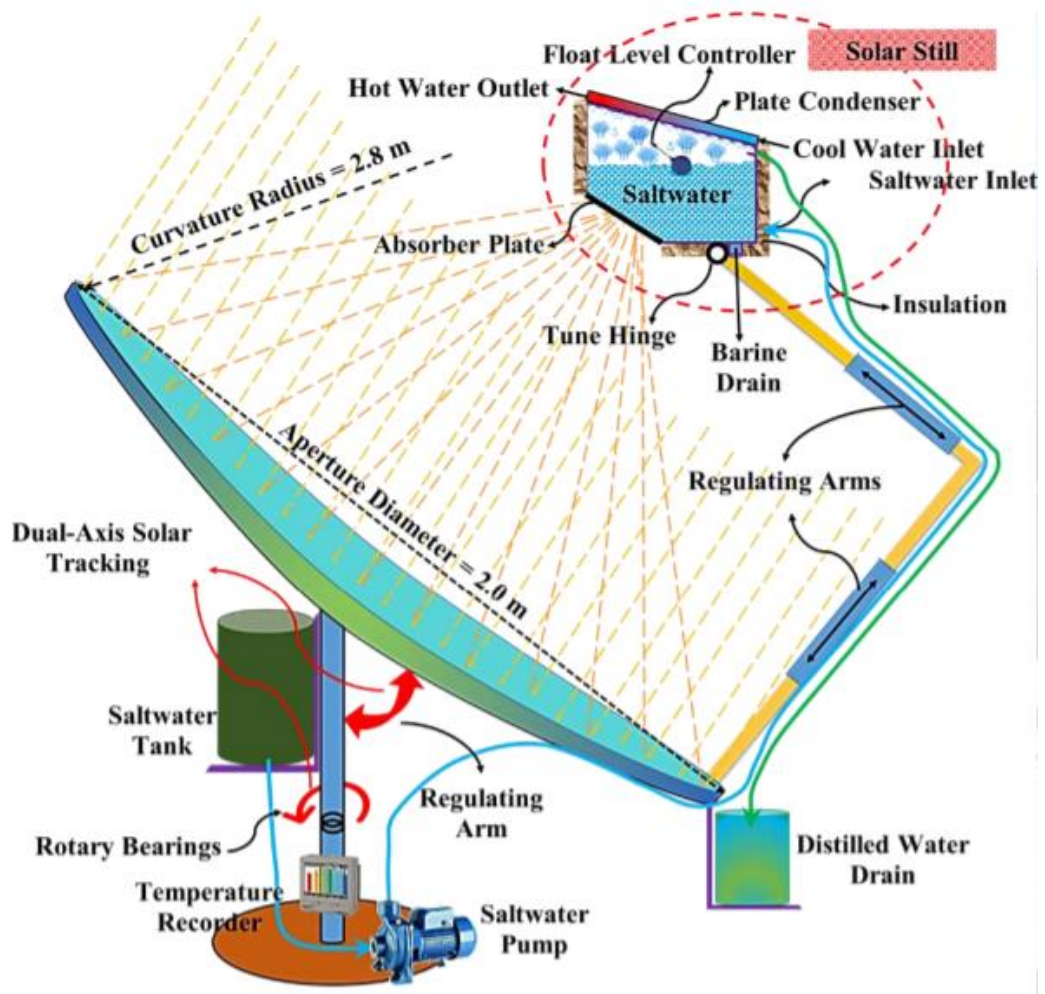


Figure 2.3: Parabolic dish solar still (Bahrami et al., 2019)

Milad Bahrami (2019) experimentally and theoretically studied a modified solar still coupled with a parabolic dish solar collector. The basin of the solar still was located at the focal point of a huge parabolic dish. A solar absorber was placed at the bottom of the still to receive concentrated solar radiation directly from the solar collector. The solar collector was integrated with

a dual-axis solar tracking system. Under optimum condition, where the dimension of the solar collector was changed to 3m in diameter, the solar still was recorded producing 75 kg of water yield in a day.

T. Arunkumar (2015b) experimentally studied a modified single slope solar still coupled with a parabolic solar collector. The modified solar still uses a copper semi-spherical basin as solar absorber to receive concentrated solar radiation from the solar dish collector located beneath the solar still. Saline water is stored in the semi-spherical absorber so that the heat can transfer with minimum heat loss. Moreover, the solar still is coupled with PCM and top cover cooling to improve the performance. Condensation of water vapour occurs on the inner surface of the top cover with inclination of 11° . In optimum condition, the cold water with flow rate of 100 mL/min was applied on the cover to enhance the rate of condensation. The optimum water yield obtained from the modified solar still is $3.8 \text{ L/m}^2 \text{ day}$.

2.6.2 Parabolic Trough Concentrator (PTC)

PTC consists of a huge U-shape trough made with reflective materials and a long tube solar receiver located at the middle of the trough (Abdullah, et al., 2018). Unlike solar dish, PTC does not have a focal point. Instead, the sunlight is concentrated from the trough onto a line parallel to the tube solar receiver. In large scale solar power plant, PTC often constructed with numerous trough parallel to each other (Abdullah, et al., 2018). The trough is aligned parallel to the north-south axis. Thus, PTC is often integrated with a single-axis solar tracker to maximize the solar intensity concentrated on the solar receiver

throughout the effective working hour. The thermal energy collected were transferred to the application chamber through thermal transfer fluid.

In the field of solar desalination, PTC can be used on both tubular solar still and basin solar still. In PCT tubular solar still, the tubular still itself is located at the middle of PTC, acted as a solar receiver (Elashmawy, 2019). Great amount of solar intensity was subjected on the tubular still to evaporate the water inside the still. In PCT basin solar still, water or thermal transfer fluid are preheated by PTC. The heated fluids are later circulated to the basin (Arunkumar et al., 2016). The heat is transferred to the feed water, aiming to increase the evaporation rate. Figure 2.4 shows the schematic diagram of the basin solar still coupled with compound PTC tubular solar still (Arunkumar et al., 2016).

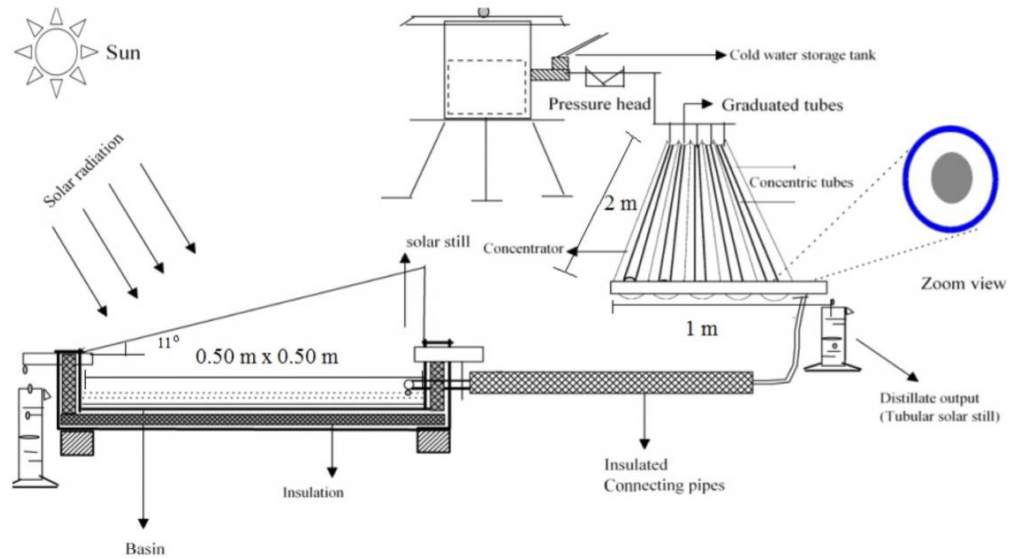


Figure 2.4: Basin solar still coupled with compound PTC tubular solar still (Arunkumar et al., 2016)

Arunkumar (2016) has experimentally evaluated a modified single slope solar still coupled with compound parabolic concentrator concentric tubular solar still. The working concept of the solar still is by preheating saline water using parabolic trough concentrator before entering single slope solar still, the initial temperature of the saline water is higher thus increases the rate of evaporation. Heated saline water will flow to single slope solar still. The water yield of the modified still is found to be $3.23 \text{ L/m}^2 \text{ day}$.

Elashmaway (2019) experimentally studied a high-temperature parabolic trough concentrator tubular solar still which integrated with a cover cooling system. Water spraying solar still and outer layer tubular cooling method was used in the modified tubular stills. The result of the experiment showed that the cover cooling gives a negative impact on the performance of stills. The temperature of the saline water for water spraying, tubular cooling modified still

are 100 °C and 92 °C, respectively, which are lower than tubular still without a cooling system, 102 °C. Cover cooling on tubular still will cause heat loss and reduce the rate of evaporation in the solar still.

2.6.3 The Weakness of Conventional CSP

CSP indeed plays an important role in solar energy applications. However, in small scale solar desalination, CSP technology is not economically feasible (Sathyamurthy, et al., 2017). Most of the CSP being used on solar applications was a reflective solar collector. To maintain high reflectivity, reflective CSP requires high maintenance frequency (Kumar, et al., 2015a). Moreover, reflective CSP often integrated with a solar tracker, as high tracking precision is needed on reflective CSP (Kumar, et al., 2015a).

It is undeniable that CSP can provide a huge improvement on the thermal input of the desalination system. However, these properties make CSP only favourable on active solar still. Thus, refractive CSP with lower cost and less maintenance-intensive properties are a great alternative solution for small scale solar desalination system (Kumar, R.L. Shrivastava, et al., 2015a; W. T. Xie et al., 2011).

2.6.4 Fresnel Lens (FRL)

Refractive solar concentrator concentrates sunlight on the focal point based on the principle of refraction. Refraction of light is a phenomenon that, when light enters a medium with greater density, the direction of the light will

bend away from normal, and vice versa (Kumar, et al., 2015b). Conventional lens utilises this concept in both imaging and non-imaging light performance.

Modified from the conventional lens, FRL is a refractive lens with only the contour profile left (Kumar, et al., 2015). Therefore, FRL possesses the advantages of compact volume and lightweight. Figure 2.5 shows the difference in thickness between FRL and conventional lens (Xie, et al., 2011). There are layers of tiny fragments on the surface of transparent FRL, each refracts the light passed through it onto the focal point. The application of FRL can be classified into imaging systems and non-imaging systems (Xie, et al., 2011). For imaging type systems, FRL is used to form a sharp and detailed image, thus required high cost for precise fabrication (Kumar, et al., 2015). On the other hand, solar thermal application is under the category of non-imaging system. In non-imaging system, FRL is used to concentrate solar flux on the focal point. FRL being used on such CSP applications are designed to have short focal length and the high concentration ratio (Xie, et al., 2011). At the same time, non-imaging FRL is relatively less tracking intensive due to its high acceptance angle (Xie, et al., 2011). Generally, FRL is made with transparent glass with high transmittance. Polymethylmethacrylate (PMMA) is another choice of material for FRL for its great optical characteristic, lightweight, and lower fabrication difficulty (Xie, et al., 2011). In short, FRL possesses high optical efficiency, along with its compact size and can be fabricated with low cost. Such advantages have proven its potential on solar thermal applications such as solar cooking and water heating (Xie, et al., 2011).

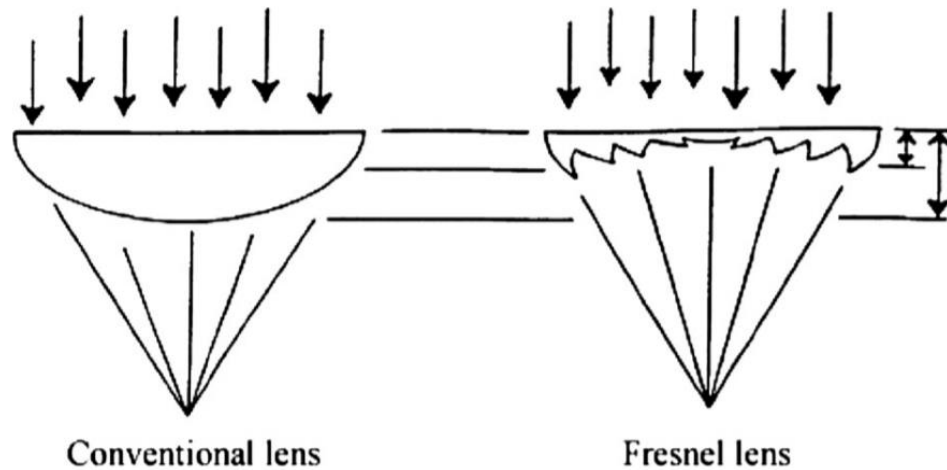


Figure 2.5: Difference between FRL and conventional lens (Xie et al., 2011)

The refraction based FRL also enables it to be used on direct solar still. The FRL can be installed on top of a solar still, transmitting the concentrated solar flux directly on the basin. Contrary to reflective CSP, such configuration does not require thermal transfer fluid nor the circulation system (Kumar, et al., 2015).

2.7 Thermal Energy Storage (TES)

The main purpose of TES is to store thermal energy and supply the stored thermal energy to the designed system at a later time (Cabeza et al., 2015). The thermal energy is usually pre-charged into a thermal storage material and then transferred to a cooler medium, actively or passively. For solar energy applications, two types of TES were mainly used, which are sensible heat storage and latent heat storage (Cabeza et al., 2015).

2.7.1 Sensible Heat Storage

Sensible heat storage refers to the thermal energy stored while increasing the temperature of the TES materials (Cabeza et al., 2015). While the thermal energy is charged in the form of sensible heat, the phase of the TES material remains (Al-Maghalseh and Mahkamov, 2018). The sensible heat TES materials should hold properties such as high specific heat capacity, high thermal conductivity, and chemically stable (Cabeza et al., 2015). The specific heat capacity of the TES material is the key consideration as it is directly affecting the amount of thermal energy storage capacity. Generally, sensible heat TES can be stored in liquid or solid phase, dependent on the thermal storage system of the applications (Cabeza et al., 2015). Liquid sensible heat materials such as water and oil can be used in the circulating system, thus preferable in the active storage system. Solid sensible heat material such as concretes, on the other hand, are preferred in passive applications. The thermal energy stored can be calculated with Equation 2.1 (Cabeza et al., 2015).

$$Q = m C_p \Delta T \quad (2.1)$$

where,

Q = Thermal energy stored, J

m = Material mass, kg

C_p = Specific heat capacity, J/kg.K

ΔT = Change in temperature, K

2.7.2 Latent Heat Storage

Latent heat storage is the thermal energy stored in the TES material while phase transition was carried out (Cabeza et al., 2015). In other words, the temperature of the TES material remains almost constant while latent heat is being discharged. This resulted in better discharge rate compared to sensible heat, as the rate of heat transfer is driven by temperature difference. Most of the latent heat storage material used relies on phase transition between solid-liquid (Cabeza et al., 2015). The TES material was preheated to a temperature where its phase is completely changed (melting). The melted material is then applied to its designed application, constantly discharge the thermal energy up until it is solidified. For latent heat TES material, also known as phase change material (PCM), phase transition temperature (melting or solidification) and phase change enthalpy (the latent heat of fusion) are the main considerations in different applications. The thermal energy stored in the latent heat storage can be calculated with Equation 2.2 (Cabeza et al., 2015).

$$Q = m \Delta h \quad (2.2)$$

where,

Q = Thermal energy stored, J

m = Material mass, kg

Δh = Phase change enthalpy (J/kg)

2.7.3 Phase Change Material (PCM)

PCM possesses both sensible and latent heat storage capability. This made PCM capable to hold a great amount of heat capacity. Moreover, PCM has a wide temperature range that is suitable for varieties of applications. Most PCM is also easily accessible and low in cost. These properties made PCM stands in a strong position on TES application (Chandel and Agarwal, 2017). Generally, PCM is classified into three categories, which is organic PCM, inorganic PCM, and eutectics PCM (Chandel and Agarwal, 2017).

Organic PCM has the properties of high latent heat of fusion, low thermal conductivity, chemically stable, and has no phase segregation (Chandel and Agarwal, 2017). Paraffin wax is the most common organic PCM being used as thermal storage. The melting point of paraffin wax can be altered by modifying the ratio of molecular mass and chain length of carbon and hydrogen compound (Chandel and Agarwal, 2017). Its wide variety of melting points made paraffin wax available in a range of applications (Chandel and Agarwal, 2017). Paraffin wax is also chosen to be used in this research.

Inorganic PCM refers to metals and salt hydrates TES. Contrary to organic PCM, inorganic PCM is corrosive and suffer significant effect from subcooling and phase segregation (Chandel and Agarwal, 2017). However, its high latent heat capacity, high specific heat capacity, and high thermal conductivity are still favourable in certain applications (Chandel and Agarwal, 2017).

Eutectic PCM, also known as composite PCM, is the mixture of organic PCM and high thermal conductivity compounds to overcome the low conductivity problem faced by organic PCM. Such eutectic PCM possess the advantages of high phase change temperature and no segregation effects (Chandel and Agarwal, 2017). In spite of that, eutectic PCM is difficult to obtain and is often more costly than the other two PCM (Chandel and Agarwal, 2017). While selecting the PCM to be used, certain conditions must be considered. In term of thermal storage capability, the PCM selected must hold high latent heat of fusion and specific heat capacity. Other than that, the PCM should be chemically stable to prevent corrosion. Moreover, the PCM should have low subcooling and phase separation effect. Most importantly, the melting point of the PCM must be chosen wisely as it will cause a direct impact to its application. Kabeel evaluated the performance comparison between paraffin wax with different melting points, thermal conductivity, and latent heat (Kabeel et al., 2018b). It was found that using paraffin wax with a different melting point, the productivity of the solar still will be affected. Thermal storage with low melting point could not hold sufficient latent heat, while high melting point is not consistent in effective phase transition process. It is found that, paraffin wax with a melting point of 48 °C has the best performance, while paraffin wax with higher or lower melting point possesses a reduction in productivity.

2.7.4 Performance of PCM Solar Still

Kabeel et al. experimentally studied the improvement of single slope single basin solar still integrated with paraffin wax as PCM (Kabeel and Abdelgaied, 2016a). Solar stills with and without PCM were built with an

effective absorbing area of 0.615 m^2 and 0.72 m^2 respectively. The difference in the area of absorber plate is because of the PCM reservoir. 17.5 kg of paraffin wax with a melting point of $56 \text{ }^\circ\text{C}$ was placed beneath the absorber plate. The solar still with PCM is found 67.18% higher than conventional solar still in terms of productivity. Figure 2.6 illustrates the schematic diagrams of the conventional solar still and PCM solar still (Kabeel and Abdelgaied, 2016b).

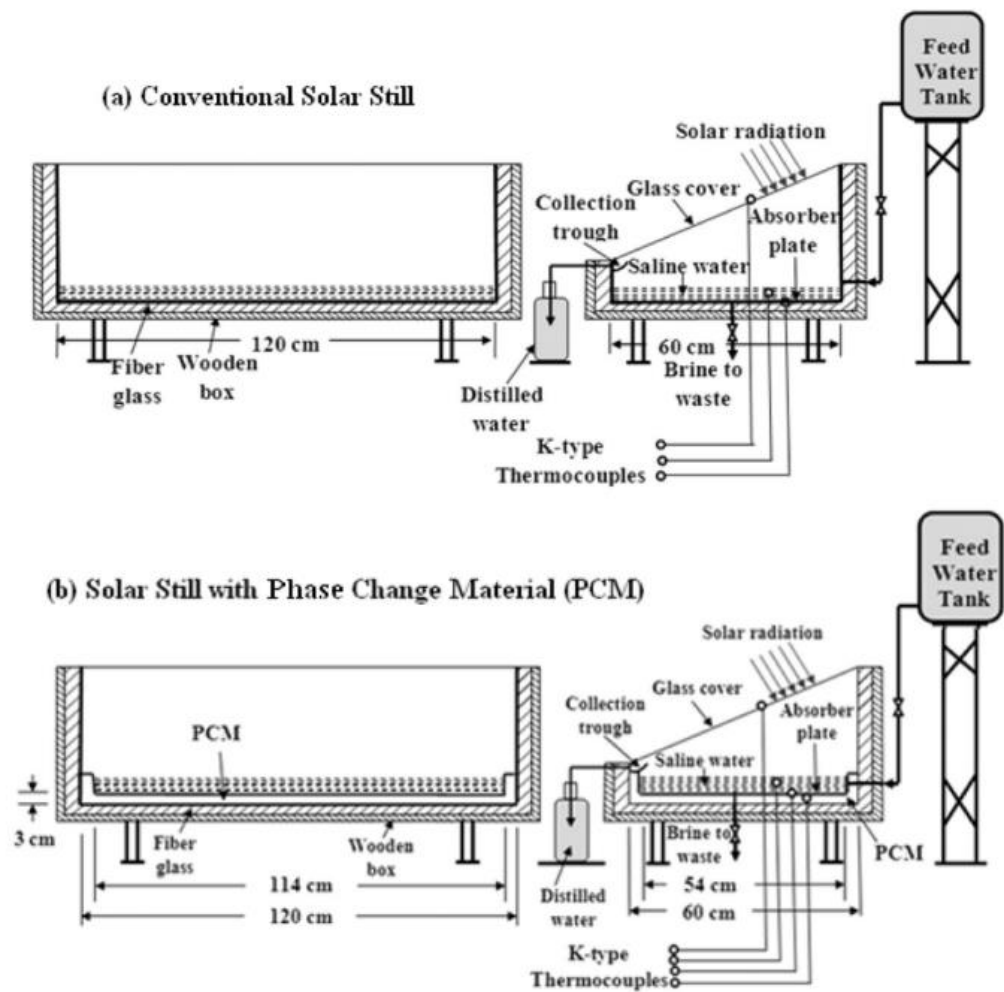


Figure 2.6 : schematic diagram of the conventional solar still and PCM solar still (A.E. Kabeel and Abdelgaied, 2016)

Kabeel et al. (2017) also analysed the productivity of pyramid solar still integrated with PCM and C-corrugated solar absorber. A conventional pyramid was used for comparison. The modified solar still has a corrugated v-trough plate

placed on the basin functioned as the solar absorber. A layer of PCM was placed between the absorber plate and basin. The PCM used has a melting point of 56 °C. The water yield of the conventional pyramid still and modified pyramid still are 3.5 L/m² day and 6.6 L/m² day, respectively, which the modified still has 87.4% improvement in water productivity.

2.8 Summary

This project aims to fabricate a portable and small scale solar still with least maintenance-intensive solar still to serve the community in arid and rural regions. Such considerations were concerned while conducting literature reviews.

Direct thermal desalination was preferred over indirect solar thermal desalination for it fulfilled the requirement of less complicated design. Indirect solar thermal desalination was not cost effective for small scale desalination. Single effect double slope single basin passive solar still was chosen as the origin for prototypes.

The variables affecting the performance of solar still were investigated. In order to obtain great solar still performance, basin type solar still must be designed with a larger surface area with lower height to provide larger free surface area and less water depth for feed water. Moreover, the slope angle of the solar still is better closed to the latitude of the experiment location to obtain the highest transmittance of sunlight. Approaches must be made to lower down

the temperature of the cover in order to obtain huge temperature gap between feed water and cover. Such arrangements aimed to enhance the evaporation rate and condensation rate of the feed water.

Point focus Fresnel lens was chosen to be used as the solar collector of the solar still. FRL is a novel refractive based solar collector that is capable to be used as an alternative of reflective based CSP for its outstanding optical efficiency and low cost. However, research related to the performance of FRL on passive solar desalination is yet published. Thus, the result obtained in this study could contribute to the research gap.

Organic PCM paraffin wax was chosen to be used as the TES for the solar stills for its high thermal storage capacities contributed by its sensible and latent heat storage. The PCM was expected to prolong the desalination process of the solar still. Studies have shown that PCM provides positive effect on solar still. However, no research has been done on combining PCM and with concentrated solar power in passive solar still.

CHAPTER 3

RESEARCH METHODOLOGY

3.1 Introduction

In this section, the design of the solar stills, the preliminary test, and the experimental procedures are discussed. In this study, two prototypes namely **Model A** and **Model B** have been used to carry out the experiments with four different configurations as listed in Table 3.1. Model A was firstly designed and fabricated by performing preliminary tests. Model B with a similar design but with a smaller size was constructed based on the preliminary results obtained. Figure 3.1 illustrates the overall flow chart of the research.

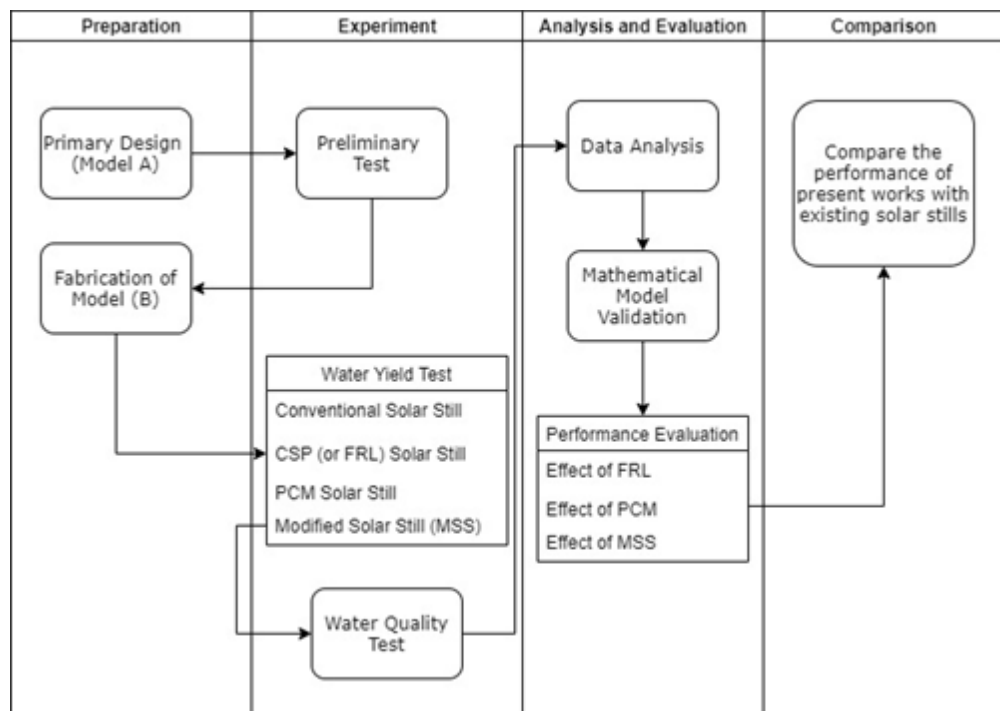
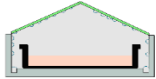
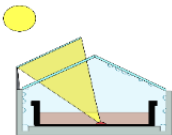
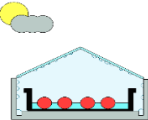
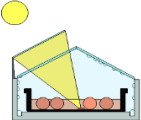


Figure 3.1: Overall flow chart of the research

Such configuration aims to understand and identify the effects of Fresnel Lens (FRL) and Paraffin Wax (PCM) towards the efficiency and performance of the passive solar still. The reason of utilizing two prototypes with similar design but different aspect ratios is to obtain a consistent and repeatable result.

Table 3.1: Solar Still Configurations

Experimental Setup	Details
<p data-bbox="391 696 740 730">Conventional Solar Still</p> 	<p data-bbox="762 696 1390 808">Double Slope Single Basin Passive Solar Still without any approach or modification.</p>
<p data-bbox="391 931 592 965">FRL Solar Still</p> 	<p data-bbox="762 931 1390 1189">Double Slope Single Basin Passive Solar Still associated with Fresnel Lens only. The Fresnel Lens concentrates the solar radiation on the basin to heat up the water rapidly.</p>
<p data-bbox="391 1225 600 1258">PCM Solar Still</p> 	<p data-bbox="762 1225 1390 1482">Double Slope Single Basin Passive Solar Still with PCM tubes inside the basin. PCM acted as thermal storage and alternate thermal source under different circumstances.</p>
<p data-bbox="391 1518 651 1552">Modified Solar Still</p> 	<p data-bbox="762 1518 1390 1630">Double Slope Single Basin Passive Solar Still with the combined effect of FRL and PCM.</p>

3.2 Design of the Solar Still

The study aims to construct a solar still that is viable in the rural region while at the same time study the performance of FRL and PCM. The solar still was expected to have low cost, simple design and portable. Thus, direct passive solar still is the ideal choice for the research.

Single effect double slope basin type solar still is chosen as the experimental prototype for the research. The solar still has a simple working mechanism that makes it highly adaptive to both FRL and PCM. Moreover, basin type solar still has relatively lesser variables affecting its performance. This makes the effect of FRL and PCM more significant when coupled with the solar still. At the same time, the solar still should also have strong durability so that least maintenance is required.

Figure 3.2 demonstrates the CAD design of the solar still. The solar still consists of 3 major parts, which is the roof structure, basin, and the outer base. The roof structure was made with aluminium bars as the supporting frame. Two transparent acrylic sheets were attached on the slopes with the aids of silicone glue. Other sides of the roof were covered with the smaller acrylic board as well. The gaps between components were sealed to make sure it is airtight so that the leakage of water vapour from the solar still to ambient can be minimised during the desalination process. Two-point Fresnel Lens was mounted above the slope with aluminium bars as shown in Figure 3.2. The focal point of the Fresnel Lens was subjected on the basin and thus heat up the saline water in it.

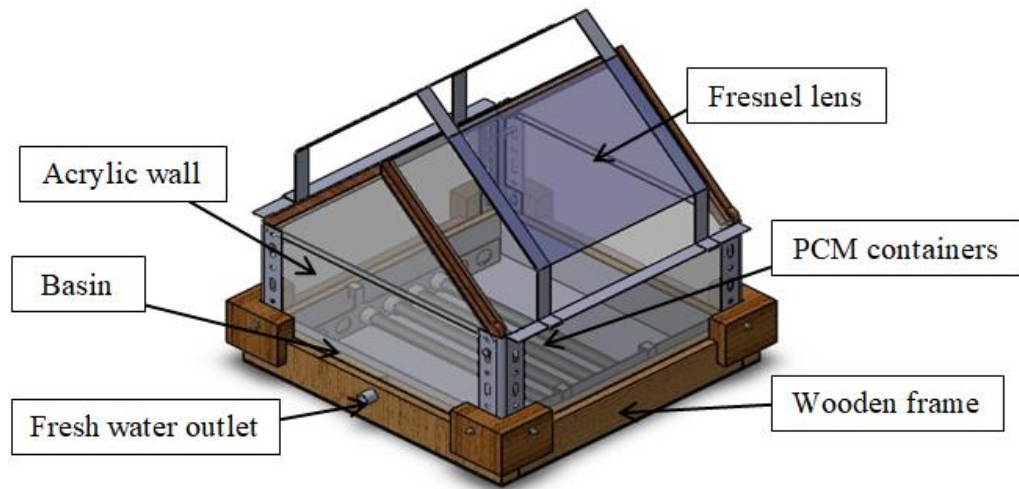


Figure 3.2: CAD drawing of double slope single basin solar still

A black-painted stainless steel basin was used as the solar receiver while holding the saline water at the same time. The outer layer of the base is made of wood, while the inner layer is covered with polystyrene to enhance the thermal insulation. As the solar still constantly receives the heat energy from solar radiation, saline water in the basin will evaporate. Water vapour would condense on the cooler surface beneath the acrylic cover and drip down eventually. Drainage made of PVC pipes were installed at the bottom edge of the acrylic wall to collect the condensates. An outlet connecting all the pipes will channel the condensates collected into a detachable bottle. The desalination process is illustrated in Figure 3.3.

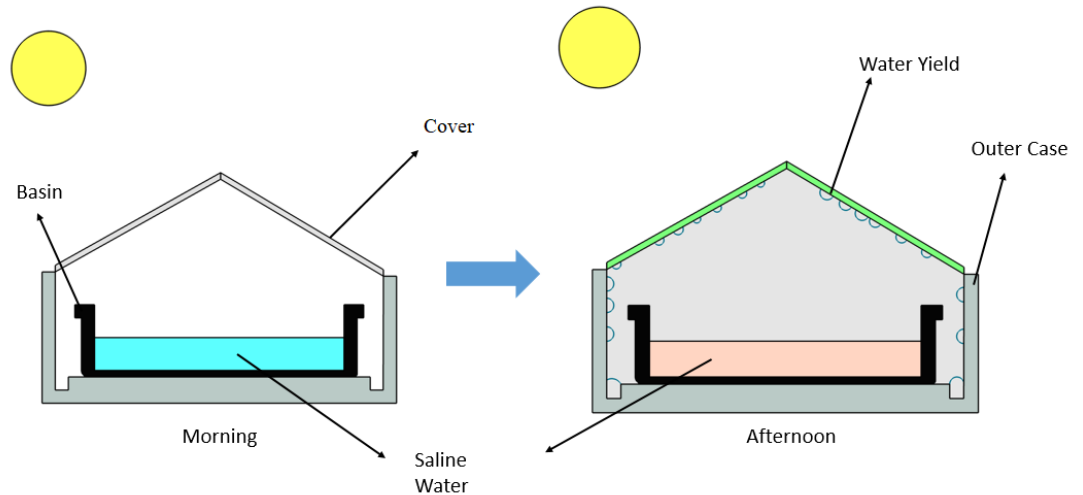


Figure 3.3: Desalination process

A crucial factor in designing slope solar still is the slope angle of the transparent cover. The slope angle of passive solar still decides the solar power received by the absorber (Loss due to reflectivity of the slope). Theoretically, the reflectivity of the slope would be minimal when the solar ray is perpendicular to the slope (Belessiotis et al., 2016).

The research was conducted in Universiti Tunku Abdul Rahman (UTAR) Sungai Long Campus, Kuala Lumpur from April 2019 to September 2019. The elevation angle of the sun was examined to identify the best slope angle for the transparent condensing cover of the still. Figure 3.4 shows the solar path diagram and the specific elevation angle of the sun in a day at Kuala Lumpur. Solar flux is at its strongest magnitude within 10 a.m. to 2 p.m. Within that time, the elevation angle of the sun ranged from 55° to 60° . Thus, the slope of the prototype was made 30° from the horizontal, which the solar ray could pass through the slope perpendicularly. Figure 3.5 shows the schematic drawing of the slope angle of the prototype.

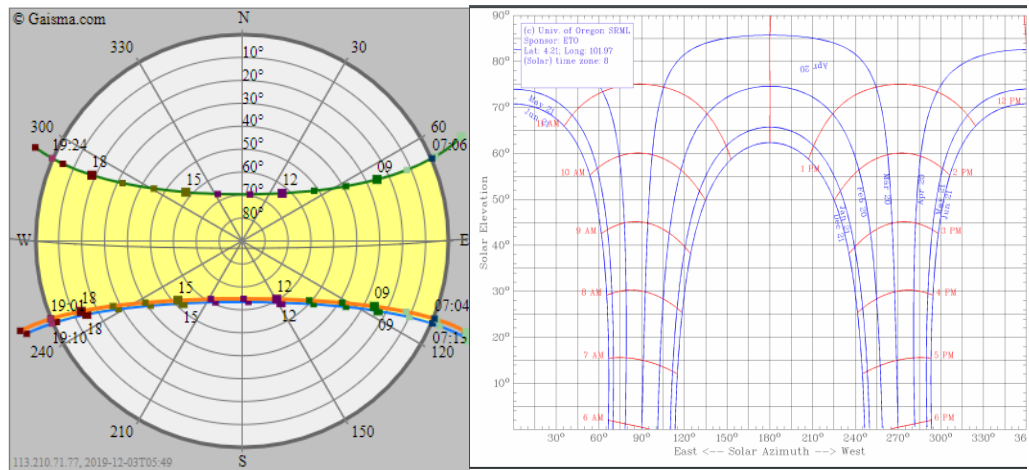


Figure 3.4: Solar Path Diagram and Sun Chart

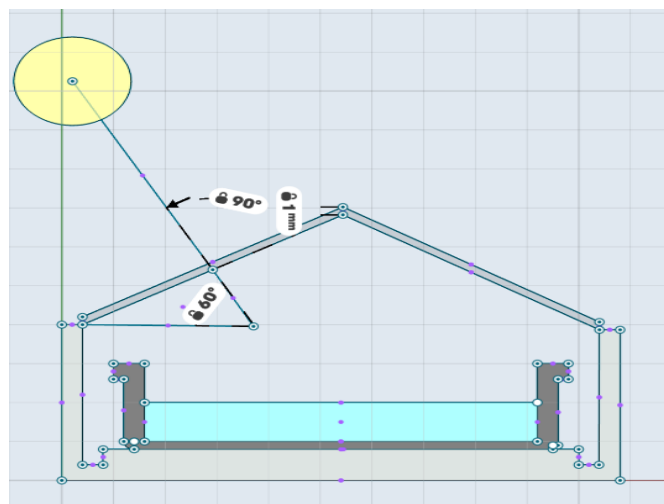


Figure 3.5: Schematic Drawing of the slope angle of the prototype

A prototype (Model A) was constructed based on the design considerations mentioned earlier, which are simple mechanism, least maintenance and highly adaptive to enhancement features. The present design of the prototype still poses the limitation of inefficient and low productivity as it does not undergo any modification yet. Moreover, leakage and small degree of thermal deformation were expected for the very first prototype. Figure 3.6 shows

the photograph of prototype setup for the preliminary test. Temperature range of the experimental location together with PCM performance test was carried out with the prototype, while the results were used to improve the design of the solar stills.

A prototype (Model A) was constructed based on the design considerations mentioned early. Figure 3.6 shows the photograph of prototype setup for the preliminary test. Temperature range of the experimental location together with PCM performance test was carried out with the prototype, while the results were used to improve the design of the solar stills.

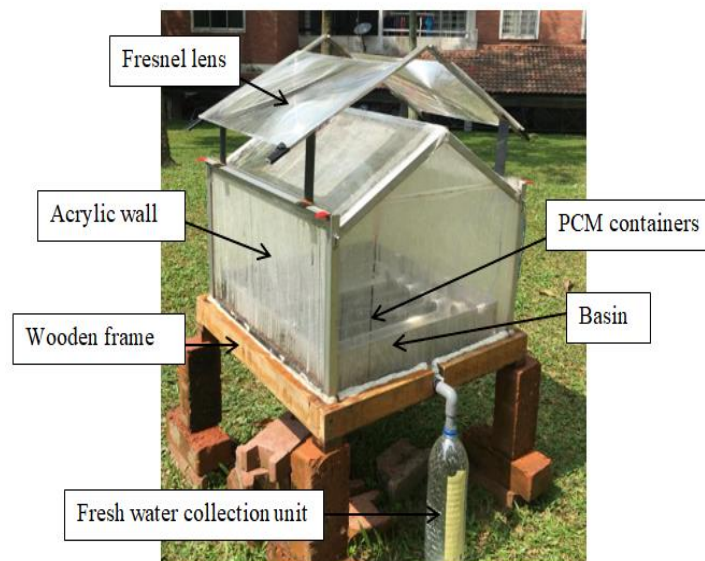


Figure 3.6: Photograph of prototype solar still for preliminary test

3.3 Preliminary Test

In order to aid the construction of the solar stills, certain conditions must first be discovered.

3.3.1 Temperature Range Test

PCM is mainly used to store thermal energy as sensible heat and latent heat. To utilise the latent heat storage, the temperature of the feed water must reach beyond the melting point of PCM under natural condition (with and without FRL). The prototype Model A was filled with 1200 mL of saline water with a salinity of 35000 ppm. The prototype was later placed under the sun to identify the highest water temperature it could reach. From Figure 3.7, it can be noticed that without FRL, the temperature of the saline water falls within 40 °C to 55 °C for most of the time. While in Figure 3.8, it shows that the temperature of the saline water in prototype with FRL is ranged between 50 °C to 60 °C. Knowing this, the melting point of the PCM to be used should not exceed 60 °C.

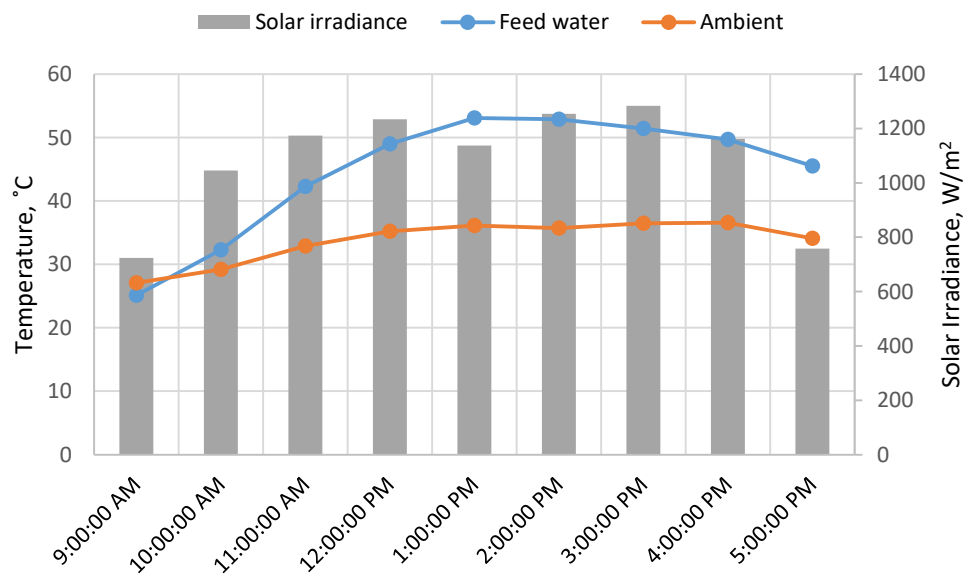


Figure 3.7: Temperature Range of Model A (Without FRL)

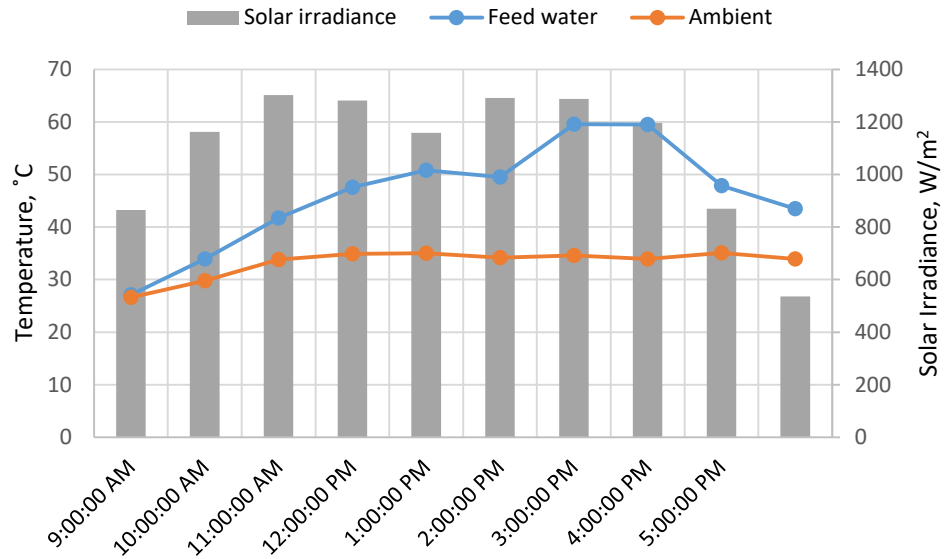


Figure 3.8: Temperature Range of Model A (With FRL)

3.3.2 PCM Selection

It must be pointed out that, the melting point of PCM does not need to be close to the boiling point of saline water. The purpose of the PCM is to discharge energy in the form of sensible and latent heat to stabilize the temperature of the saline water to prolong the desalination process. The PCM used in the study was sealed into 4 aluminium tubes as illustrated in Figure 3.9. The aluminium tubes designed has the length of 48.7 cm and diameter of 1.27 cm.

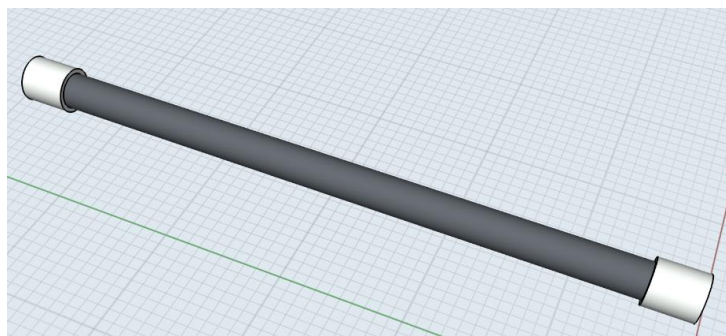


Figure 3.9: PCM tubes CAD drawing

According to the finding of previous research conducted, with same solar still setup, petroleum Jelly (paraffin wax with a low melting point) with a melting point of 37 °C mixed with aluminium scraps has the highest enhancement compared with paraffin wax with a melting point of 58 °C (Bahar et al., 2019). Figures 3.10, 3.11, 3.12, and 3.13 show the performance of the PCM associated solar still. It can be observed that the temperature of the saline water drops as the solar irradiation decreased in the afternoon. The solar still associated with PCM has its saline water temperature reduced in a relatively smoother trend, as compared to the solar still without the PCM. As solar irradiation begins to drop, the water temperature will eventually become lower than the temperature of PCM. PCM will discharge its heat energy back to the saline water, therefore acted as an alternative heat source to maintain the saline water at a higher temperature for a certain amount of time. The discharge can be observed in Figures 3.11, 3.12 and 3.13 at around 2 pm to 3 pm.

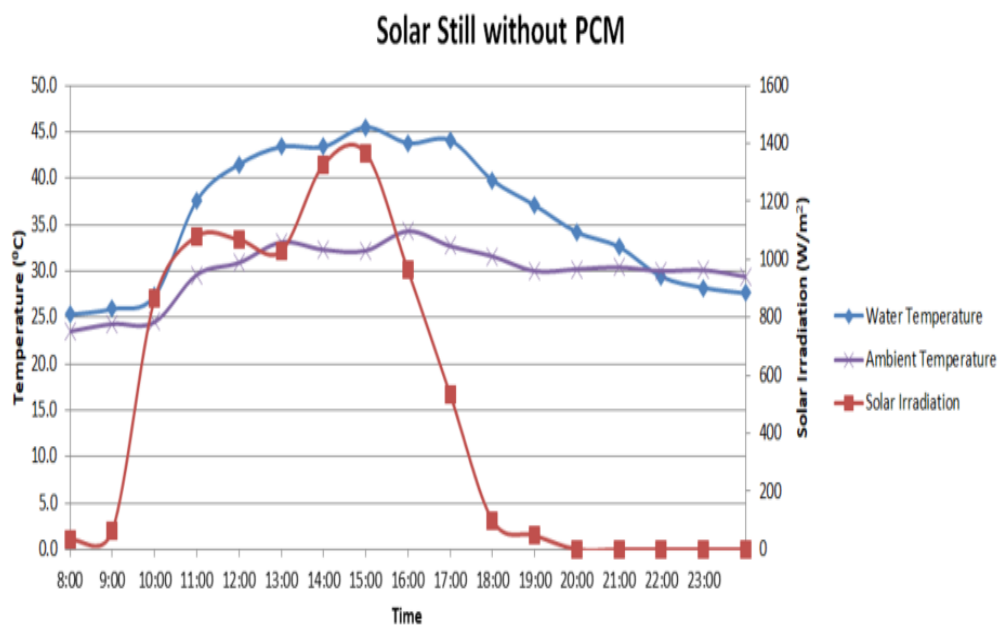


Figure 3.10: Temperature trend of Solar Still without PCM (Bahar et al., 2019)

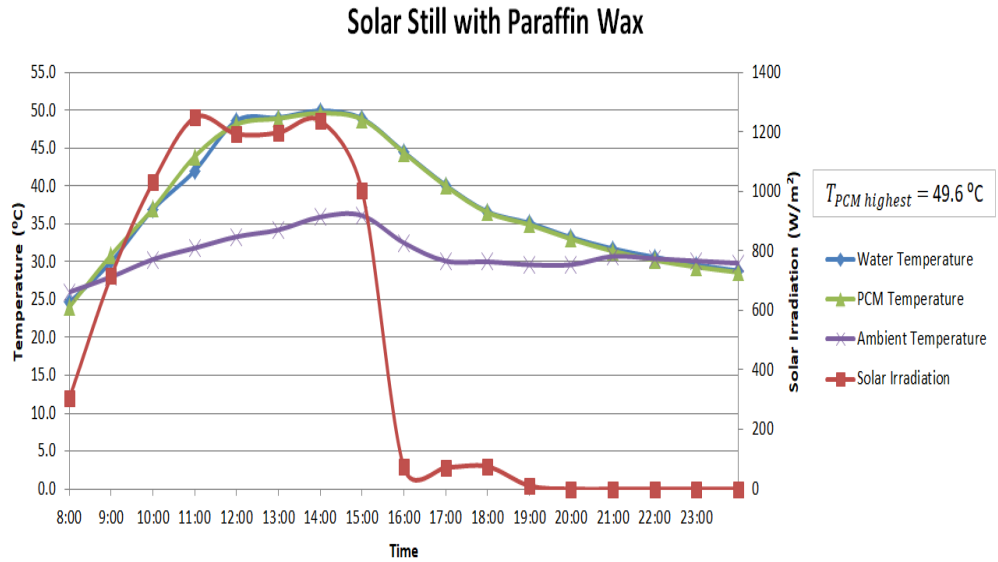


Figure 3.11: Temperature trend of Solar Still with Paraffin Wax (Bahar et al., 2019)

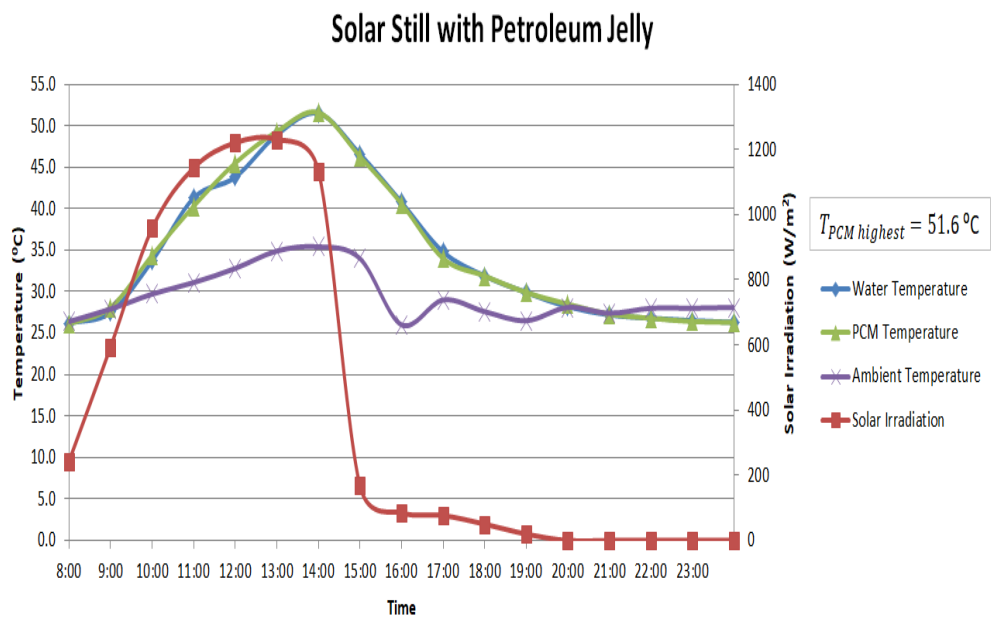


Figure 3.12: Temperature trend of Solar Still with Petroleum Jelly (Bahar et al., 2019)

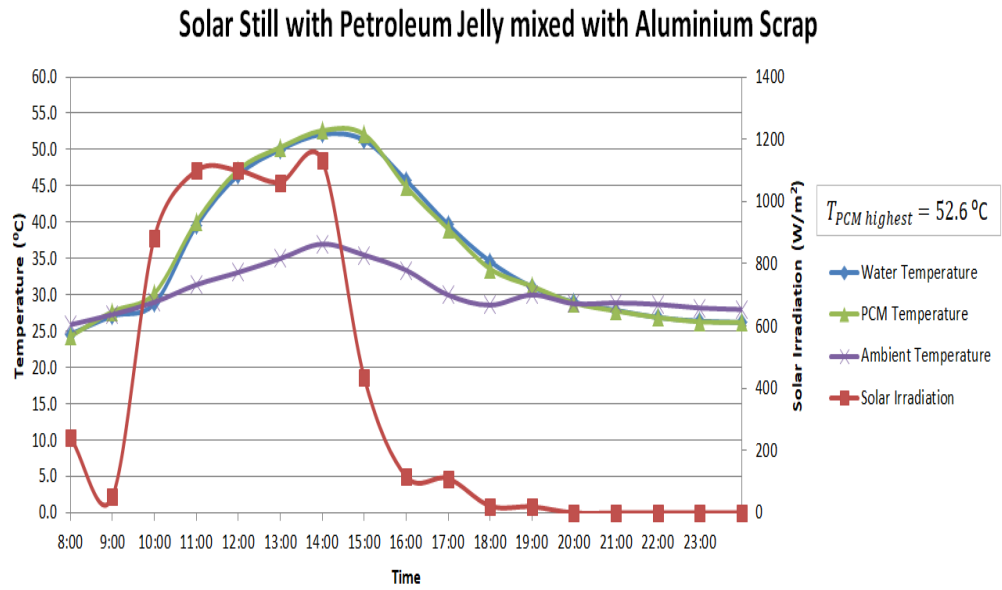
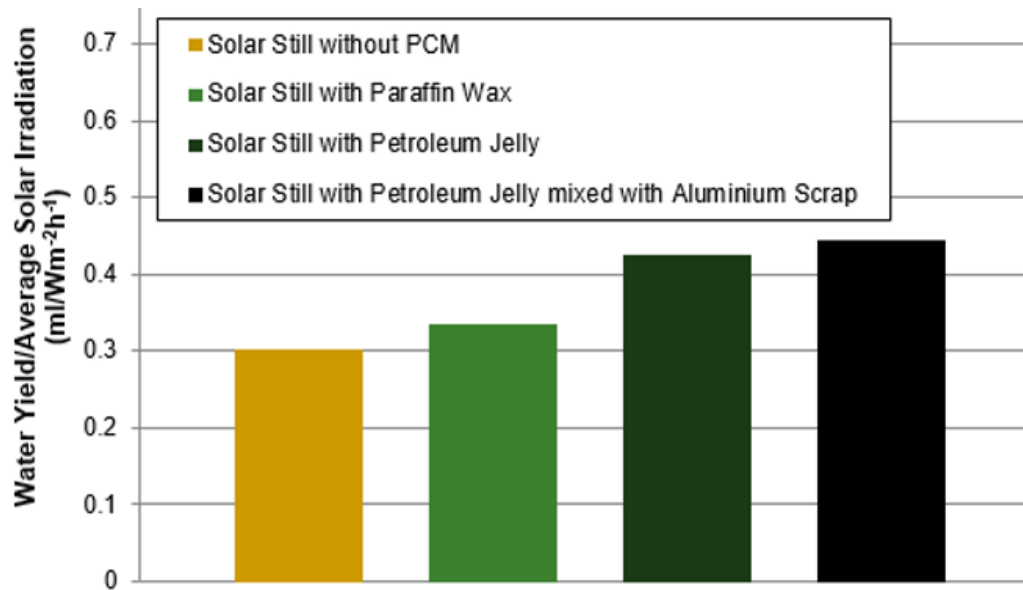


Figure 3.13: Temperature trend of Solar Still with Petroleum Jelly with Scraps (Bahar et al., 2019)

The paraffin wax used in the experiment has the melting point of 58 °C, while petroleum jelly has the melting point of 37 °C. Based on the result, petroleum jelly with lower melting points could carry out phase transition completely without taking too much thermal energy from the saline water. At the same time, the use of scrap metal increases the overall heat transfer coefficient, improving the rate of discharge. In term of water yield per average solar irradiation, Figures 3.14 shows that the solar still associated with petroleum jelly has the highest increment of 47.9%. Therefore, petroleum jelly mixed with scrap is relatively more appropriate and thus was used as the PCM in this study. Figure 3.15 illustrates the actual PCM used in the study.



Figures 3.14: Water Yield per average solar irradiation (Bahar et al., 2019)

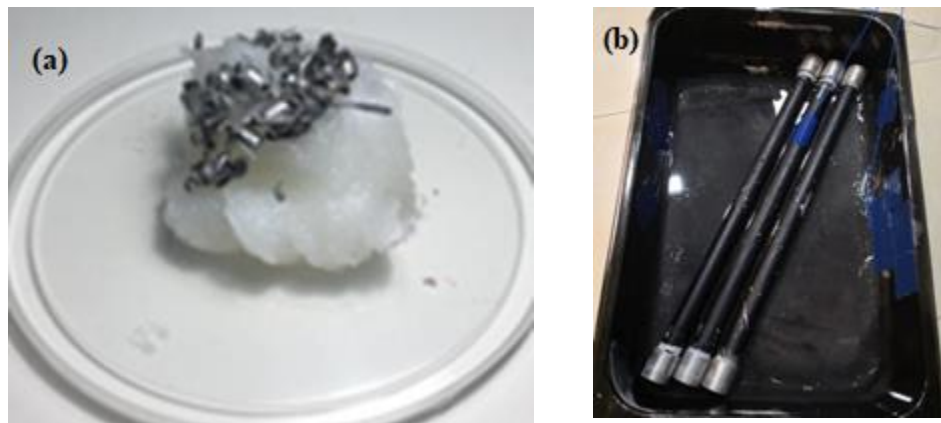


Figure 3.15: (a) Petroleum Jelly (b) PCM tubes

3.4 Experimental Procedures

Two new prototypes, Model A and Model B passive double slope single basin solar still were designed and constructed. A FRL (400 x 300-mm) was used to incorporate with the solar stills. The details of the solar stills were listed in Table 3.2. The parameters of FRL and PCM used were listed in Table 3.3. An

adjustable holder was designed and fabricated to hold the FRL above its focal distance (600mm) to ensure that the focal point can stay on the basin. The glazing material of the slope in both solar still was replaced with glass instead of acrylic. Acrylic is found inappropriate as it cannot withstand the high heat contributed by the FRL. Figure 3.16 shows the deformation of the acrylic cover during the experiment.

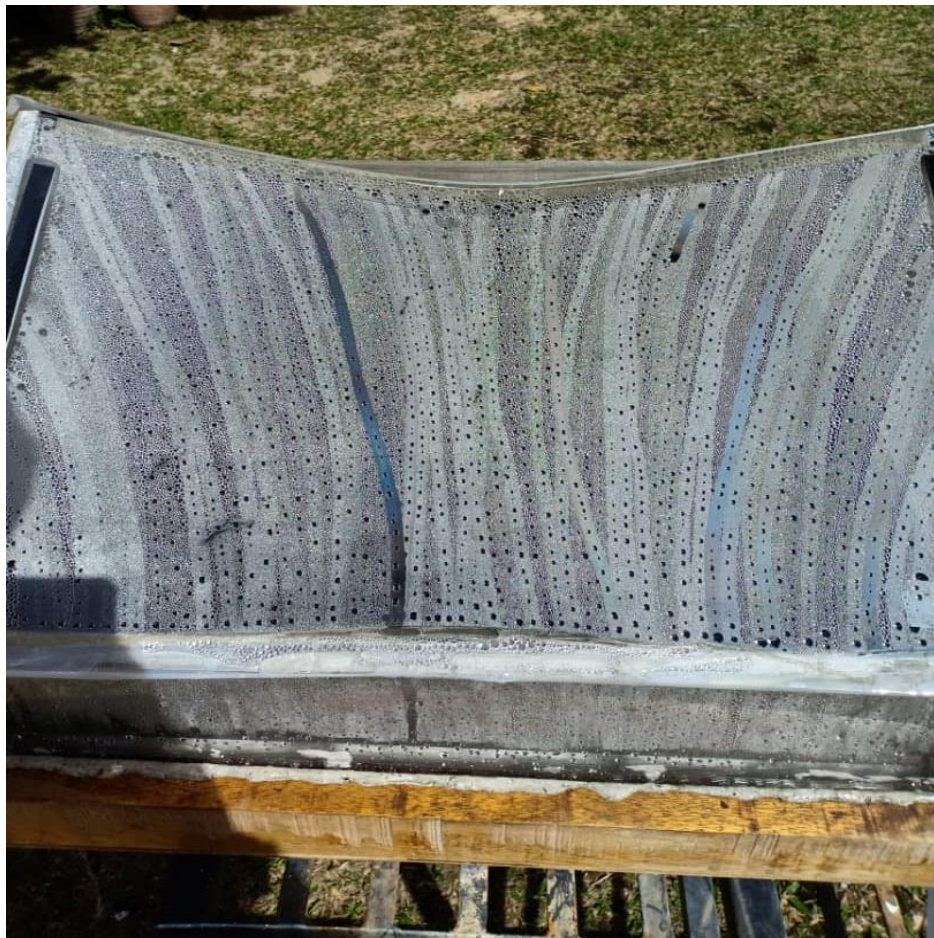


Figure 3.16: Deformation of the acrylic board

The experimental study was carried out from April 2019 to September 2019. The solar stills were tested at Sungai Long, Malaysia, from 9 a.m. to 5 p.m. (8 hours). Figure 3.17 shows the photograph of the solar stills. Model A was

designed based on the conventional double sloped solar still, while Model B was the enhanced version of Model A. Both models are passive solar stills and hence only utilised direct solar energy conversion. The basin of both solar stills was painted black to increase solar irradiance absorption. The yields were collected in the form of batch operation (Belessiotis et al., 2016).



Model A



Model B

Figure 3.17: Photograph of the solar stills

Table 3.2: Parameter of Solar Stills

	Solar Still			Basin					
	Length (m)	Width (m)	Height (m)	Length (m)	Width (m)	Height (m)	Slope Angle	Glazing Material	Insulation
Model A	0.6	0.6	0.61	0.5	0.5	0.1	30°	Glass	Polystyrene
Model B	0.55	0.4	0.5	0.45	0.3	0.1	30°	Glass	Polystyrene

Table 3.3: Properties of PCM and FRL

Thermal Properties	Petroleum Jelly	Properties	Point FRL
Melting Point	38°C	Material	Acrylic
Heat Capacity	2.0 kJ/kg K	Dimension (mm)	400*300
Density	849.9 kg/m ³	Thickness (mm)	2
Latent heat	220 kJ/kg	Focal Distance (mm)	600

**Retrieved from Take It Global Sdn Bhd, Cameo Chemical, and Shenzhen Meiying Optics Co., Ltd.*

The experiments were conducted following the procedure listed below.

Figure 3.18 shows a flow chart of the experiment routine on each setup. The instruments used are listed in Table 3.4.

1. Basin filled with 1200 mL of saline water (35g of sea salt mixed with every 1000 mL of tap water) was placed into the solar still.
2. Thermocouple sensors were attached on PCM tubes and the inner surface of the glass cover. Another thermocouple was immersed in the saline water. The temperature of the desalination system was measured with 30 minutes interval.
3. The glass cover was closed to seal the desalination system.
4. The configured setup was placed outdoor. Natural sunlight was used in the experiment. The solar irradiance subjected on the solar still was measured on 30 minutes interval with a solar power meter.
5. The setup was monitored throughout the experiment. The water yield was collected in a container fastened to the outlet of the solar still.

6. The experiment was conducted and repeated from 9 a.m. to 5 p.m. on each configuration.

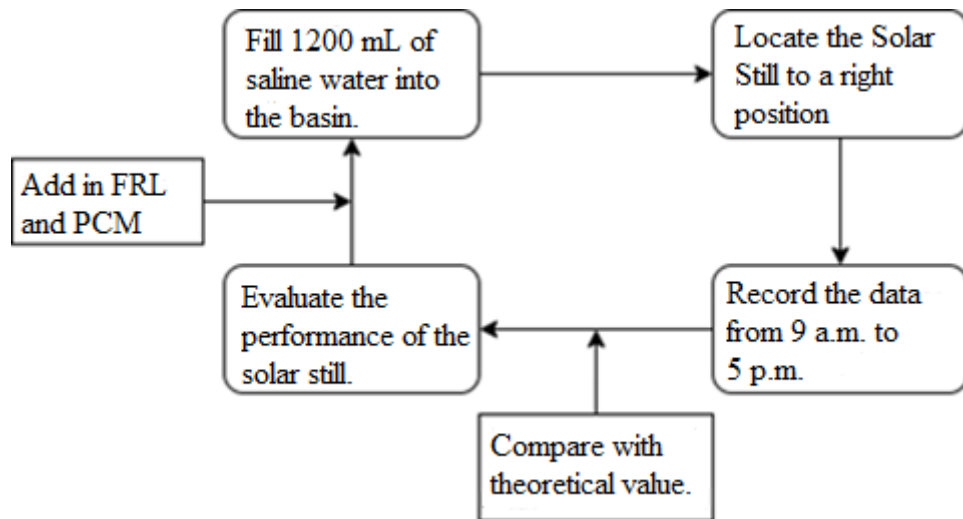


Figure 3.18: Flow chart of the experiment routine

Table 3.4: Instruments for different measurement

Instrument	Resolution	Error Range	Recorded Parameter
Digital 4 Channel K-type Thermocouple	0.1°C	0.2°C	-Temperature of Cover -Temperature of Feed Water -Temperature of PCM -Ambient Temperature
SM206 Digital Solar Power Meter	0.1 W/m ²	10 W/m ²	Solar Irradiance
Digital Weight Scale	0.1g	0.2g	Water Yield
FIXON9657 Digital TDS EC Meter	0-9999ppm	+/-2%	Total Dissolved Solid (TDS)

It should be noticed that conducting the above experiments on different days will not affect the purpose of the experiment (Abujazar, et al., 2018). The experiments were conducted on different days with similar weather criteria. The small deviation in the input will not bring a strong impact on the result (Abujazar, et al., 2018). Both Solar stills are double sloped single basin but with different aspect ratio. Model A is slightly bigger than Model B. The validity of the effect of FRL can be verified when both solar stills show similar trends in term of performance and efficiency. The difference in the performance between the solar stills could contribute to future numerical analysis in the aspect of different parameters.

3.5 Theoretical Calculation

The ultimate goal of the performance evaluation is the productivity and efficiency of the still. Both parameters are capable to showcase the performance of the solar stills under certain constraints. It is possible to calculate the productivity and efficiency of the solar stills by utilizing a mathematical model with the temperature of the glass lid and saline water as input. The result recorded from the experiment is used to validate the theoretical results obtained from Equation (3.1) to Equation (3.13). Theoretically, the thermal energy being used in the evaporation should have a direct influence with the total yield, and thus the productivity. Therefore, from equation 3.2 and 3.3, the temperature gap between the glass lid (condensation surface) and feed water would bring large impact to the water yield. Figure 3.19 shows the schematic diagram of the solar desalination system with the elements being used in the mathematical modelling.

Assumption:

- Solar still is vapour leakage proof
- No heat loss from the basin to the surrounding

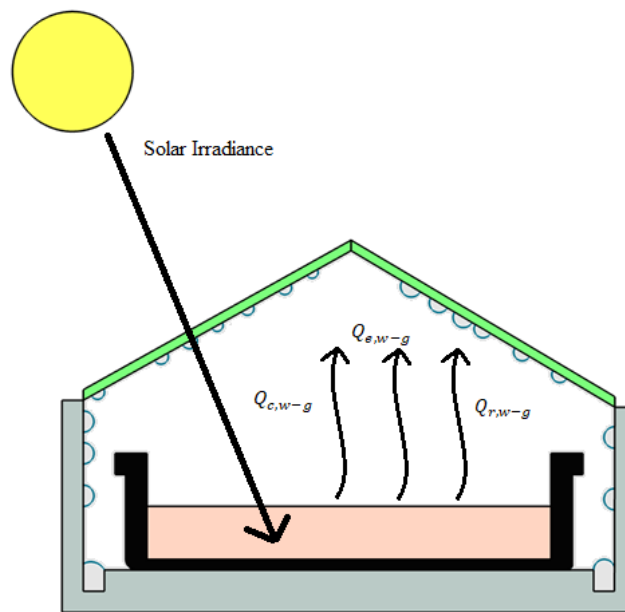


Figure 3.19: Schematic of the modelling element

The average temperature for water and glass was calculated by using the measured temperature values from previous to the current time period.

$$T = \frac{(T_{n+1} + T_n)}{2} \quad (3.1)$$

Convective heat transfer from saline water to glass lid can be calculated with the equation below (Kabeel et al., 2012; Abujazar, S. Fatihah, et al., 2018),

$$Q_{c,w-g} = 0.884 \left[(T_w - T_g) + \frac{p_w - p_g}{268.9 \times 10^3 - p_w} T_w \right]^{\frac{1}{3}} (T_w - T_g) \quad (3.2)$$

Evaporative heat transfer from saline water to glass lid can be calculated using (Abujazar, S. Fatihah, et al., 2018; Kabeel et al., 2012),

$$Q_{e,w-g} = (16.276 \times 10^{-3}) \frac{p_w - p_g}{T_w - T_g} Q_{c,w-g} \quad (3.3)$$

Water Saturation Pressure above water surface and below glass lid (Alduchov et al., 1996),

$$p_w = 614.17 e^{\frac{17.625T_w}{T_w + 243.04}} \quad (3.4)$$

$$p_g = 610.94 e^{\frac{17.625T_g}{T_g + 243.04}} \quad (3.5)$$

Water Saturation Pressure above saline water surface (Nayar et al., 2016),

$$\ln \left(\frac{p_{sw}}{p_w} \right) = -4.58180 \times 10^{-4} S - 2.04430 \times 10^{-6} S^2 \quad (3.6)$$

Mass of Yield (Badusha and Arjunan, 2013; Abujazar, Suja Fatimah, et al., 2018),

$$m_{yield} = \frac{Q_{e,w-g} \times A_w \times \Delta t}{h_{fg,sw}} \quad (3.7)$$

Latent heat of vaporization of water and saline water can be estimated by using the equation (Henderson-Sellers, 1984)(Sharqawy et al., 2010),

$$h_{fg,w} = 2500 - 2.386T \quad (3.8)$$

$$h_{fg,sw} = h_{fg,w} \times \left(1 - \frac{S}{1000}\right) \quad (3.9)$$

Utilising the mathematical model above, the theoretical yield was calculated. The results were compared with the actual yield obtained. To calculate the efficiency of the solar stills, the solar energy received were calculated. As time passes, solar stills constantly receive solar irradiation from different angles. Therefore, the elevation angle of the sun must be known from time to time. Figure 3.19 illustrates the direction of the incident solar radiation towards Model B.

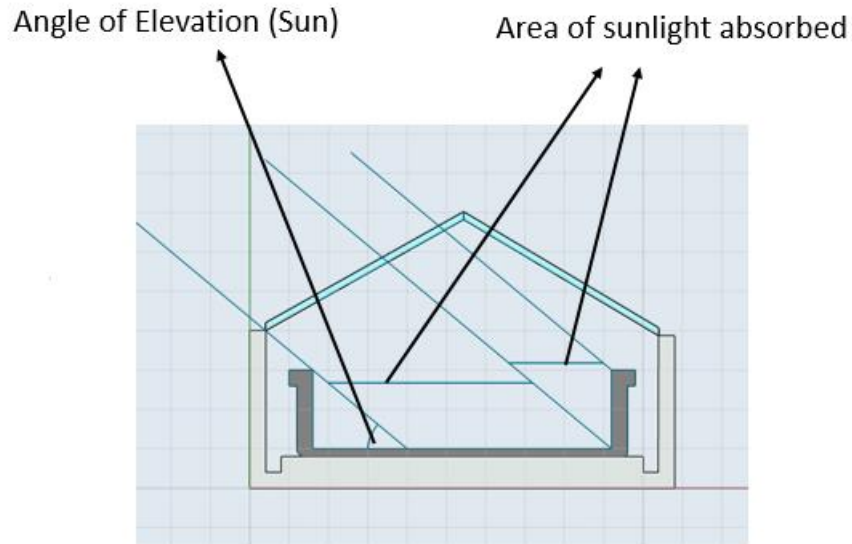


Figure 3.20: Direction of the incident solar radiation towards Model B

The elevation angle used in the calculation were obtained with the aid of the solar path diagram in Figure 3.4. Using Model B as an example, the calculation of the area which solar flux falling on it can be calculated using the example in Appendix B.

The Total Solar Irradiance and Energy absorbed by Solar Still can be calculated by using the equation below.

$$P = I(t)A_{total} \quad (3.10)$$

$$E = P\Delta T \quad (3.11)$$

The productivity and thermal efficiency of solar still can be calculated by dividing the total water yield over the solar energy absorbed throughout the experiment duration. The efficiency of the solar still can be calculated by

dividing the total energy used to evaporate the yield obtained by the total energy received from the sun.

$$Productivity = \frac{\sum m_{yield}}{\sum E} \quad (12)$$

$$Efficiency = \frac{\sum m_{yield} h_{fg,sw}}{\sum E} \quad (13)$$

It is expected that the measurement errors will cause uncertainty in the result. It is important to identify the relationship between the source of errors and the uncertainty to find out the impact of each individual measurement error. Referred to the method of Moffat, uncertainty analysis has been conducted to identify the uncertainty in productivity and efficiency of the solar stills (Moffat, 1988). It is found out that the overall uncertainty is less than 1%. The detailed of the uncertainty analysis is explained in Appendix A.

CHAPTER 4

RESULTS

4.1 Introduction

In this chapter, the experimental results obtained from each experimental setup are tabulated and analysed to identify the performance of the solar still. Conducting identical modifications and experiments on 2 different solar stills provide better understanding on the effect of modification (FRL and PCM) towards passive solar still. Table 4.1 tabulates the configuration of each setup in the experiment.

Table 4.1: Experimental Protocol

Summary of Test		Presence		
Experiments	Model	FRL	PCM	Date
Preliminary Test (Temperature Range)	A	No	No	April 2019
		No	No	
Performance evaluation FRL and PCM (Model A)	A	No	No	July and August 2019
		Yes	No	
		No	Yes	
		Yes	Yes	
Performance evaluation FRL and PCM (Model B)	B	No	No	August 2019
		Yes	No	
		No	Yes	
		Yes	Yes	
Water Volume Effect	B	Yes	No	August 2019
		Yes	Yes	

The experiment data of each setup configuration are presented in three separated graphs. The first graph illustrated the temperature and solar irradiance of the desalination system overtime for Model A, while the second graph illustrated the same set of data for Model B. The water yield of both models was compared in the third graph. Table B-1 to B2-6 in Appendix B are the experimental data used to construct the graphs.

It is to note that, while utilizing renewable energy, it is expected to have an unstable meteorological condition every day. Therefore in this study, productivity and efficiency of the stills are put into the comparison. Comparing water yield alone would not provide a clear image of the impact of FRL and PCM as the experiments were conducted on different days. Productivity and efficiency of the solar still take the amount of solar energy received into account, thus comparing these parameters could provide an accurate result in term of performance on daily basis.

4.2 Conventional Solar Still

Conventional passive solar still relies on the greenhouse effect, which traps heat absorbed from the sun to heat the water slowly, without any other approach to improve the process. In this study, Conventional (A) and (B) refer to the solar still Model A and B without FRL and PCM.

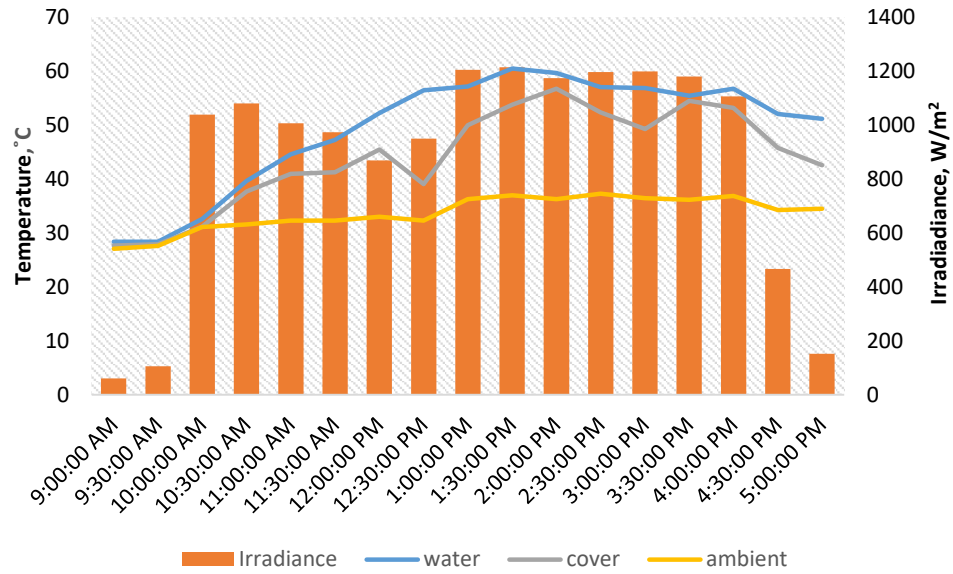


Figure 4.1: Temperature and Solar Irradiance of Conventional Model A

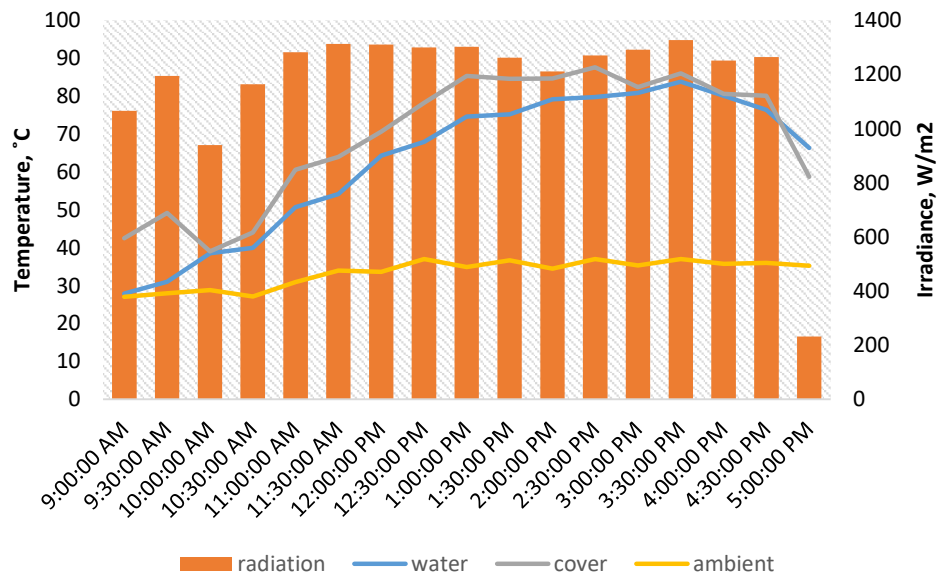


Figure 4.2: Temperature and Solar Irradiance of Conventional Model B

Figure 4.1 and Figure 4.2 show the temperature of saline water, ambient, the surface of the glass and solar irradiance cover against time in Conventional Model A and Model B. The average solar irradiance recorded was 882 W/m² and 1155 W/m² for Model A and Model B respectively. The peak temperature of

Model A and Model B are 60.5 °C and 83.8 °C, respectively. It can be observed that solar irradiance has a direct influence on water temperature as well as the temperature of the glass cover. The temperature of the cover shows significant fluctuation with the solar irradiance. In contrast, the temperature of the saline water is rather stable. This can be explained as the saline water has a higher heat capacity. The experiment was conducted during the cloudy season in Malaysia. The fluctuation of solar irradiance was due to the cloud movement.

Figure 4.3 shows the hourly water yield of the conventional solar still. The effecting working hour of the solar stills starts from 11 am to 4 pm, as the solar irradiance is at its highest around that period of time, resulting in higher hourly water yield. It is also noticed that the larger the gap between the temperature of water and cover, the larger the water yield. At the same time, provided with a constant temperature gap, the higher the water temperature, the higher the water yield at that particular time.

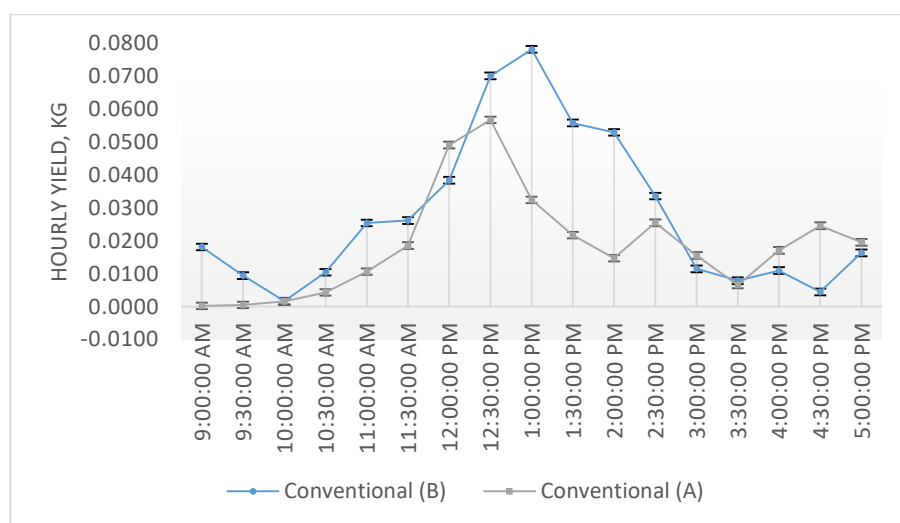


Figure 4.3: Hourly Water Yield of Conventional Still

The productivity and efficiency were calculated using the Equations (3.12) and Equation (3.13) mentioned in Chapter 3. The result obtained is tabulated in Table 4.2. It can be observed that Model B performs better in daily water yield. The productivity of Model B is 160% better than Model A, despite that the difference between water yield from both solar stills was only 62.5%. This is because Model A is a lot larger than Model B, hence receive more solar flux compared to Model B. The total solar energy received by Model A throughout the day was 5194.53 kJ, while the solar energy received by Model B was 3490.92 kJ. The efficiency of Model A and Model B was 12% and 29%, respectively. The productivity and efficiency obtained in conventional Model A and B were used as a reference for other experiments to identify the improvement and effect of the modification.

Table 4.2: Productivity and Efficiency of Conventional Solar Stills

MODEL	Yield, g	Productivity, g/kJ	Efficiency
A	280	0.05	12%
B	455	0.13	29%

4.3 Fresnel Lens Solar Still

Both Model A and Model B were associated with Fresnel lens to study the effect of FRL as CSP toward the productivity of the still. Like other CSP, FRL concentrates the solar flux from a larger area (area of the lens) to a smaller spot (area of aperture). The smaller spot is receiving more solar energy than usual. The FRL used in the experiments was all the same. The FRL was made adjustable. The focal point of the FRL was ensured to fall on the basin

throughout the experiment. Figures 4.4 and 4.5 show the temperature of the desalination system against the time of FRL Model A and Model B throughout the experiment. The average solar irradiance recorded was 1155 W/m² and 882 W/m² for FRL Model A and Model B, respectively.

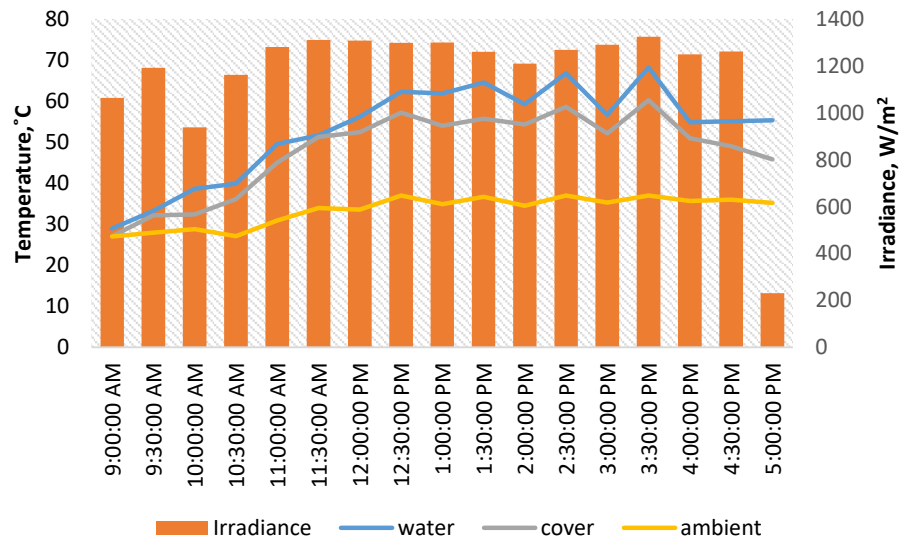


Figure 4.4: Temperature and Solar Irradiance of FRL Model A

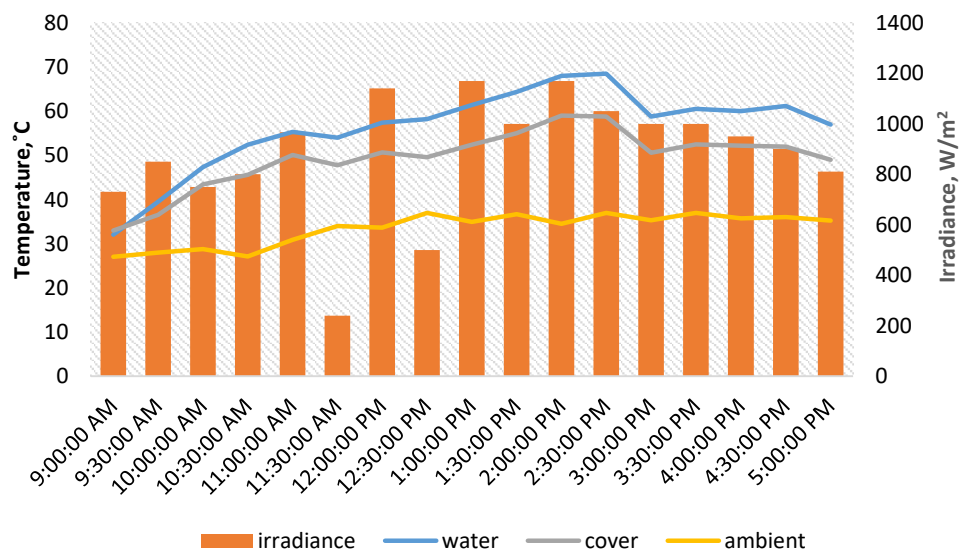


Figure 4.5: Temperature and Solar Irradiance of FRL Model B

From the result in conventional solar still Model A, the water temperature in conventional solar still A reaches its peak at 1.00 p.m. at around 60 °C and stay between 50 °C to 60 °C until 4.30 p.m., where the sun is about to set. While in the case where FRL is presented, the feed water in Model A has its peak temperature recorded at 68.3 °C, while the water temperature stays above 60 °C from 12 p.m. to 4 p.m. However, Model B with FRL shows a drop in water temperature compared to conventional model B. The peak temperature was only 68.5 °C, while most of the time the water temperature is staying at around 60 °C. This is due to the low solar irradiance. On the other hand, it can be observed that the water temperature in both solar stills with FRL presented fluctuate significantly following the solar irradiance of the particular time. This is because of the high irradiance sensitive property of CSP application. When the irradiance drops, the high thermal input of the focal point drop significantly as well, resulted in temperature drop in the desalination system.

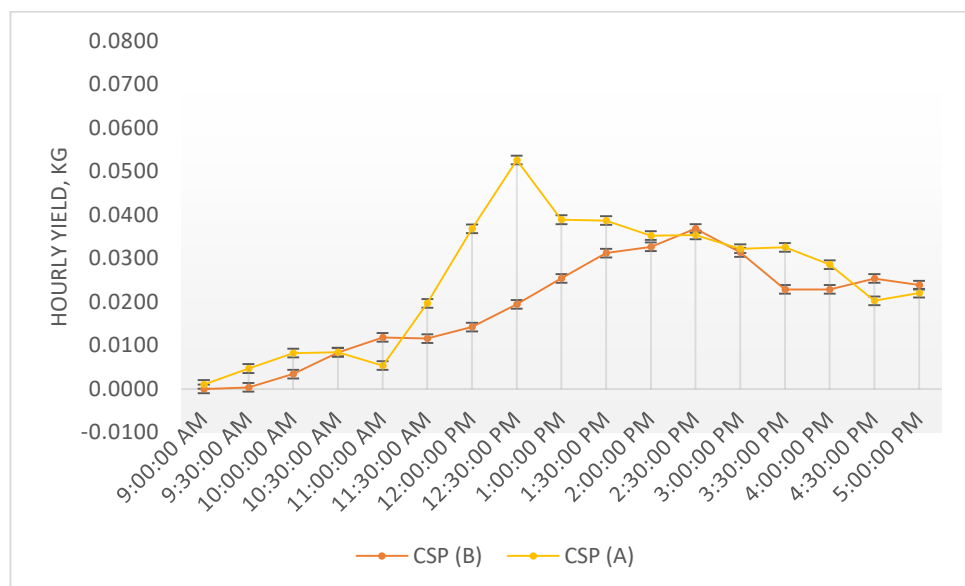


Figure 4.6: Hourly Water Yield of FRL Still

Figure 4.6 shows the hourly water yield of FRL Model A and Model B. It can be observed from Figures 4.4, 4.5 and 4.6, the water temperature is directly proportional to the rate of yield still. The solar energy received by FRL Model A and Model B throughout the experiment was 6464.67 kJ and 2646.22 kJ respectively. Table 4.3 shows the comparison between conventional Model A and Model B with FRL Model A and Model B. It can be concluded that despite the lower overall water temperature, the productivity of the solar still shows improvement as well.

Table 4.3: Productivity and Efficiency under FRL Effect

MODEL	Yield, g		Productivity, g/kJ		Efficiency	
	Conventional	FRL	Conventional	FRL	Conventional	FRL
A	280	505	0.05	0.08	12%	18%
B	455	430	0.13	0.16	29%	37%

4.4 Phase Change Material Solar Still

Similar procedures have been done to study the effect of PCM towards the productivity of Model A and B. Unlike FRL, instead of boosting the rising rate and the peak of water temperature, PCM is expected to stabilize the water temperature, enhancing the water productivity with a different approach. As thermal storage, PCM was mainly used as an alternative heat source. Figure 4.7 and 4.8 show temperature of the desalination system over time throughout the experiment of PCM Model A and Model B. The average solar irradiance recorded was 876 W/m² and 687 W/m² for FRL Model A and Model B respectively.

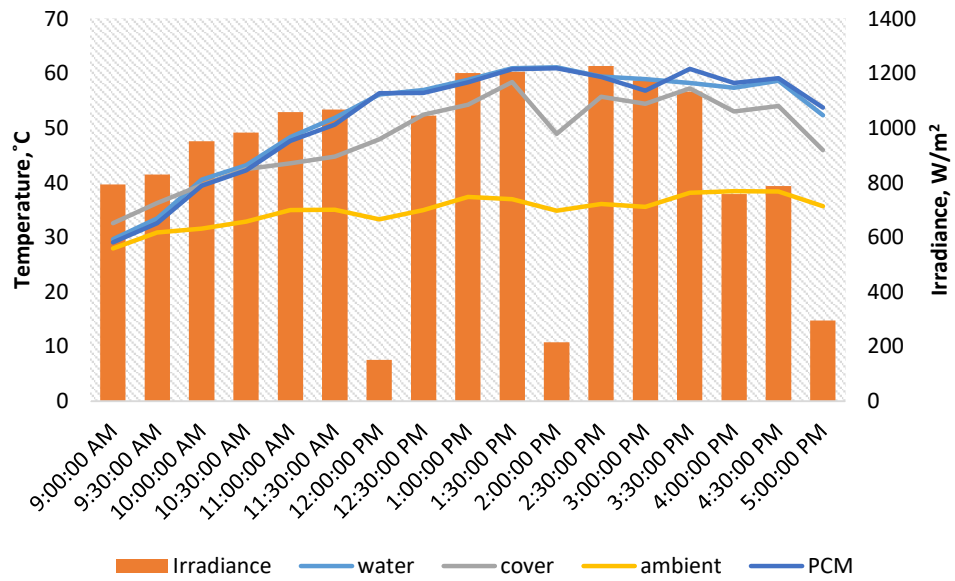


Figure 4.7: Temperature and Solar Irradiance of PCM Model A

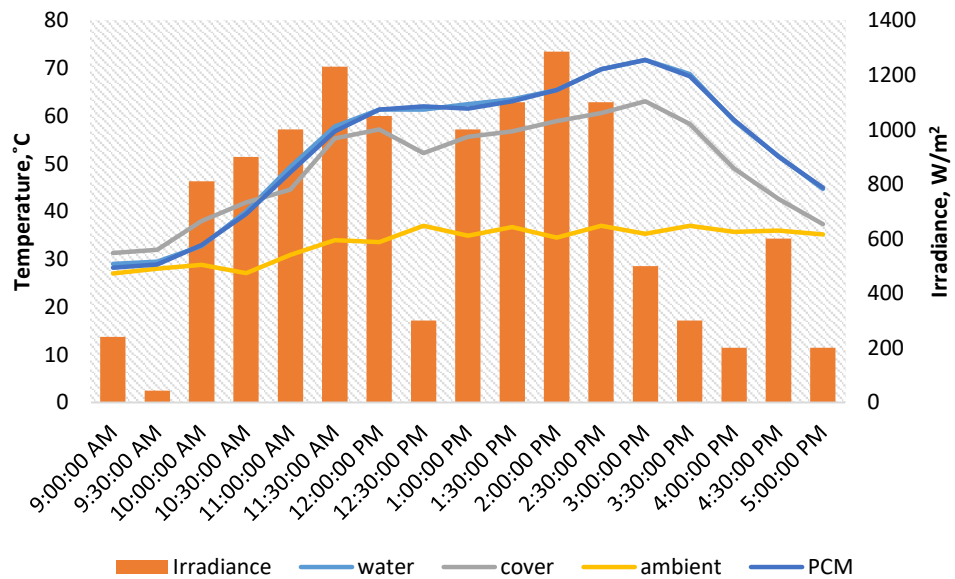


Figure 4.8: Temperature and Solar Irradiance of PCM Model B

It can be observed that the temperature of PCM was initially lower, but very close to the water temperature. This is because the PCM tubes are gradually receiving heat from the surrounding feed water. However, at a point where solar

irradiance is lower, or begin to fall, the temperature of PCM stays higher than water temperature. Compared to FRL solar still, the water temperature of PCM are rather stable. In the experiment of Model A, the water temperature increases gradually from 9 am to 2 pm, without much changes in the temperature trend. The effect of PCM can be observed at 12 pm, 2 pm, and 3.30 pm, where the temperature of PCM is higher than the feed water. A similar effect has been observed in the experiment of PCM Model B. The feed water temperature trend is rather stable compared to CSP model B. The effect of PCM can be observed at 12.30 pm, and 3.00 pm, where the solar irradiance dropped due to various reason. Figure 4.9 shows the hourly yield of PCM Model A and PCM Model B.

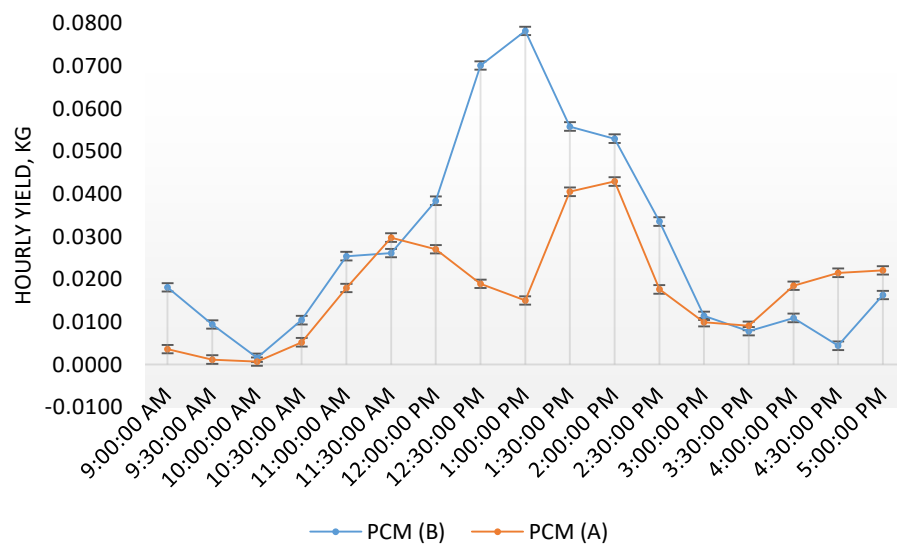


Figure 4.9: Hourly Water Yield of conventional and PCM Stills

The paraffin wax used has a relatively higher specific heat capacity than water. When thermal input is absent, it is capable to maintain its high temperature at a rate longer than feed water. As the solar irradiance decreases after the peak hours, the PCM began to discharge its energy in the form of

sensible heat, acting as an alternative thermal source to the feed water. This will reduce the fluctuation of water temperature and prolong the temperature drop of the feed water, up until the thermal energy stored in PCM are fully discharged. However, no remarkable effect has been observed throughout the experiment. Table 4.4 shows that the enhancement of PCM solar still does not seem significant. The productivity increases from 0.05 to 0.07 in Model A and had no improvement in Model B. The solar energy received by PCM Model A and Model B throughout the experiment was 4795.42 kJ and 2181.81 kJ, respectively.

Table 4.4: Productivity and Efficiency of Conventional and PCM Solar Still

MODEL	Yield, g		Productivity, g/kJ		Efficiency	
	Conventional	PCM	Conventional	PCM	Conventional	PCM
A	280	330	0.05	0.07	12%	16%
B	455	290	0.13	0.13	29%	30%

This is due to the PCM tubes used are not fully submerged into the feed water. This resulted in a form of heat loss from the desalination system to the surrounding. As evaporation continued to occur, the unsubmerged area will be exposed and thus, resulted in greater heat loss.

4.5 Combination of Fresnel Lens and Phase Change Material

Knowing the impact of both modifications, the effect using both modification together was still unknown. The experiment procedure was repeated, with both FRL and PCM utilised on the solar stills at the same time, namely, Modified Solar Still (MSS). It was expected that the advantages brought

from FRL and PCM can be obtained at the same time. In other words, the FRL could boost the water temperature rapidly, while PCM could maintain the high temperature in undesired meteorological condition. Figure 4.10 and Figure 4.11 shows the temperature of the desalination systems over time for MSS Model A and Model B throughout the experiment. The average solar irradiance recorded was 852 W/m^2 and 876 W/m^2 for FRL Model A and Model B, respectively.

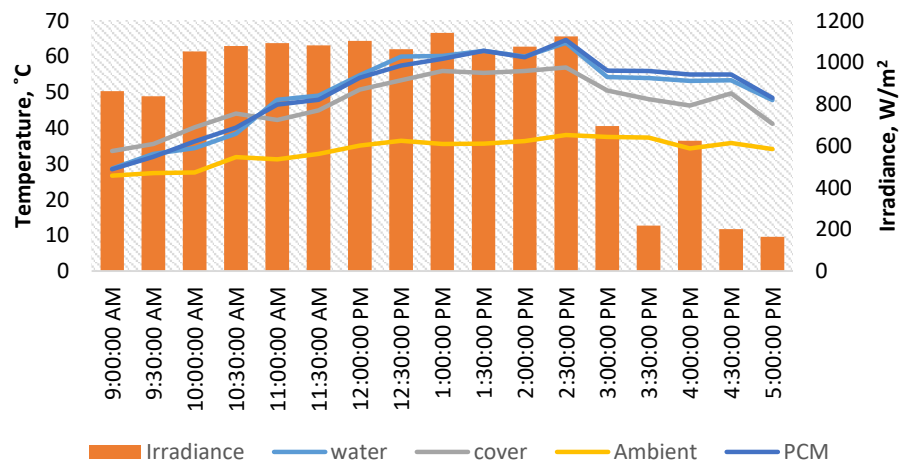


Figure 4.10: Temperature and Solar Irradiance of MSS A (with FRL and PCM)

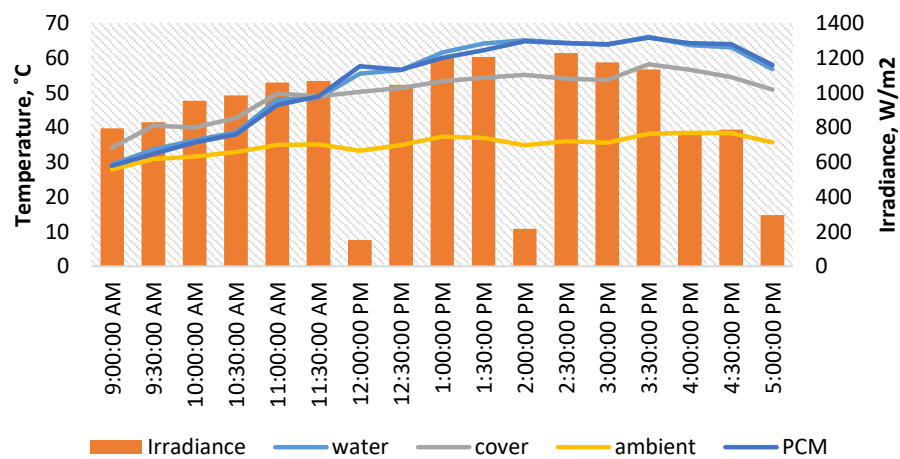


Figure 4.11: Temperature and Solar Irradiance of MSS B (with FRL and PCM)

From Figure 4.10 and 4.11, the advantage of FRL is substantially proven. Both solar still models show similar temperature trend. Model A begins to generate great amount of yields from 12 pm to 2.30 pm, where the solar flux is relatively high. The effect of PCM starts to take place after that. The solar irradiance starts to drop from 3 pm due to cloudy weather, but the temperature of feed water managed to maintain beyond 60 °C until 4.30 pm. This too reflected on the hourly yield result presented in Figure 4.12. A similar effect has been observed in the experiment of MSS Model B. Despite the unstable meteorological condition at 12 pm and 2 pm, the water temperature is capable to maintain its uptrend. From Figure 4.12, Model B begin to generate great amount of yields from 12.30 pm to 3.30 pm. Similar to Model A, as solar irradiance begin to drop in the evening, the temperature of feed water in model B maintained and decrease gradually until 4.30 pm.

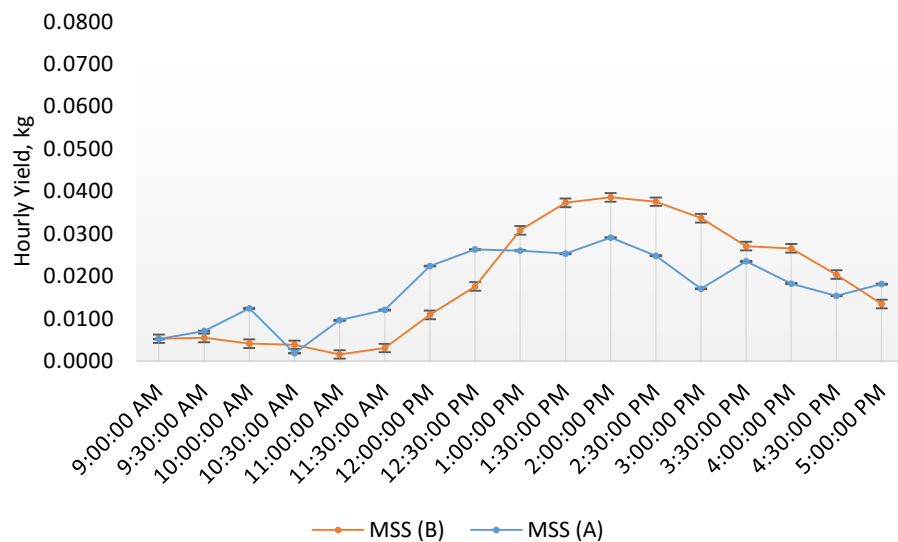


Figure 4.12: Accumulated Water Yield of Conventional and Modified Solar Stills

In spite of the performance of FRL and PCM on water temperature, the productivity and efficiency of MSS model A and B were still lower than FRL A

and B. This is because not all the heat were contributed to evaporation. Part of the gathered thermal energy was lost to the surrounding through the unsubmerged PCM. The solar energy received by MSS Model A and Model B throughout the experiment was 4702.52 kJ and 2589.53 kJ, respectively. Table 4.5 shows the productivity and efficiency of the MSS Model A and Model B. The Modified Solar Stills have their productivity and efficiency fall between FRL solar Still and PCM solar still.

Table 4.5: Productivity and Efficiency of Conventional and MSS A and B

MODEL	Yield, g		Productivity, g/kJ		Efficiency	
	Conventional	MSS	Conventional	MSS	Conventional	MSS
A	280	330	0.05	0.07	12%	16%
B	455	370	0.13	0.14	29%	32%

4.6 Effect of Water Volume

As mentioned in the previous section, PCM brought insignificant impact towards the productivity of the solar stills in the study due to the design. Therefore, another experiment was conducted to investigate the effect of PCM, with heat loss eliminated. Differ from the previous experiment, 4500 mL of saline water was poured into the basin this time to fully submerge the PCM tube. In other words, the water level in the basin was increased. The PCM tubes were fully submerged into the saline water. Only FRL and MSS Model B were involved in this experiment as it is believed that the effect of submerged PCM would be identical in both Models A and B.

Theoretically, higher water volume (water depth) will increase the water total heat capacity of water, hence reduce the productivity of solar stills as more energy is required to increase the water temperature. It is reasonable to predict that the productivity of FRL solar stills will be diminished. However, the purpose of conducting this experiment is to investigate the performance of PCM with FRL, with its full potential. Figure 4.13 and Figure 4.14 shows the temperature of the desalination system over time and hourly water yield of FRL Model B throughout the experiment with 4500 ml of saline water.

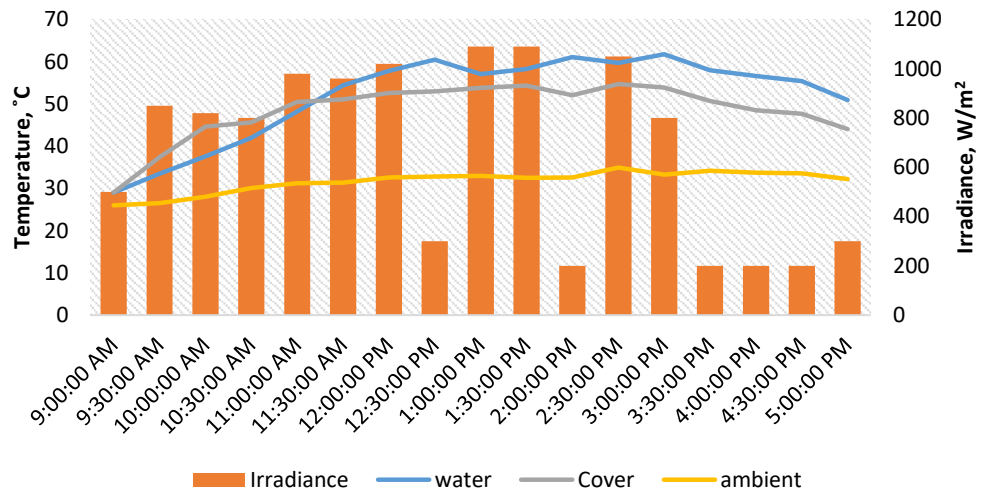


Figure 4.13: Temperature and Solar Irradiance of FRL Model B (4500mL)

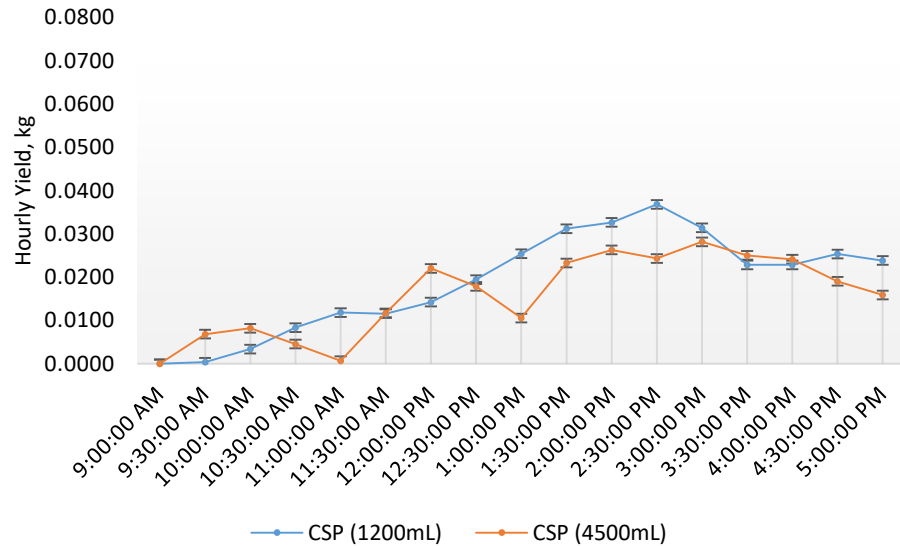


Figure 4.14: Accumulated Water Yield of FRL Model B

It can be observed that the water temperature in solar still with higher water volume takes longer time to surpass the temperature of the glass. The water temperature surpassed the temperature of the glass at 11.30 am. Moreover, the overall water temperature stays below 60 °C most of the time. This validates the assumption where more time is required to build up the water temperature. From Table 4.5, Model B with FRL has its water yield, together with productivity and thermal efficiency relatively lower compared to the identical model with lower water volume (1200 mL). This validated the hypothesis, where increasing water volume will bring a negative impact on the performance of FRL solar stills.

Figures 4.15 and 4.16 show the temperature of the desalination system over time and hourly water yield of MSS Model B throughout the experiment with 4500 ml of saline water. Contrast with FRL Model B, modified solar still shows a positive result with high water volume. From Figure 4.15, the property

of FRL and PCM are both presented. The water temperature stays high until 2.30 p.m., while right after that time, the solar irradiance drop drastically due to cloudy weather. Nevertheless, Figure 4.16 shows high yielding rate after 2.30 p.m. This can be explained as PCM plays its role at the time, discharging its heat to the water without any loss. At the same time, as PCM continues to discharge, the temperature gap between the temperature of cover and water grows wider, thus increase the yielding rate. The temperature of PCM is almost identical to the water temperature as it is fully immersed. Thus, it is not presented in Figure 4.15.

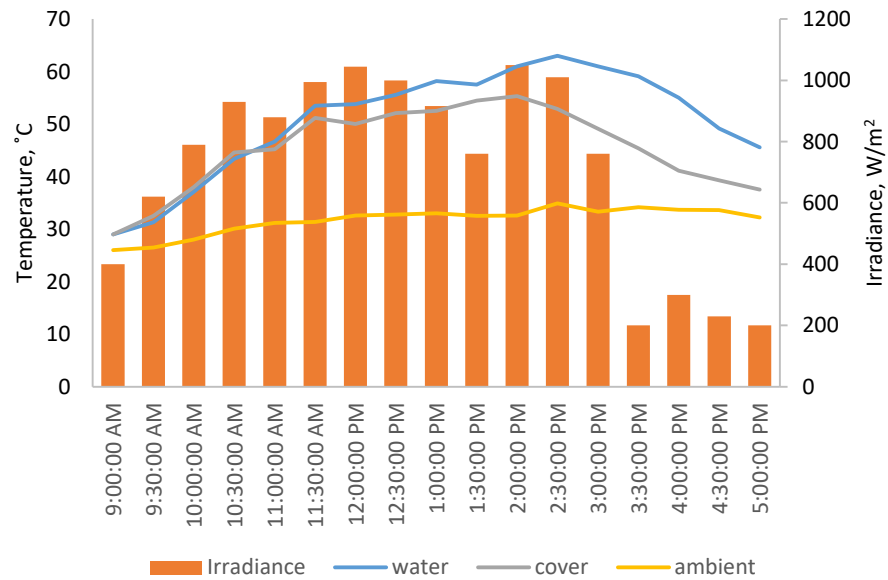


Figure 4.15: Temperature and Solar Irradiance of MSS B (4500 mL)

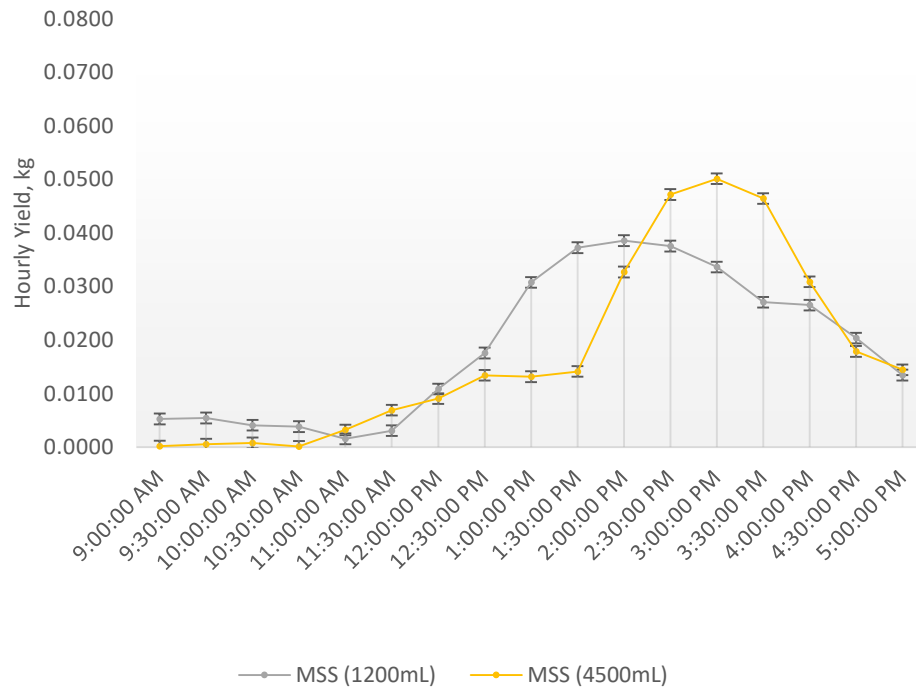


Figure 4.16: Hourly Water Yield of MSS Model B

In term of productivity and efficiency, unlike FRL Model B, MSS Model B performs better in higher water volume. It is already known that high water volume will bring negative impact to the still. The only possible explanation for the improvement is the presence of PCM. While 4500 mL of feed water is used, the PCM tubes are fully submerged in the water. This eliminates the heat loss problem mentioned in the early stage. Therefore the potential of PCM is substantially proven.

Table 4.6: Productivity and Efficiency of FRL and MSS A and B

MODEL	Yield, g		Productivity, g/kJ		Efficiency	
	1200mL	4500mL	1200mL	4500mL	1200mL	4500mL
FRL B	430	300	0.16	0.15	37%	34%
MSS B	370	320	0.14	0.15	32%	33%

4.7 Summary

In this chapter, the experimental result obtained from each enhancement on both prototypes, Model A and Model B were compared and analysed. Figures 4.17 and 4.18 show the productivity and efficiency of Model A and Model B with each configuration.

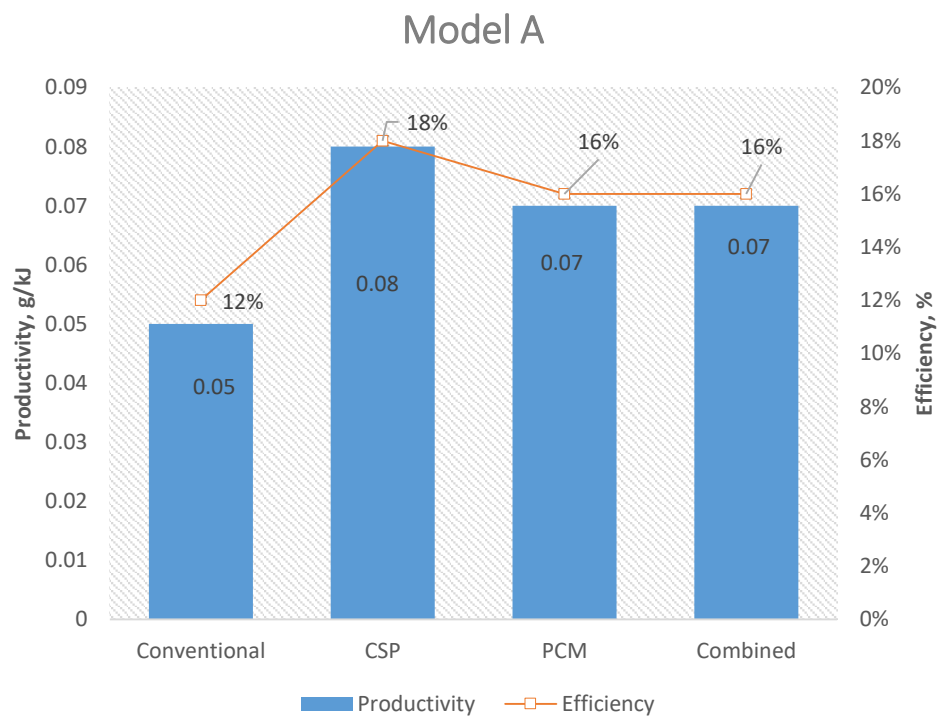


Figure 4.17: Productivity and Efficiency of Model A

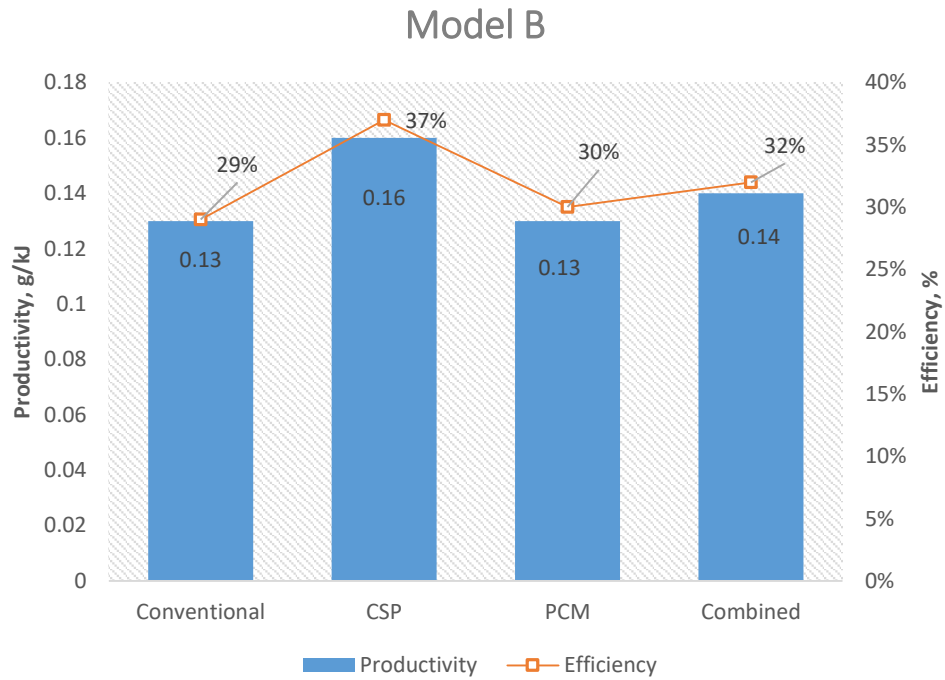


Figure 4.18: Productivity and Efficiency of Model B

Conventional setup (without FRL and PCM) has the lowest productivity and efficiency. Followed by PCM Solar Still, which the improvement in term of productivity and efficiency is insignificant. This is due to the heat loss induced by the unsubmerged PCM tubes. FRL Solar Still, on the other hand, has the highest performance among the setups. Model A and Model B associated with the FRL have significantly higher productivity and efficiency. The Modified Solar Still coupled with both FRL and PCM were expected to have the highest performance. However, the heat loss from PCM tubes turns to a drawback, dragging down the advantage from the FRL. As the result, MSS performs better than PCM solar stills, but still got outperformed by FRL solar still. The effect of both enhancement on passive double slope single basin solar still was validated as the productivity and efficiency of Model A and Model B show an identical outcome in each particular enhancing method.

It is also proven in water volume test, with higher water volume (water depth), the heat loss from PCM tubes could be eliminated. Yet, from Table 4.6, higher water volume indicates higher heat capacity to increase water temperature, which might cause a negative impact on the yield as well. Thus it can be said, the combination of FRL and PCM holds high potential as the advantage of both features are shown during the experiment. However, to utilise the full potential of solar still associated with both FRL and PCM, the container design should include considerations such as maximizing thermal transfer and minimizing heat loss.

CHAPTER 5

DISCUSSIONS

5.1 Introduction

In this chapter, the performance of the FRL and PCM associated solar still is discussed in detail. The experimental result is validated with the theoretical model in the first section. The effect of FRL and PCM is discussed in the next section, followed by the cost per litre (CPL) and total dissolved solids (TDS) in the distillate.

5.2 Theoretical Model

The experimental water yield results were compared with the corresponding theoretical yield. The mathematical model contributes to a better understanding on the thermal system of the solar still. Furthermore, the difference between the experimental and theoretical results could lead to finding of unexpected productivity catalyst. The mathematical model was made based on the equations mentioned in Chapter 3.5. The temperature of cover and saline water was used as input. From there, the convective and evaporative heat transfer from water to the cover can be calculated. The evaporative heat transfer is then used to identify the theoretical water yield using Equation (3.7). Assuming there is no heat loss and vapour leakage, the evaporated water mass should be equivalent to condensate mass. The percentage difference between experimental and theoretical yield is listed in Table 5.1.

Table 5.1: Comparison of Actual and Theoretical Yield

Model	Conventional		
	Experimental	Theoretical	Percentage Difference, %
A	280	310.9	-10%
B	455	471	-3%
Model	FRL		
	Experimental	Theoretical	Percentage Difference, %
A	505	445	13%
B	430	350	21%
Model	PCM		
	Experimental	Theoretical	Percentage Difference, %
A	330	301.7	9%
B	290	318.8	-9%
Model	MSS		
	Experimental	Theoretical	Percentage Difference, %
A	330	296	11%
B	370	317.2640	15%
Model	FRL (4500mL)		
	Experimental	Theoretical	Percentage Difference, %
B	300	268.8	11%
Model	MSS (4500mL)		
	Experimental	Theoretical	Percentage Difference, %
B	320	301.5	6%

From the result obtained, the percentage difference is mostly under 10%. However, in the experimental setup where FRL is presented, the percentage difference turns wider and could go up to 21%. Such inaccuracies could be explained by several reasons.

One of the major reasons is the unstable meteorological condition. Other than solar flux, the cover temperature could be affected by wind velocity and ambient temperature. Moreover, the experiments were conducted in a cloudy season. The sudden decrease of solar flux due to inconsistent clouds movement could cause a sudden drop in temperature of the cover, while gradually decreasing the temperature of the water and vice versa. This is because the glass cover has relatively total low heat capacity. The experimental data such as irradiance and temperature of the desalination system were recorded periodically (30 minutes), it is very difficult to notice and include such fluctuations into count. FRL, as well as all the other CSP devices, are very sensitive to solar irradiance. This fluctuation makes a more significant influence on FRL associated solar still.

Another noticeable finding is that the experimental yields from the setups where FRL is used are all more than the theoretical yield. This is because the FRL concentrates the area of solar irradiance to a particular point. Theoretically, it will keep the shaded area (glass cover) beneath the FRL away from solar ray, thus resulted in part of the cover in low temperature. In contrast, the temperature of the cover recorded was on another side of the slope, with relatively higher temperature to the shaded slope. Figure 5.1 shows the photograph of the shaded region. As validated in section 4.2, the larger the temperature difference between water and condensation surface (cover), the higher the amount of water yield. In other words, the shaded region of the cover increases the rate of condensation, thus increases the yield at the same time.

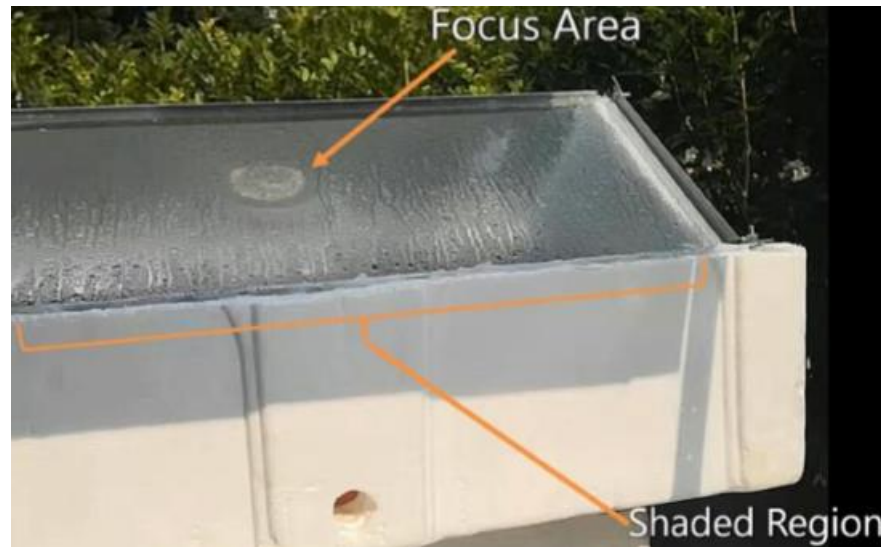


Figure 5.1: Photograph of the shaded region.

5.3 Effect of Fresnel Lens

Concentrated Solar Power (CSP) is a well-known technique that has been used in the field of solar desalination. Fresnel Lens is novel refraction based solar flux concentrated that shares similar working concept as the other CSP. Both of these techniques improve the productivity of solar still of concentrating sunlight from a larger area to a smaller spot. In CSP associated solar still, the smaller spot refers to the area of solar receiver, while the larger area refers to the area of the lens.

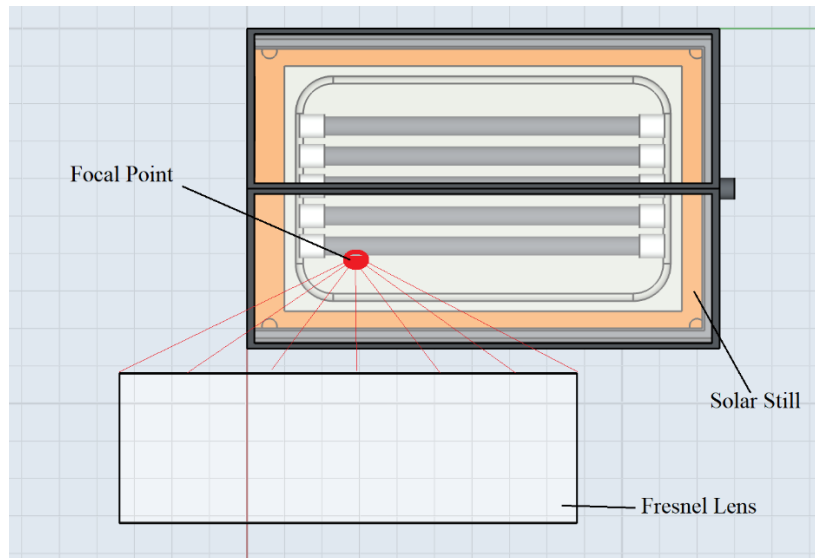


Figure 5.2: Arrangement of FRL in the experiment

The FRL used in this study has a width of 0.3 cm and a length of 0.4 cm. It is slightly smaller than the area of the basin in Model A and Model B. Theoretically, a FRL with the larger area should be used to further increase the solar energy absorbed by the basin. However, using a FRL larger than the basin defies the aim of crafting a portable solar still. Thus, an adjustable FRL frame holder was designed to solve this problem. Figure 5.2 and Figure 5.3 show the arrangement of the FRL in the experiment. The FRL is arranged slightly away from the centre, while ensured the focal point was on the basin at the same time. With this arrangement, the basin receives solar light and concentrated solar flux at the same time. Thus, as more solar energy was subjected to the basin, a higher volume of distillate was yield due to the boosted evaporation rate.



Figure 5.3: Solar flux concentrated on the side of the basin.

Another finding is that the high solar flux concentrated by Fresnel Lens induces boiling of feed water on its focal point. Figure 5.4 shows the generation of bubbles on the focal point. The bubble formation was observed shortly after the experiment. The continuous generation of air bubbles from the focal point increases the rate of evaporation. The boiling of feed water is not included in the mathematical model as it is impossible to measure the temperature of the focal point throughout the experiment. This is another reason behind the mismatch of the experimental and theoretical yield. Regardless, the boiling of feed water on the focal point indeed improved the productivity of the solar still.



Figure 5.4: Bubbles forming in CSP Solar Still where FRL is used

From the observation, it can be concluded that FRL plays a major role in improving the productivity and efficiency of solar stills. Not only did the FRL increase the overall thermal energy received by the receiver, but the boiling of feed water on the focal point also resulted in higher evaporation and productivity. This has been validated in the results obtained in Section 4.4.

5.4 Effect of Phase Change Material

According to the experiment result, the petroleum jelly performs poorly in the experiment with PCM and MSS low water volume configuration. Both Model A and Model B show least improvement in PCM associated experiment. The drawback of the PCM is due to several reasons.

5.4.1 Unsubmerged PCM Tube

The petroleum jelly was encapsulated in stainless steel tubes. Figure 5.5 illustrated the schematic diagram of the PCM tubes in the basin. The solar energy received by the basin is transferred to the saline water in the form of thermal energy. The temperature of saline water therefore increases and the thermal energy was later contributed to evaporation, convection, and radiation heat transfer from saline water to the glass cover. In the case where PCM is presented, part of the heat was transferred from saline water to PCM tubes as well. Out of which, evaporative heat transfer is crucial as it is directly affecting the water yield of the desalination system. In order to maximize the water yield, the other two forms of heat transfer must be kept minimal.

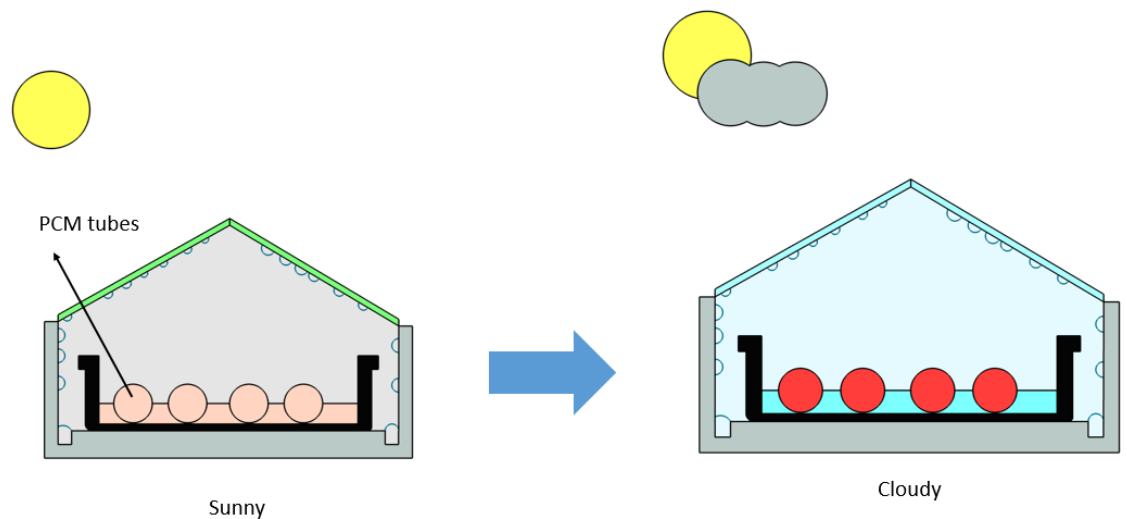


Figure 5.5: Schematic diagram of Unsubmerged PCM

The experiment used only 1200 mL of saline water as feed water in the basin. The PCM tubes were not fully submerged with the water volume. As such, the unsubmerged part acted as a portal that induces heat loss from the saline

water to the air through convective heat transfer. Instead of storing the heat, part of the heat in the PCM was lost to the air in solar still. As the result, the thermal energy received by the saline water did not contribute to the evaporation effectively. Moreover, the heat loss from the PCM tube to the air increases the temperature of the glass cover. This greatly affects the condensation rate beneath the glass cover. Other than that, the unsubmerged part of the PCM reduces the surface area of the saline water. This reduces the area available for saline water to evaporate as listed in equation (3.7). As the saline water continues to evaporate, the more unsubmerged part will get exposed, thus resulted in a greater negative impact.

5.4.2 Fully Submerged PCM Tube

In experiments where 4500 mL of feed water is used, the PCM tubes are completely submerged into the saline water. Contrast with the previous result, MSS Model B with 4500 mL of saline water has its performance improved. The productivity and efficiency of the MSS Model B were relatively higher than the FRL Model B when 4500 mL of saline water is used. This can be explained as the drawbacks of unsubmerged PCM mentioned in the previous section were solved.

First of all, the heat loss induced by the exposed PCM tubes were eliminated. During the where solar irradiation stays high and stable, the heat obtained from saline water was stored in the PCM. When fully submerged, the PCM is surrounded by saline water with the same or higher temperature, thus heat loss was prevented. The stored heat was later fully discharged back to the

saline water effectively. This fulfilled the purpose of utilizing PCM. Furthermore, the surface area of water to air interface is increased when PCM is fully submerged. The evaporation rate of the saline water was therefore increased.

As reflected in the result, the potential of PCM was shown when the PCM is fully submerged in the saline water. In other words, in order to utilize the PCM effectively, the heat transfer between PCM and feed water must be maximized.

5.5 Combination of Fresnel Lens and Phase Change Material

Both FRL and PCM could be used as individual enhancement method and their working concept are independent of each other. The initial proposal of the study was to incorporate the working concept of FRL with PCM in passive solar still to identify the feasibility of such an arrangement.

5.5.1 Mixed Solar Still in the Research

From the results obtained in Section 4.5, MSS solar still outperform the conventional solar still and PCM solar still in terms of productivity and efficiency. The improvement is mainly contributed by FRL which induced boiling of saline water and increment of solar power received. As previously mentioned, FRL is capable to concentrate a larger amount of solar flux onto the basin, while at the same time reduces the temperature of the shaded region on the glass cover. Thus, the evaporation rate and condensation rate of the solar still increase, which also contributed to the improvement on productivity and efficiency of solar still. In spite of the fact that the presence of PCM increased

the overall heat capacity of the saline water, the FRL is still able to boost up the water temperature rapidly.

Nevertheless, the unsubmerged PCM acted as a drawback in low water volume experiment as mentioned in Section 5.4.1. The exposed PCM did not fulfil its main purpose as thermal storage as part of the heat absorbed from the saline water were constantly transferred to the air and glass cover through convective heat transfer. When solar irradiance dropped, the temperature of saline water dropped drastically due to the PCM failed to discharge the heat back to the water. The exposed PCM also limited the water to air interface which directly reduces the evaporation rate of feed water. As the result, the negative impact from unsubmerged PCM neutralized the improvement brought by the FRL. This was reflected in the results in Section 4.5 in which the MSS solar still (low water volume) outperformed by the FRL solar stills.

On the other hand, the performance of MSS improved significantly relative to FRL when higher water volume (4500 mL) of feed water was used. When fully submerged, the heat transfer between saline water and PCM is maximized. The stored heat can be discharged effectively back to saline water in the form of sensible heat and latent heat. This way, the feasibility of combining the strengths of both FRL and PCM were substantially proven. Regardless, high water volume or water depth is not recommended (Rajamanickam et al., 2012; Kumar et al., 2017; Kabeel et al., 2019b) to be used on solar still as more water volume required more thermal energy to heat the feed water. Additionally, higher water depth indicates smaller water-solar

receiver interface ratio. Thus, the solar energy absorbed by the receiver is not effectively transfer to the feed water.

5.5.2 Improvement on Mixed Solar Still

In order to further improve the productivity and efficiency of the solar still, the design of PCM tubes must be changed. The PCM tubes contributed the least improvement to the solar still due to the drawbacks mentioned in section 5.4.1. Although it can be solved with high feed water volume, that would trigger another flaw, which is lower overall water temperature. This has been proven in the result mentioned in Section 4.6.

Using smaller PCM tubes would be a solution to this problem. Smaller PCM tubes can be submerged completely into feed water, even with lower water depth. The reduction in the diameters would not restrict the amount of PCM used as more PCM tubes could fit in the same basin. This is good for improving the heat transfer between PCM and saline water as the ratio PCM-saline water interface are increased.

Moreover, FRL should be arranged to ensure its focal point fell on top of the PCM tubes instead of the basin. This is because the heat received by the basin was not fully transferred to the saline water in the first place. Part of the heat was transferred to the polystyrene beneath the basin. In contrast, the fully submerged PCM tubes were surrounded by saline water. When the solar flux was subjected to the tubes, saline water is the only object to receive the thermal energy from it.

Theoretically, this would further reduce non-evaporative heat loss from the desalination system.

5.6 Quality of the Distillate

A sample from freshwater yielded from the solar stills was tested with a sample from feed water to showcase the difference and at the same time to ensure the freshwater is consumable. The result of water conducting test is listed in Table 5.2. According to the guideline from the World Health Organization (WHO), the water yield from the stills is completely safe to drink.

Table 5.2: Water Conductivity Test

Model	A	B	WHO	Feed Water
Total Dissolved Solid (ppm)	15	18	<500	~20000
pH	6.8	6.8	6.5~8.5	7.2

5.7 Cost of the Distillate

The economic feasibility of the solar still is calculated based on the study of Mohammad Behshad Shafii in order to obtain the Cost-Per-Litre (CPL) of the prototypes (Shafii et al., 2016). Table 5.3 and Table 5.4 show the CPL of Model A and Model B. Apparently, Model B offer lower cost in all configuration compared to Model A.

For Model B, conventional desalination unit has the lowest cost per litre among all. However, considering its low productivity and efficiency, FRL only solar still would be a better choice.

Table 5.3: Cost of solar still model A

Parameters	Unit	Conventional	CSP only	PCM only	Combined
Principal cost (P)	\$	96.61	106.73	102.89	113.01
Salvage Value (S, 10% of P)	\$	9.661	10.673	10.289	11.301
Life (n)	years	15	15	15	15
interest rate (i)	%	-			
Capital recovery factor (CRF)	0.117	0.117	0.117	0.117	0.117
Sink fund factor (SFF)	0.017	0.017	0.017	0.017	0.017
Annual First Cost (CRF * P)	\$	11.30	12.49	12.04	13.22
Annual salvage value (SFF * S)	\$	0.16	0.18	0.17	0.19
Annual Maintenance Cost (0.15 * annual first cost)	\$	1.70	1.87	1.81	1.98
Annual Cost (Annual first cost + annual maintenance cost - annual salvage value)	\$	12.83	14.18	13.67	15.01
Average Daily Yield (Kg/m ²)	kg/m ²	0.880	0.912	0.852	0.980
Annual Yield of the Still (average daily yield *365)	kg/m ²	321.20	332.88	310.98	357.70
Cost per Litre per unit area of still (CPL = Annual cost/ Annual Yield of Still)	\$/ (kg/m ²)	0.0400	0.0426	0.0440	0.0420
Average Daily Yield (L)	L	0.220	0.228	0.213	0.245
Annual Yield of the Still (average daily yield *365)	L	80.3	83.22	77.745	89.425
Cost per Litre per unit area of still (CPL = Annual cost/ Annual Yield of Still)	\$/L	0.1598	0.1704	0.1758	0.1679

Table 5.4: Cost of solar still model B

Parameters	Unit	Conventional	FRL only	PCM only	Combined
Principal cost (P)	\$	14.97	26.08	20.52	31.64
Salvage Value (S, 10% of P)	\$	1.497	2.608	2.052	3.164
Life (n)	years	15	15	15	15
interest rate (i)	%	-			
Capital recovery factor (CRF)	0.117	0.117	0.117	0.117	0.117
Sink fund factor (SFF)	0.017	0.017	0.017	0.017	0.017
Annual First Cost (CRF * P)	\$	1.75	3.05	2.40	3.70
Annual salvage value (SFF * S)	\$	0.03	0.04	0.03	0.05
Annual Maintenance Cost (0.15 * annual first cost)	\$	0.26	0.46	0.36	0.56
Annual Cost (Annual first cost + annual maintenance cost - annual salvage value)	\$	1.99	3.46	2.73	4.20
Average Daily Yield (Kg/m ²)	kg/m ²	2.963	3.185	2.609	3.391
Annual Yield of the Still (average daily yield *365)	kg/m ²	1081.48	1162.59	952.17	1237.83
Cost per Litre per unit area of still (CPL = Annual cost/ Annual Yield of Still)	\$/ (kg/m ²)	0.0018	0.0030	0.0029	0.0034
Average Daily Yield (L)	L	0.400	0.430	0.300	0.390
Annual Yield of the Still (average daily yield *365)	L	146	156.95	109.5	142.35
Cost per Litre per unit area of still (CPL = Annual cost/ Annual Yield of Still)	\$/L	0.0136	0.0221	0.0249	0.0295

The present work with the highest productivity, which is FRL Model B, was compared to the existing solar stills in Table 5.5. It must be mentioned that

the passive solar still in this study were purposely fabricated with a simple design and required the least maintenance. This greatly reduces the cost per litre (CPL) water of the desalination system. Moreover, from Table 5.5, the performance of the designed still is relatively high compared to other passive solar stills, in terms of daily yield and CPL.

Table 5.5: Comparison between present work and existing stills

Author	Solar Still Model	Yield, L/m² day	Efficiency	Cost per Litre
(Ahsan et al., 2013)	Triangular Solar Still (Passive Solar Still)	1.55	-	0.0255 \$/L
(Wang et al., 2018)	Floating Solar Desalination Film	1.38	22.7%	-
(Elashmawy, 2017)	Tubular Solar Still	3.6	30.22%	0.023\$/L
(Abujazar, S. Fatihah, et al., 2018)	Inclined Copper Stepped Solar Still	4.353	28.3%	-
(Rahbar et al., 2018)	Tubular Solar Still (Passive Solar Still)	2.13	35~41%	0.0683 \$/L
(Arunkumar et al., 2016)	Crescent Absorber CSP Solar Still (Passive Solar Still)	1.58	-	0.025 \$/L
Present (CSP B)	Point Focus FRL Double Slope Passive Solar Still	3.19	37%	0.0221 \$/L

5.8 Summary

In this chapter, the experimental results were validated with the theoretical model. At the same time, the effect of FRL, PCM, and the combination of both on passive solar still has been discussed. It can be concluded that the FRL has the ability to concentrate the high amount of solar flux on the solar receiver. In term of productivity and efficiency, the performance of FRL associated solar still is far better than the solar still associated with PCM. The design of the PCM containers is proved to be a crucial consideration while designing a PCM coupled solar still. The potential of combining both FRL and PCM on passive solar still is substantially proven.

CHAPTER 6

CONCLUSION AND RECOMMENDATION

6.1 Conclusion

Two portable, simple design and high efficiency double sloped passive solar still, Model A and Model B were designed and crafted. FRL and petroleum jelly were used as the CSP and PCM enhancement features of the solar stills, respectively. Few sets of experiments, including conventional stills (without enhancement), CSP solar stills, PCM solar stills, and Modified solar stills (with FRL and PCM) were conducted to evaluate the performance between each enhancement strategy.

Despite the different parameters and daily yield, Model A and Model B show similar trends on the effect of the modifications. The presence of FRL greatly improved the performance of solar stills. On the other hand, PCM has a relatively insignificant enhancement to the performance of the solar still, provided with heat loss is found from unsubmerged part of PCM tubes. The drawback from the loss brought negative effect towards Modified Solar Stills (with FRL and PCM) as well. Nevertheless, the combination of FRL and PCM still brought improvement in the productivity of the still. When higher feed water volume is provided, the combination of FRL and PCM solar still shows better performance relative to FRL solar still.

Comparing both solar stills, it can be concluded that, among the modification mentioned, FRL alone provides the highest productivity and efficiency when coupled with passive double sloped solar stills. Model B incorporated with FRL has the highest productivity of 0.16 g/kJ and thermal efficiency of up to 37%. The daily water yield of 3.19 L/m²day with low cost has been achieved. It can be concluded that the Fresnel Lens is feasible as a CSP on passive solar still, while the combination of Fresnel lens and PCM are viable when the heat transfer between saline water and PCM are maximized.

6.2 Recommendation for Future Work

The heat transfer between PCM and feed water are proven to be crucial. In order to utilize the PCM effectively, a new PCM encapsulation model must be designed. Chapter 5.5.2 suggested a smaller tubular PCM tube as it can keep up the heat transfer, without increasing the water volume. Alternative design such as corrugated PCM container, fin PCM container that possesses high water-PCM interface ratio could also be kept in the consideration.

The experiments were conducted outdoor, the input of the experiment was natural sunlight, which is highly dependent on the meteorological condition. Moreover, the experiments were conducted on different days in a range of time. Although such conditions do not cause significant influences on the result, a more consistent and accurate result could be obtained under a stable and controlled environment. An indoor solar simulator could be used to achieve the condition mentioned.

As mentioned in Section 3.5, the latent heat of vaporization is dependent to the salinity of the feed water. Water obtainable from nature possess different salinity and content from others. In order to obtain a clearer image of the performance of the prototypes, seawater and polluted water can be used as feed water in the experiment.

REFERENCES

- Abujazar, M.S.S., Fatihah, S., et al., 2018. Performance evaluation of inclined copper-stepped solar still in a wet tropical climate. *Desalination*, 425, pp.94–103.
- Abujazar, M.S.S., Fatihah, Suja, et al., 2018. Productivity modelling of a developed inclined stepped solar still system based on actual performance and using a cascaded forward neural network model. *Journal of Cleaner Production*, 170, pp.147–159.
- Ahmadvand, S. et al., 2019. Looking Beyond Energy Efficiency: An Applied Review of Water Desalination Technologies and an Introduction to Capillary-Driven Desalination. *Water*, 11(4), p.696. Available at: <https://www.mdpi.com/2073-4441/11/4/696> [Accessed: 14 January 2020].
- Al-Dohani, N.S., Nagaraj, S.N., Anarghya, A. and Abhishek, V.N., 2018. Development of Powerhouse Using Fresnel lens Raghuvir, P.B. and Mathew, T.M., (eds.). *MATEC Web of Conferences*, 144, p.04006. Available at: <https://www.matec-conferences.org/10.1051/matecconf/201814404006> [Accessed: 11 February 2020].
- Al-Maghalseh, M. and Mahkamov, K., 2018. Methods of heat transfer intensification in PCM thermal storage systems: Review paper. *Renewable and Sustainable Energy Reviews*.
- Alduchov, O.A., Eskridge, R.E., Alduchov, O.A. and Eskridge, R.E., 1996. Improved Magnus Form Approximation of Saturation Vapor Pressure. [http://dx.doi.org/10.1175/1520-0450\(1996\)035<0601:IMFAOS>2.0.CO;2](http://dx.doi.org/10.1175/1520-0450(1996)035<0601:IMFAOS>2.0.CO;2).
- Ali, M.T., Fath, H.E.S. and Armstrong, P.R., 2011. A comprehensive techno-economical review of indirect solar desalination. *Renewable and Sustainable Energy Reviews*.
- Alnaimat, F., Klausner, J. and Mathew, B., 2018. Solar Desalination. In: *Desalination and Water Treatment*. InTech.
- Altarawneh, I. et al., 2017. Experimental and numerical performance analysis and optimization of single slope, double slope and pyramidal shaped solar stills. *Desalination*.
- Arunkumar, T. et al., 2019. A review of efficient high productivity solar stills. *Renewable and Sustainable Energy Reviews*, 101, pp.197–220. Available at: <https://www.sciencedirect.com/science/article/pii/S1364032118307615> [Accessed: 2 January 2019].
- Arunkumar, T. et al., 2016. Effect of heat removal on tubular solar desalting system. *Desalination*, 379, pp.24–33.
- Arunkumar, T. et al., 2015a. Experimental study on a parabolic concentrator assisted solar desalting system. *Energy Conversion and Management*, 105, pp.665–674. Available at: <https://www.sciencedirect.com/science/article/pii/S0196890415007670> [Accessed: 2 January 2019].
- Arunkumar, T. et al., 2015b. Experimental study on a parabolic concentrator assisted solar desalting system. *Energy Conversion and Management*.
- Awasthi, A., Kumari, K., Panchal, H. and Sathyamurthy, R., 2018. Passive solar still: recent advancements in design and related performance. *Environmental Technology Reviews*, 7(1), pp.235–261.
- Badusha, R. and Arjunan, T. V., 2013. *Performance Analysis of Single Slope Solar Still*,

- Bahrami, M., Madadi Avargani, V. and Bonyadi, M., 2019. Comprehensive experimental and theoretical study of a novel still coupled to a solar dish concentrator. *Applied Thermal Engineering*, 151, pp.77–89.
- Belessiotis, V., Kalogirou, S. and Delyannis, E., 2016. Solar Distillation—Solar Stills. In: *Thermal Solar Desalination*. Elsevier, pp. 103–190.
- Cabeza, L.F. et al., 2015. Introduction to thermal energy storage (TES) systems. In: *Advances in Thermal Energy Storage Systems: Methods and Applications*. Elsevier Inc., pp. 1–28.
- Chandel, S.S. and Agarwal, T., 2017. Review of current state of research on energy storage, toxicity, health hazards and commercialization of phase changing materials. *Renewable and Sustainable Energy Reviews*.
- Chen, C. et al., 2019. Sustainably integrating desalination with solar power to overcome future freshwater scarcity in China. *Global Energy Interconnection*, 2(2), pp.98–113.
- Dawoud, M.A. and Al Mulla, M.M., 2012. *Environmental Impacts of Seawater Desalination: Arabian Gulf Case Study*,
- Delgado-Torres, A.M., García-Rodríguez, L. and del Moral, M.J., 2020. Preliminary assessment of innovative seawater reverse osmosis (SWRO) desalination powered by a hybrid solar photovoltaic (PV) - Tidal range energy system. *Desalination*, 477.
- Dsilva Winfred Rufuss, D., Iniyan, S., Suganthi, L. and Davies, P.A., 2016. Solar stills: A comprehensive review of designs, performance and material advances. *Renewable and Sustainable Energy Reviews*.
- El-Samadony, Y.A.F., El-Maghlany, W.M. and Kabeel, A.E., 2016. Influence of glass cover inclination angle on radiation heat transfer rate within stepped solar still. *Desalination*.
- Elashmawy, M., 2017. An experimental investigation of a parabolic concentrator solar tracking system integrated with a tubular solar still. *Desalination*, 411, pp.1–8. Available at: <https://www.sciencedirect.com/science/article/pii/S0011916416313212> [Accessed: 24 December 2018].
- Elashmawy, M., 2019. Effect of surface cooling and tube thickness on the performance of a high temperature standalone tubular solar still. *Applied Thermal Engineering*, 156, pp.276–286.
- Elimelech, M. and Phillip, W.A., 2011. The future of seawater desalination: Energy, technology, and the environment. *Science*, 333(6043), pp.712–717.
- Fathy, M., Hassan, H. and Salem Ahmed, M., 2018. Experimental study on the effect of coupling parabolic trough collector with double slope solar still on its performance. *Solar Energy*, 163, pp.54–61. Available at: <https://www.sciencedirect.com/science/article/pii/S0038092X18300641?via%3Dihub> [Accessed: 24 January 2019].
- Gorjian, S. and Ghobadian, B., 2015. Solar desalination: A sustainable solution to water crisis in Iran. *Renewable and Sustainable Energy Reviews*, 48, pp.571–584. Available at: <https://www.sciencedirect.com/science/article/pii/S1364032115002798> [Accessed: 4 January 2019].
- Harris Samuel, D.G. et al., 2016. Enhancing the solar still yield by increasing the surface area of water—A review. *Environmental Progress and Sustainable Energy*.
- Hassan, H., Ahmed, M.S. and Fathy, M., 2019. Experimental work on the effect

of saline water medium on the performance of solar still with tracked parabolic trough collector (TPTC). *Renewable Energy*, 135, pp.136–147. Available at: <https://www.sciencedirect.com/science/article/pii/S0960148118314319> [Accessed: 2 January 2019].

Henderson-Sellers, B., 1984. A new formula for latent heat of vaporization of water as a function of temperature. *Quarterly Journal of the Royal Meteorological Society*, 110(466), pp.1186–1190. Available at: <http://doi.wiley.com/10.1002/qj.49711046626> [Accessed: 5 May 2020].

Islam, M.T., Huda, N., Abdullah, A.B. and Saidur, R., 2018. A comprehensive review of state-of-the-art concentrating solar power (CSP) technologies: Current status and research trends. *Renewable and Sustainable Energy Reviews*, 91, pp.987–1018. Available at: <https://www.sciencedirect.com/science/article/pii/S1364032118303113> [Accessed: 28 December 2018].

Kabeel, A.E. et al., 2019a. Effect of water depth on a novel absorber plate of pyramid solar still coated with TiO₂ nano black paint. *Journal of Cleaner Production*.

Kabeel, A.E. et al., 2019b. Effect of water depth on a novel absorber plate of pyramid solar still coated with TiO₂ nano black paint. *Journal of Cleaner Production*, 213, pp.185–191.

Kabeel, A. E. and Abdelgaied, M., 2016a. Improving the performance of solar still by using PCM as a thermal storage medium under Egyptian conditions. *Desalination*, 383, pp.22–28.

Kabeel, A. E. and Abdelgaied, M., 2016b. Improving the performance of solar still by using PCM as a thermal storage medium under Egyptian conditions. *Desalination*.

Kabeel, A.E. and Abdelgaied, M., 2016. Improving the performance of solar still by using PCM as a thermal storage medium under Egyptian conditions. *Desalination*, 383, pp.22–28. Available at: <https://www.sciencedirect.com/science/article/pii/S0011916416300066> [Accessed: 24 January 2019].

Kabeel, A.E., Abdelgaied, M. and Mahgoub, M., 2016. The performance of a modified solar still using hot air injection and PCM. *Desalination*, 379, pp.102–107.

Kabeel, A.E., El-Samadony, Y.A.F. and El-Maghlany, W.M., 2018a. Comparative study on the solar still performance utilizing different PCM. *Desalination*, 432(January), pp.89–96. Available at: <http://linkinghub.elsevier.com/retrieve/pii/S0011916417324803>.

Kabeel, A.E., El-Samadony, Y.A.F. and El-Maghlany, W.M., 2018b. Comparative study on the solar still performance utilizing different PCM. *Desalination*, 432, pp.89–96. Available at: <https://www.sciencedirect.com/science/article/pii/S0011916417324803> [Accessed: 24 January 2019].

Kabeel, A.E., Khalil, A., Omara, Z.M. and Younes, M.M., 2012. Theoretical and experimental parametric study of modified stepped solar still. *Desalination*, 289, pp.12–20.

Kabeel, A.E., Teamah, M.A., Abdelgaied, M. and Abdel Aziz, G.B., 2017. Modified pyramid solar still with v-corrugated absorber plate and PCM as a thermal storage medium. *Journal of Cleaner Production*.

Khalifa, A.J.N., 2011. On the effect of cover tilt angle of the simple solar still on

- its productivity in different seasons and latitudes. *Energy Conversion and Management*. 2011
- Kumar, P.N. et al., 2017. Experimental investigation on the effect of water mass in triangular pyramid solar still integrated to inclined solar still. *Groundwater for Sustainable Development*, 5, pp.229–234. Available at: <http://dx.doi.org/10.1016/j.gsd.2017.08.003>.
- Kumar, V., Shrivastava, R.L. and Untawale, S.P., 2015b. Fresnel lens: A promising alternative of reflectors in concentrated solar power. *Renewable and Sustainable Energy Reviews*, 44, pp.376–390. Available at: <https://linkinghub.elsevier.com/retrieve/pii/S1364032114010582> [Accessed: 24 January 2019].
- Liu, J. et al., 2017. Water scarcity assessments in the past, present, and future. *Earth's Future*, 5(6), pp.545–559.
- Ma, X., Zheng, H. and Liu, S., 2019. Optimization on a cylindrical Fresnel lens and its validation in a medium-temperature solar steam generation system. *Renewable Energy*, 134, pp.1332–1343.
- Mahmoud, M.S., Farrag, T.E. and Mohamed, W.A., 2013. Experimental and Theoretical Model for Water Desalination by Humidification - dehumidification (HDH). *Procedia Environmental Sciences*, 17, pp.503–512.
- Mancosu, N., Snyder, R., Kyriakakis, G. and Spano, D., 2015. Water Scarcity and Future Challenges for Food Production. *Water*, 7(12), pp.975–992. Available at: <http://www.mdpi.com/2073-4441/7/3/975> [Accessed: 14 January 2020].
- Manikandan, V. et al., 2013. Wick type solar stills: A review. *Renewable and Sustainable Energy Reviews*.
- Manju, S. and Sagar, N., 2017. Renewable energy integrated desalination: A sustainable solution to overcome future fresh-water scarcity in India. *Renewable and Sustainable Energy Reviews*, 73, pp.594–609.
- March, H., Saurí, D. and Rico-Amorós, A.M., 2014. The end of scarcity? Water desalination as the new cornucopia for Mediterranean Spain. *Journal of Hydrology*, 519(PC), pp.2642–2651.
- Mekonnen, M.M. and Hoekstra, A.Y., 2016. Four billion people facing severe water scarcity. *Science advances*, 2(2), p.e1500323. Available at: <http://advances.sciencemag.org/cgi/doi/10.1126/sciadv.1500323> [Accessed: 31 March 2018].
- Moffat, R.J., 1988. Describing the uncertainties in experimental results. *Experimental Thermal and Fluid Science*, 1(1), pp.3–17.
- Morad, M.M., El-Maghawry, H.A.M. and Wasfy, K.I., 2017. A developed solar-powered desalination system for enhancing fresh water productivity. *Solar Energy*, 146, pp.20–29. Available at: <http://dx.doi.org/10.1016/j.solener.2017.02.002>.
- Morad, M.M., El-Maghawry, H.A.M. and Wasfy, K.I., 2015. Improving the double slope solar still performance by using flat-plate solar collector and cooling glass cover. *Desalination*.
- Mu, L. et al., 2019. Enhancing the performance of a single-basin single-slope solar still by using Fresnel lens: Experimental study. *Journal of Cleaner Production*, 239, p.118094.
- Muftah, A.F. et al., 2014. Factors affecting basin type solar still productivity: A detailed review. *Renewable and Sustainable Energy Reviews*.
- Muraleedharan, M., Singh, H., Udayakumar, M. and Suresh, S., 2019. Modified

- active solar distillation system employing directly absorbing Therminol 55–Al₂O₃ nano heat transfer fluid and Fresnel lens concentrator. *Desalination*, 457, pp.32–38.
- Nayar, K.G., Sharqawy, M.H., Banchik, L.D. and Lienhard, J.H., 2016. Thermophysical properties of seawater: A review and new correlations that include pressure dependence. *Desalination*, 390, pp.1–24.
- Omara, Z.M., Abdullah, A.S. and Dakrory, T., 2017. Improving the productivity of solar still by using water fan and wind turbine. *Solar Energy*.
- Omara, Z.M., Kabeel, A.E., Abdullah, A.S. and Essa, F.A., 2016. Experimental investigation of corrugated absorber solar still with wick and reflectors. *Desalination*, 381, pp.111–116.
- Palomino-Resendiz, S.I. et al., 2018. Design and implementation of a robotic active solar distiller based on a Fresnel concentrator and a photovoltaic system. *Energy Conversion and Management*, 166, pp.637–647. Available at: <https://www.sciencedirect.com/science/article/pii/S0196890418304175> [Accessed: 16 January 2019].
- Pham, T.T., Vu, N.H. and Shin, S., 2018. Design of Curved Fresnel Lens with High Performance Creating Competitive Price Concentrator Photovoltaic. *Energy Procedia*. 1 July 2018 Elsevier Ltd, pp. 16–32.
- Pouyfaucou, A.B. and García-Rodríguez, L., 2018a. Solar thermal-powered desalination: A viable solution for a potential market. *Desalination*, 435, pp.60–69.
- Pugsley, A., Zacharopoulos, A., Mondol, J.D. and Smyth, M., 2016. Global applicability of solar desalination. *Renewable Energy*, 88, pp.200–219. Available at: <http://dx.doi.org/10.1016/j.renene.2015.11.017>.
- Pugsley, A., Zacharopoulos, A., Mondol, J.D. and Smyth, M., 2018. Solar Desalination Potential Around the World. In: *Renewable Energy Powered Desalination Handbook: Application and Thermodynamics*. Elsevier Inc., pp. 47–90.
- Rabhi, K. et al., 2017. Experimental performance analysis of a modified single-basin single-slope solar still with pin fins absorber and condenser. *Desalination*, 416, pp.86–93.
- Rajamanickam, M.R. and Ragupathy, A., 2012. Influence of water depth on internal heat and mass transfer in a double slope solar still. *Energy Procedia*. 2012
- Saadi, Z., Rahmani, A., Lachtar, S. and Soualmi, H., 2018. Performance evaluation of a new stepped solar still under the desert climatic conditions. *Energy Conversion and Management*, 171, pp.1749–1760.
- Sampathkumar, K., Arjunan, T. V., Pitchandi, P. and Senthilkumar, P., 2010. Active solar distillation-A detailed review. *Renewable and Sustainable Energy Reviews*, 14(6), pp.1503–1526.
- Sathyamurthy, R., El-Agouz, S.A., et al., 2017. A Review of integrating solar collectors to solar still. *Renewable and Sustainable Energy Reviews*, 77, pp.1069–1097. Available at: <https://www.sciencedirect.com/science/article/pii/S1364032116309935> [Accessed: 2 January 2019].
- Shafii, M.B., Shahmohamadi, M., Faegh, M. and Sadrhosseini, H., 2016. Examination of a novel solar still equipped with evacuated tube collectors and thermoelectric modules. *Desalination*, 382, pp.21–27.
- Sharon, H., Reddy, K.S., Krithika, D. and Philip, L., 2017. Experimental

performance investigation of tilted solar still with basin and wick for distillate quality and enviro-economic aspects. *Desalination*, 410, pp.30–54.

Sharqawy, M.H., Lienhard V, J.H. and Zubair, S.M., 2010. Thermophysical properties of seawater: A review of existing correlations and data. *Desalination and Water Treatment*, 16(1–3), pp.354–380.

Shatat, M., Riffat, S. and Gan, G., 2016. An innovative psychometric solar-powered water desalination system. *International Journal of Low-Carbon Technologies*, 11(2), pp.254–265. Available at: <https://academic.oup.com/ijlct/article-lookup/doi/10.1093/ijlct/cts075> [Accessed: 14 January 2020].

Shatat, M., Worall, M. and Riffat, S., 2013. Opportunities for solar water desalination worldwide: Review. *Sustainable Cities and Society*.

Sriram, V. et al., 2019. Investigation of effect of the Fresnel lens on the performance of the double slope single basin solar still. *International Journal of Ambient Energy*.

Srithar, K. et al., 2016. Stand alone triple basin solar desalination system with cover cooling and parabolic dish concentrator. *Renewable Energy*, 90, pp.157–165.

Tanaka, H., 2009. Experimental study of a basin type solar still with internal and external reflectors in winter. *Desalination*.

Tiwari, G.N., Dimri, V. and Chel, A., 2009. Parametric study of an active and passive solar distillation system: Energy and exergy analysis. *Desalination*.

Wang, H., Huang, J., Song, M. and Yan, J., 2019. Effects of receiver parameters on the optical performance of a fixed-focus Fresnel lens solar concentrator/cavity receiver system in solar cooker. *Applied Energy*, 237, pp.70–82.

Wang, Q., Zhu, Z. and Zheng, H., 2018. Investigation of a floating solar desalination film. *Desalination*, 447, pp.43–54.

Xie, W. T., Dai, Y.J., Wang, R.Z. and Sumathy, K., 2011. Concentrated solar energy applications using Fresnel lenses: A review. *Renewable and Sustainable Energy Reviews*.

Xie, W T, Dai, Y.J., Wang, R.Z. and Sumathy, K., 2011. Concentrated solar energy applications using Fresnel lenses: A review. *Renewable and Sustainable Energy Reviews*, 15, pp.2588–2606. Available at: <https://pdfs.semanticscholar.org/dbd1/ad08468552b3cd8b7de0196a0464640781f3.pdf> [Accessed: 9 April 2018].

Xiong, J., Xie, G. and Zheng, H., 2013. Experimental and numerical study on a new multi-effect solar still with enhanced condensation surface. *Energy Conversion and Management*, 73, pp.176–185.

Yousef, M.S., Hassan, H., Kodama, S. and Sekiguchi, H., 2019. An experimental study on the performance of single slope solar still integrated with a PCM-based pin-finned heat sink. *Energy Procedia*. 1 January 2019 Elsevier Ltd, pp. 100–104.

Zhao, Y. et al., 2018. Development and performance studies of a novel portable solar cooker using a curved Fresnel lens concentrator. *Solar Energy*, 174, pp.263–272.

APPENDICES

Appendix A: Experimental Error and Uncertainty Analysis

Uncertainty Analysis for Productivity (Sample: FRL Model B)

$$E = P\Delta T = \frac{I(t)_1 + I(t)_2}{2} A_{total} \Delta T, \text{ Taking time} = 9.00 \text{ am as sample.}$$

$$\text{Let } A_{total} = 0.053 \text{ m}^2, \Delta T = 1800\text{s}, \delta I(t) = 10 \text{ W/m}^2$$

$$E = 47.7I(t)_1 + 47.7I(t)_2$$

$$\delta E = \left[\left(\frac{dE}{dI(t)_1} \delta I(t)_1 \right)^2 + \left(\frac{dE}{dI(t)_2} \delta I(t)_2 \right)^2 \right]^{0.5}$$

$$\delta E = [(47.7 * 10)^2 + (47.7 * 10)^2]^{0.5}$$

$$\delta E = 674.58 \text{ J}, \text{ while } E = 75008.655 \text{ J. Thus, } \delta E = \pm 0.9\%$$

Approach 1, Experimental Uncertainty Percentile.

$$\text{Productivity} = \frac{\sum m_{yield}}{\sum E}$$

$$\text{Let } \sum m_{yield} = 430 \text{ g}, \sum E = 2646.2 \text{ kJ}, \delta m_{yield} = 0.2 \text{ g}, \sum \delta E = \pm 0.9\% = 23.82 \text{ kJ}$$

$$\delta \text{Productivity} = \left[\left(\frac{d\text{Productivity}}{dm_{yield}} \delta m_{yield} \right)^2 + \left(\frac{d\text{Productivity}}{dE} \delta E \right)^2 \right]^{0.5}$$

$$\delta \text{Productivity} = \left[\left(\frac{1}{E} * 0.2 \right)^2 + \left(-\frac{m_{yield}}{E^2} * 23.82 \right)^2 \right]^{0.5}$$

$$\delta \text{Productivity} = 1.46 * 10^{-3}, \text{ while Productivity} = 0.16. \text{ Thus,}$$

$$\delta \text{Productivity} = \pm 0.9\%$$

Approach 2, Using Table

$$Productivity = \frac{\sum m_{yield}}{\sum E}$$

Let $\sum m_{yield} = 430g$, $\sum E = 2646.2kJ$, $\delta m_{yield} = 0.2g$, $\sum \delta E = 20.64kJ$

$$\delta Productivity = \left[\left(\frac{dProductivity}{dm_{yield}} \delta m_{yield} \right)^2 + \left(\frac{dProductivity}{dE} \delta E \right)^2 \right]^{0.5}$$

$$\delta Productivity = \left[\left(\frac{1}{E} * 0.2 \right)^2 + \left(-\frac{m_{yield}}{E^2} * 20.64 \right)^2 \right]^{0.5}$$

$\delta Productivity = 1.27 * 10^{-3}$, while **Productivity = 0.16. Thus,**

$\delta Productivity = \pm 0.8\%$ error. The calculation is referred to Table A-1.

Table A-1: Thermal Energy Data from FRL Model B

			Irradiance (W/m2)		Heat absorbed, J	
Time	total area, m2	Time, S	Measured	Delta	Calculated	Delta
9:00:00 AM	0.053	1800	730	10	75008.65	671.3814
9:30:00 AM	0.053	1800	850	10	93914.69	671.3814
10:00:00 AM	0.079	1800	750	10	110694.7	1009.973
10:30:00 AM	0.079	1800	800	10	144445.2	1009.973
11:00:00 AM	0.100	1800	967	10	108982.6	1276.923
11:30:00 AM	0.100	1800	240	10	139133.2	1276.923
12:00:00 PM	0.114	1800	1140	10	168982.1	1457.175
12:30:00 PM	0.114	1800	500	10	178180	1457.175
1:00:00 PM	0.120	1800	1170	10	234918.3	1530.989
1:30:00 PM	0.120	1800	1000	10	231367.1	1530.989
2:00:00 PM	0.117	1800	1170	10	233593	1488.065
2:30:00 PM	0.117	1800	1050	10	206226.5	1488.065
3:00:00 PM	0.106	1800	1000	10	191486.6	1354.015
3:30:00 PM	0.106	1800	1000	10	171468.9	1354.015
4:00:00 PM	0.089	1800	950	10	147465.7	1127.286
4:30:00 PM	0.089	1800	900	10	117943.1	1127.286
5:00:00 PM	0.063	1800	810	10	92406.09	806.6787
				Sum	2646216	20638.3

Uncertainty Analysis for Efficiency (Sample: FRL Model B)

$$h_{fg,w} = 2500 - \frac{2.386(T_2 + T_1)}{2}$$

$$h_{fg,sw} = h_{fg,w} * (1 - \frac{S}{1000}), S = 35g$$

$$h_{fg,sw} = 2412.5 - 1.151(T_2 + T_1)$$

$$\delta h_{fg,sw} = \left[\left(\frac{dh_{fg,sw}}{dT_1} \delta T_1 \right)^2 + \left(\frac{dh_{fg,sw}}{dT_2} \delta T_2 \right)^2 \right]^{0.5}, \delta T = 0.2^\circ C$$

$$\delta h_{fg,sw} = 0.326 \frac{kJ}{kg}$$

$$h_{fg,avg} = \sum(h_{fg,sw1} + h_{fg,sw2} + \dots + h_{fg,swn})/n, n = 17$$

$$\delta h_{fg,avg} = \left[\left(\frac{dE}{dh_{fg,sw1}} \delta h_{fg,sw1} \right)^2 + \left(\frac{dE}{dh_{fg,sw2}} \delta h_{fg,sw2} \right)^2 + \dots + \right.$$

$$\left. \left(\frac{dE}{dh_{fg,sw17}} \delta h_{fg,sw17} \right)^2 \right]^{0.5}$$

$$\delta h_{fg,avg} = 0.079 \text{ kJ/kg}$$

Approach 1, Experimental Uncertainty by Table

$$\text{Efficiency} = \frac{\sum m_{yield} h_{fg,avg}}{\sum E}, \text{ the data is referred to Table A-2}$$

$$\text{Let } \sum m_{yield} = 0.430 \text{ kg}, \sum E = 2646.2 \text{ kJ}, \delta m_{yield} = 0.2 \text{ g}, \sum \delta E = 20.64 \text{ kJ},$$

$$h_{fg,average} = 2340.31 \frac{kJ}{kg}$$

$$\delta \text{Efficiency} = \left[\left(\frac{d\text{Efficiency}}{dm_{yield}} \delta m_{yield} \right)^2 + \left(\frac{d\text{Efficiency}}{dE} \delta E \right)^2 + \left(\frac{d\text{Efficiency}}{dh_{fg,avg}} \delta h_{fg,avg} \right)^2 \right]^{0.5}$$

$$\delta\text{Efficiency} = \left[\left(\frac{h_{fg,avg}}{E} * 0.0002 \right)^2 + \left(-\frac{m_{yield} h_{fg,avg}}{E^2} * 20.64 \right)^2 + \left(\frac{m_{yield}}{E} * 0.079 \right)^2 \right]^{0.5}$$

$\delta\text{Efficiency} = 2.9 * 10^{-3}$ (Or 0.29%), while **Efficiency = 0.37 (or 37%).**

Thus, $\delta\text{Efficiency} = \pm 0.78\%$ error.

Table A-2: Latent Heat of Vaporization Data from FRL Model B

Time	Temperature (°C)		h _{fg} , salt water (kJ/kg)	
	Water	Delta	Calculated	Delta
9:00:00 AM	32	0.2	2338.536	0.325835
9:30:00 AM	39.5	0.2	2329.9035	0.325835
10:00:00 AM	47.3	0.2	2312.2932	0.325835
10:30:00 AM	52.4	0.2	2297.4453	0.325835
11:00:00 AM	55.3	0.2	2288.2373	0.325835
11:30:00 AM	54	0.2	2286.3957	0.325835
12:00:00 PM	57.4	0.2	2283.9786	0.325835
12:30:00 PM	58.2	0.2	2279.1444	0.325835
1:00:00 PM	61.4	0.2	2274.5404	0.325835
1:30:00 PM	64.4	0.2	2267.4042	0.325835
2:00:00 PM	68	0.2	2259.8076	0.325835
2:30:00 PM	68.5	0.2	2255.0885	0.325835
3:00:00 PM	58.8	0.2	2265.6777	0.325835
3:30:00 PM	60.5	0.2	2274.8857	0.325835
4:00:00 PM	60	0.2	2273.5045	0.325835
4:30:00 PM	61.2	0.2	2272.6988	0.325835
5:00:00 PM	57	0.2	2276.1518	0.325835
		Average	2284.452541	0.079067

Table A-3: Uncertainty in Model A

Model A	Productivity	Del Productivity	Efficiency	Del Efficiency	Percent Error	
					Productivity	Efficiency
Conventional	0.05	0.000397	0.12	0.000917	0.8%	0.8%
CSP	0.08	0.000462	0.18	0.001061	0.6%	0.6%
PCM	0.07	0.000548	0.16	0.001262	0.8%	0.8%
MSS	0.07	0.000570	0.16	0.001314	0.8%	0.8%

Table A-4: Uncertainty in Model B

Model B	Productivity	Del Productivity	Efficiency	Del Efficiency	Percent Error	
					Productivity	Efficiency
Conventional	0.13	0.000771	0.29	0.001754	0.6%	0.6%
CSP	0.16	0.001267	0.37	0.002900	0.8%	0.8%
PCM	0.13	0.001257	0.3	0.002886	1.0%	1.0%
MSS	0.13	0.001139	0.3	0.002614	0.9%	0.9%

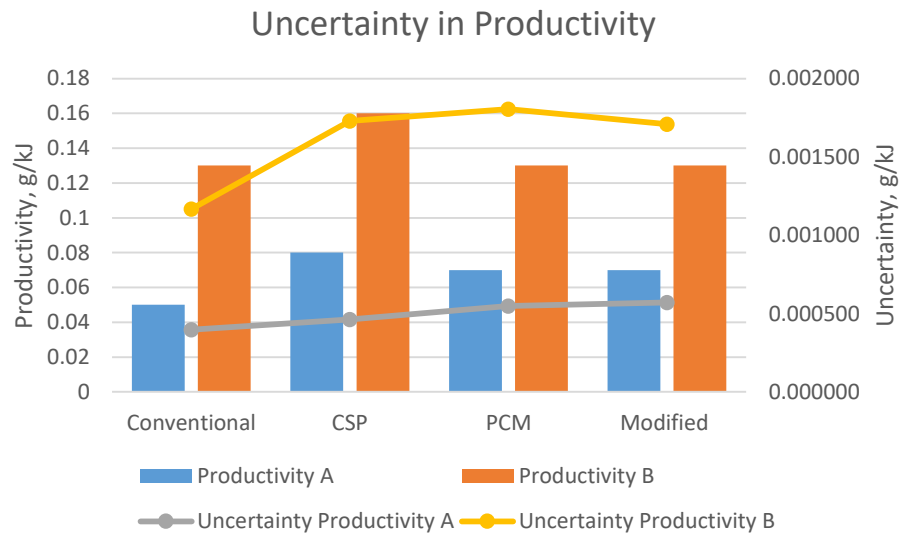


Figure A-1: Uncertainty in Productivity

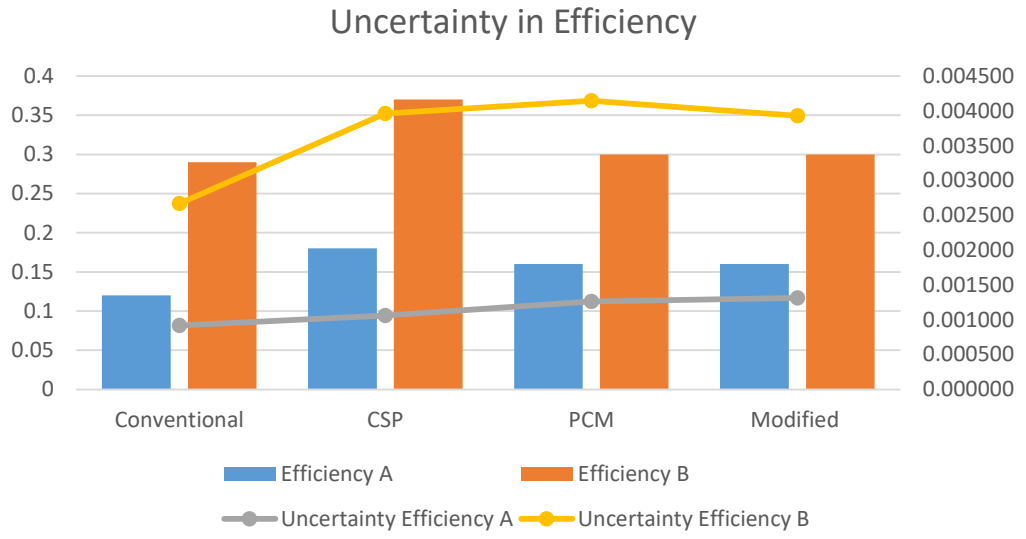


Figure A-2: Uncertainty in Efficiency

Appendix B: Experimental Data

Calculation of actual receiver area with different elevation angle

θ = elevation angle, height = 0.098 m, length = 0.45 m

$$a = \frac{0.098}{\tan \theta}, b = 0.3 - a, c = b \sin \theta$$

$$A_{water} = 0.45 * C$$

$$A_{water} = 0.45 \left(0.3 - \frac{0.098}{\tan \theta} \right) \sin \theta$$

$$d = 0.098 \cos \theta$$

$$A_{basin} = 0.45 * d$$

$$A_{basin} = 0.45(0.098) \cos \theta$$

$$A_{total} = A_{water} + A_{total}$$

Table B – 1: Experimental Data for Conventional Solar Still Model A

Time	Irradiance (W/m²)	Temperature of Feed water (K)	Temperature of Cover (K)
9:00:00 AM	61	301.4	300.7
9:30:00 AM	105.8	301.4	300.9
10:00:00 AM	1039.4	305.6	304.2
10:30:00 AM	1081.3	312.7	310.7
11:00:00 AM	1007.3	317.6	314
11:30:00 AM	973.6	320.3	314.3
12:00:00 PM	869.8	325.3	318.5
12:30:00 PM	949.9	329.5	312.1
1:00:00 PM	1206.1	330.2	323
1:30:00 PM	1215.6	333.5	326.8
2:00:00 PM	1175.2	332.7	329.8
2:30:00 PM	1197.7	330.1	325.4
3:00:00 PM	1199.6	329.9	322.3
3:30:00 PM	1180.8	328.5	327.5
4:00:00 PM	1107.1	329.8	326.2
4:30:00 PM	467.1	325.1	318.8
5:00:00 PM	152	324.2	315.6

Actual Yield = 0.28 kg

Table B – 2: Theoretical Yield for Conventional Solar Still Model A

Time	Q_{wge}	Q_{wgr}	Q_{wgc}	P_g	P_{sw}	Yield (kg)
9:00:00 AM	1.04	4.12	0.47	3729.74	3811.71	0.0002
9:30:00 AM	2.63	2.94	0.88	4128.33	4302.65	0.0005
10:00:00 AM	8.63	8.55	1.97	5448.62	5907.01	0.0015
10:30:00 AM	23.75	13.05	3.95	7122.24	8157.46	0.0043
11:00:00 AM	58.81	24.43	8.27	7840.47	9938.70	0.0106
11:30:00 AM	102.43	41.30	12.39	8825.97	12077.09	0.0185
12:00:00 PM	270.03	48.88	29.47	8331.53	15142.91	0.0491
12:30:00 PM	310.70	123.86	30.64	9369.85	17033.59	0.0567
1:00:00 PM	177.48	54.05	14.74	13581.10	18724.20	0.0324
1:30:00 PM	118.37	51.95	9.12	16025.73	19852.43	0.0217
2:00:00 PM	80.17	22.71	6.60	15493.61	18331.75	0.0147
2:30:00 PM	139.41	35.65	12.36	12894.36	17155.67	0.0255
3:00:00 PM	84.86	56.79	7.65	13581.10	16513.21	0.0155
3:30:00 PM	35.89	7.60	3.31	14940.44	16473.75	0.0065
4:00:00 PM	93.48	27.37	9.10	12055.58	15179.60	0.0171
4:30:00 PM	135.15	45.30	15.32	9201.33	13238.64	0.0246
5:00:00 PM	107.53	60.67	14.54	7493.84	10811.23	0.0195

Total Theoretical Yield: 0.3189 kg

Table B –3: Solar Power received by Conventional Solar Still Model A

Time	Ir ,W/m²	A_w, m²	A_b, m²	A_{Total}, m²	Power, W
9:00:00 AM	61	0.052	0.046	0.098	5.959
9:30:00 AM	105.8	0.052	0.046	0.098	10.335
10:00:00 AM	1039.4	0.106	0.040	0.147	152.736
10:30:00 AM	1081.3	0.106	0.040	0.147	158.893
11:00:00 AM	1007.3	0.152	0.033	0.186	187.142
11:30:00 AM	973.6	0.152	0.033	0.186	180.881
12:00:00 PM	869.8	0.186	0.026	0.212	184.408
12:30:00 PM	949.9	0.186	0.026	0.212	201.390
1:00:00 PM	1206.1	0.200	0.023	0.223	268.661
1:30:00 PM	1215.6	0.200	0.023	0.223	270.777
2:00:00 PM	1175.2	0.192	0.025	0.217	254.438
2:30:00 PM	1197.7	0.192	0.025	0.217	259.310
3:00:00 PM	1199.6	0.166	0.031	0.197	236.324
3:30:00 PM	1180.8	0.166	0.031	0.197	232.621
4:00:00 PM	1107.1	0.126	0.038	0.164	181.581
4:30:00 PM	467.1	0.126	0.038	0.164	76.611
5:00:00 PM	152	0.073	0.044	0.117	17.840

Total Heat Absorbed: 5194.53 kJ

Table B – 4: Experimental Data for Conventional Solar Still Model B

Time	Irradiance (W/m²)	Temperature of Feed water (K)	Temperature of Cover (K)
9:00:00 AM	1065.2	300.9	315.5
9:30:00 AM	1194.4	304	322.2
10:00:00 AM	939.1	311.5	312
10:30:00 AM	1164	313	317
11:00:00 AM	1282.5	323.7	333.6
11:30:00 AM	1313	327.2	337
12:00:00 PM	1310.6	337.3	343.6
12:30:00 PM	1300.2	340.9	351.2
1:00:00 PM	1301.8	347.6	358.3
1:30:00 PM	1262.4	348.2	357.6
2:00:00 PM	1211.2	352.2	357.7
2:30:00 PM	1270.8	352.8	360.6
3:00:00 PM	1292.3	353.9	355.4
3:30:00 PM	1327.3	356.8	359
4:00:00 PM	1251.8	353.1	353.6
4:30:00 PM	1264.3	349.4	353.1
5:00:00 PM	231.3	339.3	331.7

Actual Yield = 0.455kg

Table B – 5: Theoretical Yield for Conventional Solar Still Model B

Time	Q_{wge}	Q_{wgr}	Q_{wgc}	P_g	P_{sw}	Yield (kg)
9:00:00 AM	245.07	0.00	41.37	10019.40	4050.69	0.0181
9:30:00 AM	126.82	0.00	19.76	9153.67	5467.47	0.0094
10:00:00 AM	21.64	0.00	3.00	7987.20	6991.04	0.0016
10:30:00 AM	139.36	0.00	14.12	13850.89	9636.88	0.0104
11:00:00 AM	336.08	0.00	23.92	22272.61	13770.02	0.0254
11:30:00 AM	344.47	0.00	19.27	27921.08	19079.08	0.0261
12:00:00 PM	500.67	0.00	21.45	38019.64	26116.95	0.0384
12:30:00 PM	910.92	0.00	31.22	51597.61	32774.08	0.0701
1:00:00 PM	1009.09	0.00	30.61	58683.01	38325.12	0.0782
1:30:00 PM	719.49	0.00	20.89	57985.54	42218.97	0.0558
2:00:00 PM	680.10	0.00	18.40	61544.36	46444.29	0.0530
2:30:00 PM	430.64	0.00	11.49	58799.94	48094.16	0.0336
3:00:00 PM	146.73	0.00	3.49	56952.51	52173.57	0.0114
3:30:00 PM	100.17	0.00	2.31	54933.17	51335.02	0.0078
4:00:00 PM	140.36	0.00	3.91	48734.12	44105.47	0.0109
4:30:00 PM	57.19	0.00	3.00	30635.37	32916.47	0.0044
5:00:00 PM	212.30	0.00	13.05	20069.75	26116.95	0.0080

Total Theoretical Yield: 0.4712 kg

Table B –6: Solar Power received by Conventional Solar Still Model B

Time	Ir ,W/m²	A_w, m²	A_b, m²	A_{Total}, m²	Power, W
9:00:00 AM	1065.2	0.011	0.041	0.053	56.188
9:30:00 AM	1194.4	0.011	0.041	0.053	63.003
10:00:00 AM	939.1	0.043	0.036	0.079	74.519
10:30:00 AM	1164	0.043	0.036	0.079	92.365
11:00:00 AM	1282.5	0.070	0.030	0.100	128.666
11:30:00 AM	1313	0.070	0.030	0.100	131.726
12:00:00 PM	1310.6	0.091	0.024	0.114	150.046
12:30:00 PM	1300.2	0.091	0.024	0.114	148.855
1:00:00 PM	1301.8	0.100	0.020	0.120	156.588
1:30:00 PM	1262.4	0.100	0.020	0.120	151.849
2:00:00 PM	1211.2	0.094	0.022	0.117	141.606
2:30:00 PM	1270.8	0.094	0.022	0.117	148.574
3:00:00 PM	1292.3	0.079	0.028	0.106	137.477
3:30:00 PM	1327.3	0.079	0.028	0.106	141.200
4:00:00 PM	1251.8	0.055	0.034	0.089	110.869
4:30:00 PM	1264.3	0.055	0.034	0.089	111.976
5:00:00 PM	231.3	0.024	0.040	0.063	14.659

Total Heat Absorbed: 3490.92 kJ

Table B – 7: Experimental Data for FRL Solar Still Model A

Time	Irradiance (W/m²)	Temperature of Feed water (K)	Temperature of Cover (K)
9:00:00 AM	1065.2	302	300.1
9:30:00 AM	1194.4	306.3	305.2
10:00:00 AM	939.1	311.7	305.4
10:30:00 AM	1164	312.9	309.2
11:00:00 AM	1282.5	322.6	318.1
11:30:00 AM	1313	324.7	324.3
12:00:00 PM	1310.6	329.3	325.5
12:30:00 PM	1300.2	335.4	330.3
1:00:00 PM	1301.8	335	327.1
1:30:00 PM	1262.4	337.6	328.8
2:00:00 PM	1211.2	332.3	327.4
2:30:00 PM	1270.8	339.9	331.7
3:00:00 PM	1292.3	329.7	325.2
3:30:00 PM	1327.3	341.3	333.3
4:00:00 PM	1251.8	327.9	324
4:30:00 PM	1264.3	328.2	322.1
5:00:00 PM	231.3	328.4	318.9

Actual Yield = 0.505kg

Table B – 8: Theoretical Yield for FRL Solar Still Model A

Time	Q_{wge}	Q_{wgr}	Q_{wgc}	P_g	P_{sw}	Yield (kg)
9:00:00 AM	5.54	0.00	1.63	4152.19	4465.38	0.0082
9:30:00 AM	25.16	0.00	5.56	4829.89	5858.49	0.0084
10:00:00 AM	44.05	0.00	8.42	5403.32	7009.86	0.0057
10:30:00 AM	45.14	0.00	6.66	7634.93	9343.02	0.0054
11:00:00 AM	30.10	0.00	3.47	11292.83	12599.36	0.0197
11:30:00 AM	28.39	0.00	2.88	13581.10	14852.06	0.0368
12:00:00 PM	103.44	0.00	8.20	15719.77	19168.70	0.0526
12:30:00 PM	192.42	0.00	13.86	16336.80	21879.35	0.0389
1:00:00 PM	275.01	0.00	19.45	15757.74	23010.12	0.0387
1:30:00 PM	202.80	0.00	14.83	15872.12	21629.10	0.0352
2:00:00 PM	202.90	0.00	14.11	17015.13	22800.88	0.0354
2:30:00 PM	183.34	0.00	13.40	16141.78	21480.14	0.0322
3:00:00 PM	185.95	0.00	13.20	16773.00	22182.91	0.0185
3:30:00 PM	167.40	0.00	12.28	16297.64	21282.89	0.0325
4:00:00 PM	97.53	0.00	9.26	12391.44	15625.99	0.0286
4:30:00 PM	171.26	0.00	16.70	10899.66	15815.29	0.0202
5:00:00 PM	150.41	0.00	16.15	9739.99	14145.92	0.0220

Total Theoretical Yield: 0.445 kg

Table B –9: Solar Power received by FRL Solar Still Model A

Time	Ir ,W/m²	A_w, m²	A_b, m²	A_{Total}, m²	Power, W
9:00:00 AM	1065.2	0.052	0.046	0.098	104.052
9:30:00 AM	1194.4	0.052	0.046	0.098	116.672
10:00:00 AM	939.1	0.106	0.040	0.147	137.997
10:30:00 AM	1164	0.106	0.040	0.147	171.046
11:00:00 AM	1282.5	0.152	0.033	0.186	238.271
11:30:00 AM	1313	0.152	0.033	0.186	243.937
12:00:00 PM	1310.6	0.186	0.026	0.212	277.863
12:30:00 PM	1300.2	0.186	0.026	0.212	275.658
1:00:00 PM	1301.8	0.200	0.023	0.223	289.978
1:30:00 PM	1262.4	0.200	0.023	0.223	281.202
2:00:00 PM	1211.2	0.192	0.025	0.217	262.232
2:30:00 PM	1270.8	0.192	0.025	0.217	275.136
3:00:00 PM	1292.3	0.166	0.031	0.197	254.587
3:30:00 PM	1327.3	0.166	0.031	0.197	261.482
4:00:00 PM	1251.8	0.126	0.038	0.164	205.314
4:30:00 PM	1264.3	0.126	0.038	0.164	207.364
5:00:00 PM	231.3	0.073	0.044	0.117	27.147

Total Heat Absorbed: 6464.67 kJ

Table B – 10: Experimental Data for FRL Solar Still Model B

Time	Irradiance (W/m²)	Temperature of Feed water (K)	Temperature of Cover (K)
9:00:00 AM	730	316.4	312.95
9:30:00 AM	850	322.85	317.5
10:00:00 AM	750	326.85	320.85
10:30:00 AM	800	327.65	321.95
11:00:00 AM	967	328.7	322.25
11:30:00 AM	240	330.8	323.15
12:00:00 PM	1140	332.8	324
12:30:00 PM	500	335.9	326.7
1:00:00 PM	1170	339.2	330
1:30:00 PM	1000	341.25	331.9
2:00:00 PM	1170	336.65	327.7
2:30:00 PM	1050	332.65	324.55
3:00:00 PM	1000	333.25	325.35
3:30:00 PM	1000	333.6	325.1
4:00:00 PM	950	332.1	323.5
4:30:00 PM	900	327	319.25
5:00:00 PM	810	321	313.75

Actual Yield = 0.43kg

Table B – 11: Theoretical Yield for FRL Solar Still Model B

Time	Q_{wge}	Q_{wgr}	Q_{wgc}	P_g	P_{sw}	Yield (kg)
9:00:00 AM	33.55	23.16	5.25	7355.02	8710.07	0.0034
9:30:00 AM	82.10	37.84	9.77	9345.62	12107.28	0.0084
10:00:00 AM	115.68	43.91	11.69	11094.74	14744.25	0.0118
10:30:00 AM	112.87	42.08	10.98	11727.62	15327.16	0.0116
11:00:00 AM	138.64	47.92	13.03	11905.54	16122.28	0.0142
11:30:00 AM	189.22	57.63	16.57	12453.36	17819.50	0.0195
12:00:00 PM	246.44	67.16	20.23	12990.59	19576.46	0.0254
12:30:00 PM	302.03	72.09	22.00	14831.87	22593.27	0.0312
1:00:00 PM	314.70	74.27	22.22	18228.23	26234.24	0.0326
1:30:00 PM	354.48	76.83	23.11	19929.79	28739.93	0.0368
2:00:00 PM	303.35	70.69	21.35	15568.69	23380.26	0.0314
2:30:00 PM	221.85	61.93	18.13	13348.77	19439.72	0.0229
3:00:00 PM	221.75	60.79	17.63	13884.94	19991.65	0.0229
3:30:00 PM	246.06	65.44	19.46	13715.43	20319.79	0.0254
4:00:00 PM	231.78	65.28	19.52	12672.21	18945.33	0.0239
4:30:00 PM	159.24	56.34	16.39	10226.94	14852.06	0.0163
5:00:00 PM	108.79	49.94	14.44	7675.66	11032.46	0.0111

Total Theoretical Yield: 0.349 kg

Table B –12: Solar Power received by FRL Solar Still Model B

Time	Ir ,W/m²	A_w, m²	A_b, m²	A_{Total}, m²	Power, W
9:00:00 AM	730	0.011	0.041	0.053	38.507
9:30:00 AM	850	0.011	0.041	0.053	44.836
10:00:00 AM	750	0.043	0.036	0.079	59.513
10:30:00 AM	800	0.043	0.036	0.079	63.481
11:00:00 AM	967	0.070	0.030	0.100	97.014
11:30:00 AM	240	0.070	0.030	0.100	24.078
12:00:00 PM	1140	0.091	0.024	0.114	130.515
12:30:00 PM	500	0.091	0.024	0.114	57.243
1:00:00 PM	1170	0.100	0.020	0.120	140.734
1:30:00 PM	1000	0.100	0.020	0.120	120.286
2:00:00 PM	1170	0.094	0.022	0.117	136.789
2:30:00 PM	1050	0.094	0.022	0.117	122.759
3:00:00 PM	1000	0.079	0.028	0.106	106.381
3:30:00 PM	1000	0.079	0.028	0.106	106.381
4:00:00 PM	950	0.055	0.034	0.089	84.140
4:30:00 PM	900	0.055	0.034	0.089	79.711
5:00:00 PM	810	0.024	0.040	0.063	51.337

Total Heat Absorbed: 2646.22 kJ

Table B – 13: Experimental Data for PCM Solar Still Model A

Time	Irradiance (W/m ²)	Temperature of Feed water (K)	Temperature of Cover (K)	Temperature of PCM (K)
9:00:00 AM	794.7	302.7	305.6	302.1
9:30:00 AM	830.5	306.5	309.3	305.6
10:00:00 AM	952.8	313.6	312.6	312.5
10:30:00 AM	984.5	316.2	315.5	315.3
11:00:00 AM	1059	321.4	316.6	320.7
11:30:00 AM	1068.5	324.9	317.8	323.7
12:00:00 PM	151.9	329.2	321	329.4
12:30:00 PM	1045.9	330	325.5	329.5
1:00:00 PM	1202.9	331.9	327.3	331.4
1:30:00 PM	1206.6	334	331.5	333.8
2:00:00 PM	216.4	334.2	322	334
2:30:00 PM	1228.2	332.5	328.8	332.4
3:00:00 PM	1175.1	332	327.5	329.9
3:30:00 PM	1134	331.3	330.3	333.9
4:00:00 PM	758.8	330.4	326.1	331.3
4:30:00 PM	788.4	331.7	327.1	332.2
5:00:00 PM	296.2	325.4	319	326.8

Actual Yield = 0.33kg

Table B – 14: Theoretical Yield for PCM Solar Still Model A

Time	Q_{wge}	Q_{wgr}	Q_{wgc}	P_g	P_{sw}	Yield (kg)
9:00:00 AM	19.57	0.00	3.95	5448.62	4581.16	0.0036
9:30:00 AM	6.37	0.00	0.88	6603.79	6205.53	0.0012
10:00:00 AM	3.80	0.00	0.79	7798.99	8050.67	0.0007
10:30:00 AM	27.84	0.00	3.93	8665.96	9862.49	0.0052
11:00:00 AM	95.27	0.00	11.28	9201.33	12289.83	0.0180
11:30:00 AM	157.27	0.00	16.13	10305.72	14888.15	0.0298
12:00:00 PM	142.23	0.00	12.86	12515.55	16831.80	0.0270
12:30:00 PM	99.49	0.00	8.35	14616.77	17946.40	0.0189
1:00:00 PM	78.83	0.00	6.10	16893.69	19714.03	0.0150
1:30:00 PM	212.05	0.00	16.15	14867.98	20796.56	0.0405
2:00:00 PM	224.66	0.00	17.80	13919.06	20084.94	0.0429
2:30:00 PM	92.42	0.00	7.35	15910.40	19079.08	0.0176
3:00:00 PM	52.12	0.00	4.29	16494.28	18548.90	0.0099
3:30:00 PM	47.62	0.00	4.05	15948.76	17861.71	0.0091
4:00:00 PM	97.12	0.00	8.12	14759.87	18031.42	0.0185
4:30:00 PM	112.85	0.00	10.55	12391.44	16006.56	0.0215
5:00:00 PM	116.66	0.00	12.60	10096.80	13736.28	0.0221

Total Theoretical Yield: 0.302 kg

Table B –15: Solar Power received by PCM Solar Still Model A

Time	Ir ,W/m²	A_w, m²	A_b, m²	A_{Total}, m²	Power, W
9:00:00 AM	794.7	0.052	0.046	0.098	77.629
9:30:00 AM	830.5	0.052	0.046	0.098	81.126
10:00:00 AM	952.8	0.106	0.040	0.147	140.010
10:30:00 AM	984.5	0.106	0.040	0.147	144.669
11:00:00 AM	1059	0.152	0.033	0.186	196.748
11:30:00 AM	1068.5	0.152	0.033	0.186	198.513
12:00:00 PM	151.9	0.186	0.026	0.212	32.205
12:30:00 PM	1045.9	0.186	0.026	0.212	221.743
1:00:00 PM	1202.9	0.200	0.023	0.223	267.948
1:30:00 PM	1206.6	0.200	0.023	0.223	268.772
2:00:00 PM	216.4	0.192	0.025	0.217	46.852
2:30:00 PM	1228.2	0.192	0.025	0.217	265.913
3:00:00 PM	1175.1	0.166	0.031	0.197	231.498
3:30:00 PM	1134	0.166	0.031	0.197	223.401
4:00:00 PM	758.8	0.126	0.038	0.164	124.454
4:30:00 PM	788.4	0.126	0.038	0.164	129.309
5:00:00 PM	296.2	0.073	0.044	0.117	34.764

Total Heat Absorbed: 4795.42 kJ

Table B – 16: Experimental Data for PCM Solar Still Model B

Time	Irradiance (W/m ²)	Temperature of Feed water (K)	Temperature of Cover (K)	Temperature of PCM (K)
9:00:00 AM	240.3	302.25	304.65	301.2
9:30:00 AM	43.5	304.15	308	301.9
10:00:00 AM	810	309.4	312.95	306
10:30:00 AM	900	317.65	316.25	312.5
11:00:00 AM	1000	326.55	322.95	321.2
11:30:00 AM	1230	332.55	329.25	329.8
12:00:00 PM	1050	334.3	327.7	334.3
12:30:00 PM	300	334.9	326.9	335
1:00:00 PM	1000	336	329.2	334.5
1:30:00 PM	1100	337.45	330.85	336.1
2:00:00 PM	1286	340.6	332.75	338.4
2:30:00 PM	1100	343.75	334.85	342.8
3:00:00 PM	500	343.25	333.7	344.7
3:30:00 PM	300	336.9	326.65	341.3
4:00:00 PM	200	328.3	318.8	332.2
4:30:00 PM	600	321.15	312.95	324.5
5:00:00 PM	21	315.55	308.55	318

Actual Yield = 0.29kg

Table B – 17: Theoretical Yield for PCM Solar Still Model B

Time	Q_{wge}	Q_{wgr}	Q_{wgc}	P_g	P_{sw}	Yield (kg)
9:00:00 AM	0.00	-14.45	3.11	4655.32	4004.19	0.0000
9:30:00 AM	28.67	-23.79	5.89	5617.57	4465.38	0.0029
10:00:00 AM	33.97	-23.05	5.42	7355.02	5988.65	0.0034
10:30:00 AM	9.84	9.60	1.57	8757.08	9294.81	0.0010
11:00:00 AM	58.87	26.57	5.92	12329.78	14530.63	0.0060
11:30:00 AM	69.99	25.76	5.51	16773.00	19349.02	0.0072
12:00:00 PM	187.59	51.57	14.03	15568.69	20989.93	0.0194
12:30:00 PM	243.98	62.46	18.16	14976.78	21579.35	0.0252
1:00:00 PM	211.34	53.91	14.80	16732.94	22696.87	0.0219
1:30:00 PM	218.46	53.06	14.41	18099.39	24245.49	0.0226
2:00:00 PM	314.15	64.55	18.63	19790.68	27924.20	0.0326
2:30:00 PM	424.27	74.92	22.63	21816.18	32069.99	0.0442
3:00:00 PM	449.87	79.81	24.69	20686.02	31378.85	0.0469
3:30:00 PM	359.07	80.67	25.55	14795.83	23647.75	0.0372
4:00:00 PM	215.59	69.34	21.62	9993.72	15815.29	0.0221
4:30:00 PM	126.88	56.32	16.99	7355.02	11116.42	0.0129
5:00:00 PM	78.93	45.83	13.37	5791.06	8330.89	0.0080

Total Theoretical Yield: 0.314 kg

Table B –18: Solar Power received by PCM Solar Still Model B

Time	Ir ,W/m²	A_w, m²	A_b, m²	A_{Total}, m²	Power, W
9:00:00 AM	240.3	0.011	0.041	0.053	12.676
9:30:00 AM	43.5	0.011	0.041	0.053	2.295
10:00:00 AM	810	0.043	0.036	0.079	64.274
10:30:00 AM	900	0.043	0.036	0.079	71.416
11:00:00 AM	1000	0.070	0.030	0.100	100.325
11:30:00 AM	1230	0.070	0.030	0.100	123.399
12:00:00 PM	1050	0.091	0.024	0.114	120.211
12:30:00 PM	300	0.091	0.024	0.114	34.346
1:00:00 PM	1000	0.100	0.020	0.120	120.286
1:30:00 PM	1100	0.100	0.020	0.120	132.314
2:00:00 PM	1286	0.094	0.022	0.117	150.351
2:30:00 PM	1100	0.094	0.022	0.117	128.605
3:00:00 PM	500	0.079	0.028	0.106	53.191
3:30:00 PM	300	0.079	0.028	0.106	31.914
4:00:00 PM	200	0.055	0.034	0.089	17.714
4:30:00 PM	600	0.055	0.034	0.089	53.141
5:00:00 PM	21	0.024	0.040	0.063	1.331

Total Heat Absorbed: 2181.81 kJ

Table B – 19: Experimental Data for MSS Solar Still Model A

Time	Irradiance (W/m ²)	Temperature of Feed water (K)	Temperature of Cover (K)	Temperature of PCM (K)
9:00:00 AM	863.5	301.7	306.6	301.5
9:30:00 AM	837.9	305.8	308.6	305
10:00:00 AM	1053	307.4	313.2	309.3
10:30:00 AM	1079.4	311.4	317.1	313.1
11:00:00 AM	1092.9	320.9	317.2	319.6
11:30:00 AM	1081.8	322.1	318	320.9
12:00:00 PM	1104.2	327.8	323.8	327.1
12:30:00 PM	1064.3	333	326.4	330.5
1:00:00 PM	1141.6	333.2	329	332.4
1:30:00 PM	1057.7	334.6	328.4	334.6
2:00:00 PM	1076.6	333	329	332.8
2:30:00 PM	1124.8	336.9	330	337.7
3:00:00 PM	695.9	327.3	323.5	329.1
3:30:00 PM	219.2	327	321.1	329
4:00:00 PM	625.5	326.2	319.3	328
4:30:00 PM	201.2	326.4	322.7	328
5:00:00 PM	164.6	320.8	314.2	321.5

Actual Yield = 0.33 kg

Table B – 20: Theoretical Yield for PCM Solar Still Model A

Time	Q_{wge}	Q_{wgr}	Q_{wgc}	P_g	P_{sw}	Yield (kg)
9:00:00 AM	28.07	0.00	5.88	5494.25	4364.62	0.0052
9:30:00 AM	38.12	0.00	6.91	6585.90	5127.99	0.0071
10:00:00 AM	66.71	0.00	10.35	8266.01	5988.65	0.0124
10:30:00 AM	9.98	0.00	1.06	9177.47	8597.02	0.0019
11:00:00 AM	51.04	0.00	6.37	9394.14	11314.49	0.0096
11:30:00 AM	63.67	0.00	6.85	11122.85	13435.80	0.0120
12:00:00 PM	117.89	0.00	10.18	13715.43	17484.87	0.0224
12:30:00 PM	137.70	0.00	10.66	15568.69	19852.43	0.0263
1:00:00 PM	136.40	0.00	10.21	16336.80	20604.71	0.0260
1:30:00 PM	132.40	0.00	9.94	16336.80	20509.36	0.0253
2:00:00 PM	152.37	0.00	10.96	16974.56	21629.10	0.0291
2:30:00 PM	129.62	0.00	10.45	14867.98	18945.33	0.0248
3:00:00 PM	89.73	0.00	8.84	11935.42	14960.56	0.0170
3:30:00 PM	123.83	0.00	12.71	10734.81	14566.05	0.0235
4:00:00 PM	96.37	0.00	9.88	11179.26	14354.66	0.0183
4:30:00 PM	81.26	0.00	9.34	9815.52	12568.10	0.0154
5:00:00 PM	96.16	0.00	12.74	7861.29	10921.36	0.0181

Total Theoretical Yield: 0.295 kg

Table B –21: Solar Power received by MSS Solar Still Model A

Time	Ir ,W/m²	A_w, m²	A_b, m²	A_{Total}, m²	Power, W
9:00:00 AM	863.5	0.052	0.046	0.098	84.349
9:30:00 AM	837.9	0.052	0.046	0.098	81.848
10:00:00 AM	1053	0.106	0.040	0.147	154.734
10:30:00 AM	1079.4	0.106	0.040	0.147	158.614
11:00:00 AM	1092.9	0.152	0.033	0.186	203.046
11:30:00 AM	1081.8	0.152	0.033	0.186	200.984
12:00:00 PM	1104.2	0.186	0.026	0.212	234.104
12:30:00 PM	1064.3	0.186	0.026	0.212	225.644
1:00:00 PM	1141.6	0.200	0.023	0.223	254.293
1:30:00 PM	1057.7	0.200	0.023	0.223	235.604
2:00:00 PM	1076.6	0.192	0.025	0.217	233.091
2:30:00 PM	1124.8	0.192	0.025	0.217	243.526
3:00:00 PM	695.9	0.166	0.031	0.197	137.094
3:30:00 PM	219.2	0.166	0.031	0.197	43.183
4:00:00 PM	625.5	0.126	0.038	0.164	102.591
4:30:00 PM	201.2	0.126	0.038	0.164	33.000
5:00:00 PM	164.6	0.073	0.044	0.117	19.319

Total Heat Absorbed: 4702.52 kJ

Table B – 22: Experimental Data for MSS Solar Still Model B

Time	Irradiance (W/m ²)	Temperature of Feed water (K)	Temperature of Cover (K)	Temperature of PCM (K)
9:00:00 AM	1065.2	302.3	307.2	302
9:30:00 AM	1194.4	306.7	313.5	305.4
10:00:00 AM	939.1	309.3	313	308.7
10:30:00 AM	1164	311.6	315.7	311
11:00:00 AM	1282.5	321	322.8	319.5
11:30:00 AM	1313	321.5	322	322
12:00:00 PM	1310.6	328.5	323.3	330.6
12:30:00 PM	1300.2	329.5	324.4	329.6
1:00:00 PM	1301.8	334.6	326.3	333
1:30:00 PM	1262.4	337.2	327.3	335.2
2:00:00 PM	1211.2	338.1	328.1	337.8
2:30:00 PM	1270.8	337.4	327	337.3
3:00:00 PM	1292.3	336.8	326.7	337
3:30:00 PM	1327.3	339.1	331.2	338.8
4:00:00 PM	1251.8	336.7	329.6	337.3
4:30:00 PM	1264.3	336.1	327.5	337
5:00:00 PM	231.3	329.8	323.9	331

Actual Yield = 0.37 kg

Table B – 23: Theoretical Yield for MSS Solar Still Model B

Time	Q_{wge}	Q_{wgr}	Q_{wgc}	P_g	P_{sw}	Yield (kg)
9:00:00 AM	52.79	0.00	10.33	6391.84	4555.21	0.0053
9:30:00 AM	54.39	0.00	9.09	7473.87	5543.80	0.0055
10:00:00 AM	40.83	0.00	6.19	7924.03	6342.36	0.0041
10:30:00 AM	38.06	0.00	4.42	10226.94	8664.70	0.0038
11:00:00 AM	15.35	0.00	1.32	11995.37	11172.70	0.0016
11:30:00 AM	30.30	0.00	3.31	12146.39	13468.90	0.0031
12:00:00 PM	106.13	0.00	9.70	12894.36	16355.87	0.0109
12:30:00 PM	171.36	0.00	14.06	13884.94	18900.93	0.0176
1:00:00 PM	298.41	0.00	21.70	14904.17	22593.27	0.0308
1:30:00 PM	360.25	0.00	24.75	15568.69	24466.03	0.0373
2:00:00 PM	372.41	0.00	25.59	15456.19	24576.94	0.0386
2:30:00 PM	362.83	0.00	25.61	14940.44	23863.63	0.0376
3:00:00 PM	325.43	0.00	21.77	16533.85	24800.06	0.0337
3:30:00 PM	261.27	0.00	17.13	17717.53	24744.12	0.0271
4:00:00 PM	256.72	0.00	17.96	16219.55	23115.36	0.0266
4:30:00 PM	197.18	0.00	15.72	14125.29	19714.03	0.0204
5:00:00 PM	131.08	0.00	11.68	12926.37	16993.07	0.0135

Total Theoretical Yield: 0.317 kg

Table B –24: Solar Power received by MSS Solar Still Model B

Time	Ir ,W/m²	A_w, m²	A_b, m²	A_{Total}, m²	Power, W
9:00:00 AM	794.7	0.011	0.041	0.053	41.919
9:30:00 AM	830.5	0.011	0.041	0.053	43.808
10:00:00 AM	952.8	0.043	0.036	0.079	75.606
10:30:00 AM	984.5	0.043	0.036	0.079	78.121
11:00:00 AM	1059	0.070	0.030	0.100	106.244
11:30:00 AM	1068.5	0.070	0.030	0.100	107.197
12:00:00 PM	151.9	0.091	0.024	0.114	17.390
12:30:00 PM	1045.9	0.091	0.024	0.114	119.741
1:00:00 PM	1202.9	0.100	0.020	0.120	144.692
1:30:00 PM	1206.6	0.100	0.020	0.120	145.137
2:00:00 PM	216.4	0.094	0.022	0.117	25.300
2:30:00 PM	1228.2	0.094	0.022	0.117	143.593
3:00:00 PM	1175.1	0.079	0.028	0.106	125.009
3:30:00 PM	1134	0.079	0.028	0.106	120.637
4:00:00 PM	758.8	0.055	0.034	0.089	67.205
4:30:00 PM	788.4	0.055	0.034	0.089	69.827
5:00:00 PM	296.2	0.024	0.040	0.063	18.773

Total Heat Absorbed: 2589.53 kJ

Table B – 25: Experimental Data for High Water Volume FRL Model B

Time	Irradiance (W/m²)	Temperature of Feed water (K)	Temperature of Cover (K)
9:00:00 AM	500	304.25	306.2
9:30:00 AM	850	308.55	314
10:00:00 AM	820	312.8	318.1
10:30:00 AM	800	318.1	321.05
11:00:00 AM	980	324.3	323.8
11:30:00 AM	960	329.1	324.85
12:00:00 PM	1020	332.15	325.8
12:30:00 PM	300	331.8	326.4
1:00:00 PM	1090	330.7	327.05
1:30:00 PM	1090	332.7	326.2
2:00:00 PM	200	333.4	326.4
2:30:00 PM	1050	333.75	327.3
3:00:00 PM	800	332.9	325.3
3:30:00 PM	200	330.3	322.6
4:00:00 PM	200	329	321.1
4:30:00 PM	200	326.15	318.85
5:00:00 PM	300	323.9	317

Actual Yield = 0.3 kg

Table B – 26: Theoretical Yield for High Water Volume FRL Model B

Time	Q_{wge}	Q_{wgr}	Q_{wgc}	P_g	P_{sw}	Yield (kg)
9:00:00 AM	9.93	-11.95	2.35	5081.01	4574.70	0
9:30:00 AM	55.70	-35.42	9.53	7778.31	5821.67	0.0068
10:00:00 AM	66.49	-35.85	9.39	9640.07	7334.79	0.0082
10:30:00 AM	36.84	-20.75	4.40	11207.56	9691.04	0.0046
11:00:00 AM	5.64	3.67	0.44	12862.42	13254.63	0.0007
11:30:00 AM	93.47	32.01	7.64	13547.70	16741.10	0.0117
12:00:00 PM	175.12	48.72	13.27	14194.62	19344.24	0.0220
12:30:00 PM	142.28	41.47	10.70	14616.77	19028.88	0.0179
1:00:00 PM	84.22	27.97	6.34	15086.26	18066.34	0.0106
1:30:00 PM	184.92	50.08	13.74	14474.86	19848.88	0.0233
2:00:00 PM	208.59	54.16	15.23	14616.77	20507.45	0.0263
2:30:00 PM	193.04	50.19	13.73	15270.26	20843.71	0.0243
3:00:00 PM	223.62	58.37	16.88	13850.89	20035.16	0.0282
3:30:00 PM	199.44	57.73	16.82	12116.06	17726.85	0.0251
4:00:00 PM	192.41	58.47	17.21	11235.92	16661.13	0.0241
4:30:00 PM	152.37	52.76	15.20	10019.40	14515.92	0.0191
5:00:00 PM	127.45	48.93	13.90	9106.22	12994.71	0.0159

Total Theoretical Yield: 0.269 kg

Table B –27: Solar Power received by High Water Volume FRL Model B

Time	Ir ,W/m²	A_w, m²	A_b, m²	A_{Total}, m²	Power, W
9:00:00 AM	500	0.011	0.041	0.053	26.374
9:30:00 AM	850	0.011	0.041	0.053	44.836
10:00:00 AM	820	0.043	0.036	0.079	65.068
10:30:00 AM	800	0.043	0.036	0.079	63.481
11:00:00 AM	980	0.070	0.030	0.100	98.318
11:30:00 AM	960	0.070	0.030	0.100	96.312
12:00:00 PM	1020	0.091	0.024	0.114	116.776
12:30:00 PM	300	0.091	0.024	0.114	34.346
1:00:00 PM	1090	0.100	0.020	0.120	131.112
1:30:00 PM	1090	0.100	0.020	0.120	131.112
2:00:00 PM	200	0.094	0.022	0.117	23.383
2:30:00 PM	1050	0.094	0.022	0.117	122.759
3:00:00 PM	800	0.079	0.028	0.106	85.105
3:30:00 PM	200	0.079	0.028	0.106	21.276
4:00:00 PM	200	0.055	0.034	0.089	17.714
4:30:00 PM	200	0.055	0.034	0.089	17.714
5:00:00 PM	300	0.024	0.040	0.063	19.014

Total Heat Absorbed: 1999.83 kJ

Table B – 28: Experimental Data for High Water Volume MSS Model B

Time	Irradiance (W/m²)	Temperature of Feed water (K)	Temperature of Cover (K)
9:00:00 AM	400	303.15	303.75
9:30:00 AM	620	307.2	308.25
10:00:00 AM	790	313.25	314.3
10:30:00 AM	930	318.05	317.9
11:00:00 AM	880	323.1	321.2
11:30:00 AM	994	326.65	323.6
12:00:00 PM	1045	327.7	324.05
12:30:00 PM	1000	329.9	325.3
1:00:00 PM	916	330.85	326.5
1:30:00 PM	760	332.25	327.9
2:00:00 PM	1050	335	327.1
2:30:00 PM	1010	335	324
3:00:00 PM	760	333.05	320.25
3:30:00 PM	200	330.05	316.25
4:00:00 PM	300	325.1	313.2
4:30:00 PM	230	320.4	311.4
5:00:00 PM	200	318.6	310.5

Actual Yield = 0.32 kg

Table B – 29: Theoretical Yield for High Water Volume MSS Model B

Time	Q_{wge}	Q_{wgr}	Q_{wgc}	P_g	P_{sw}	Yield (kg)
9:00:00 AM	1.65	-3.61	0.48	4422.69	4295.90	0.0002
9:30:00 AM	4.73	-6.59	1.04	5695.86	5401.71	0.0006
10:00:00 AM	6.44	-6.99	1.07	7903.07	7513.39	0.0008
10:30:00 AM	1.21	1.04	0.09	9541.04	9666.07	0.0001
11:00:00 AM	25.87	13.69	2.53	11292.83	12488.04	0.0032
11:30:00 AM	55.29	22.59	4.84	12735.34	14874.05	0.0069
12:00:00 PM	72.51	27.22	6.19	13022.81	15651.00	0.0091
12:30:00 PM	106.96	34.85	8.53	13850.89	17392.87	0.0134
1:00:00 PM	104.87	33.28	7.99	14688.17	18195.08	0.0132
1:30:00 PM	112.41	33.71	8.09	15719.77	19435.17	0.0142
2:00:00 PM	259.26	61.76	18.08	15122.91	22083.56	0.0327
2:30:00 PM	373.90	84.81	27.79	12990.59	22083.56	0.0472
3:00:00 PM	398.17	96.16	33.26	10762.14	20175.86	0.0502
3:30:00 PM	370.03	100.38	35.81	8757.08	17517.47	0.0465
4:00:00 PM	247.26	83.38	28.54	7453.95	13787.94	0.0309
4:30:00 PM	143.85	61.14	19.24	6766.74	10901.80	0.0179
5:00:00 PM	116.56	54.32	16.58	6444.27	9943.85	0.0145

Total Theoretical Yield: 0.3015 kg

Table B –30: Solar Power received by High Water Volume MSS Model B

Time	Ir ,W/m²	A_w, m²	A_b, m²	A_{Total}, m²	Power, W
9:00:00 AM	400	0.011	0.041	0.053	21.099
9:30:00 AM	620	0.011	0.041	0.053	32.704
10:00:00 AM	790	0.043	0.036	0.079	62.687
10:30:00 AM	930	0.043	0.036	0.079	73.796
11:00:00 AM	880	0.070	0.030	0.100	88.286
11:30:00 AM	994	0.070	0.030	0.100	99.723
12:00:00 PM	1045	0.091	0.024	0.114	119.638
12:30:00 PM	1000	0.091	0.024	0.114	114.486
1:00:00 PM	916	0.100	0.020	0.120	110.182
1:30:00 PM	760	0.100	0.020	0.120	91.417
2:00:00 PM	1050	0.094	0.022	0.117	122.759
2:30:00 PM	1010	0.094	0.022	0.117	118.083
3:00:00 PM	760	0.079	0.028	0.106	80.850
3:30:00 PM	200	0.079	0.028	0.106	21.276
4:00:00 PM	300	0.055	0.034	0.089	26.570
4:30:00 PM	230	0.055	0.034	0.089	20.371
5:00:00 PM	200	0.024	0.040	0.063	12.676

Total Heat Absorbed: 2182.31 kJ

Appendix C: Publication

1. Ho Zhi Yong, Rubina Bahar, PERFORMANCE ANALYSIS OF A SOLAR DESALINATION SYSTEM WITH CONCENTRATED SOLAR POWER (CSP), IOP Conf. Ser.: Earth Environ. Sci. 268 012023
2. Ho Zhi Yong, Rubina Bahar, SOLAR DESALINATION ASSOCIATED WITH CONCENTRATED SOLAR POWER (CSP) AND PHASE CHANGE MATERIAL (PCM), FEIIC International Conference on Engineering Education and Research 2019. Available at: <http://myset.org.my/ficeer2019/>
3. Wing Sum Choong, Zhi Yong Ho, Rubina Bahar, "Solar Desalination Using Fresnel Lens as Concentrated Solar Power Device: An Experimental Study in Tropical Climate", Frontiers in Energy Research, Frontiers Media, Volume 8, pp 1-8, October 2020 (ISSN: 2296-598X).
4. Zhi Yong Ho, Rubina Bahar & Chai Hoon Koo (2021) A comprehensive review on small-scale passive solar stills for desalination, Environmental Technology Reviews, 10:1, 188-212, DOI: [10.1080/21622515.2021.1921056](https://doi.org/10.1080/21622515.2021.1921056)
5. Jun-Yan Tan, Jun Wei Ding, Zhi Yong Ho, & Rubina Bahar, EXPERIMENTAL STUDY ON A PASSIVE SOLAR DESALINATION UNIT ASSOCIATED WITH FRESNEL LENS AND THERMAL STORAGE, Proceedings of the ASME 2021 15th International Conference on Energy Sustainability ES2021